九州大学学術情報リポジトリ
Kyushu University Institutional Repository

Analysis of Pesticides by Gas Chromatography/Multiphoton Ionization/Time-of-flight Mass Spectrometry Using a Femtosecond Laser

楊, 希翔

https://hdl.handle.net/2324/1937183

出版情報：九州大学, 2018, 博士（工学）, 課程博士
バージョン：
権利関係：

Analysis of Pesticides by Gas Chromatography/Multiphoton Ionization/Time-of-flight Mass Spectrometry Using a Femtosecond Laser

Department of Applied Chemistry

Graduate School of Engineering

Kyushu University

Xixiang Yang

2/28/2018

Contents

Chapter 1 Introduction

1.1. General information

During the past centuries, a variety of pesticides have been developed to increase the production rate of the agriculture products for human beings[1]. From the invisible bacteria to the moist weather and from the overgrown weeds to the gluttonous pests, people have struggled in the battle against every kind of antagonist in the environment. However, most of the pesticides not only strike a mortal blow for the pests but also provide some crucial damages to human beings and also to the habitat. What was worse, some of the chemical compounds have extremely-high stability in the natural environment and it takes more than several human generations for decomposition. For more effective use of the pesticide resistive against some pests, farmers would increase the amount and the frequency of pesticides in the agreculature[2], which make the condition of the environment worse (pour oil on the flame). Regret to say, nobody can escape from the deteriorated environment and avoid possible diseases arising from the pesticides. Just like a coin having two faces, the pesticides pollution has become a lingering nightmare for the living animals and also for human beings on the earth.

According to the definition by the Food and Agriculture Organization (FAO)[3], pesticides can be defined as follows, “any substance or mixture of substances intended for preventing, destroying, or controlling any pest, including vectors of human or animal disease, unwanted species of plants or animals, causing harm during or otherwise interfering with the

production, processing, storage, transport, or marketing of food, agricultural commodities, wood and wood products or animal feedstuffs, or substances that may be administered to animals for the control of insects, arachnids, or other pests in or on their bodies". The term includes substances intended for use as a plant growth regulator, defoliant, desiccant, or agent for thinning fruit or preventing the premature fall of fruit. Also, they are used as substances applied to crops either before or after harvest to protect the commodity from deterioration during storage and transport.

Briefly, pesticides are the chemicals used for the destruction of insects, weeds, fungi, bacteria, and so on. They are generally called insecticides, fungicides, bactericides, herbicides. The pesticide demand in the world is increasing all the time, especially in the developing countries[4]. In Fig.1-1, the world pesticide demand is shown, according to the data of years and continents.

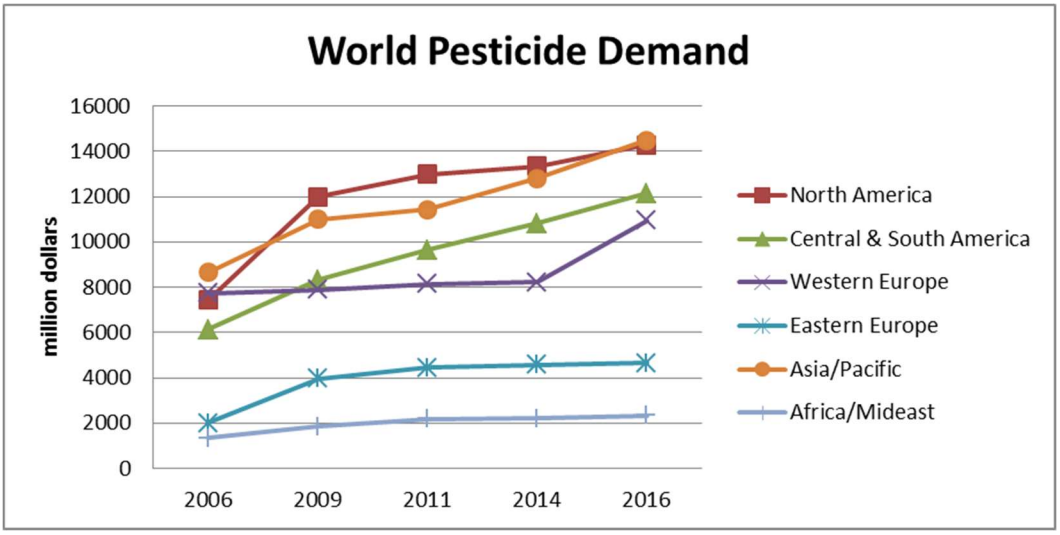

Fig. 1-1. The world pesticide demand

1.2. Pesticides and residues

In 1962, *Silent Spring* was published. As an environmental science book, it describes a world with no birds, bees and butterflies, due to a large-scale use of the DDT (Dichloro Diphenyl Trichloroethane) and other synthetic pesticides[5-6]. Since then, the issue of the protection of the environmental has been brought into people's eyes and caused widespread public and social concerns.

For better understanding and control of the pollution, basic knowledge of pesticides are of importance. In recent centuries, almost thousands of pesticides have been developed and can be categorized into several groups. Table 1-1. shows one classification of pesticides by chemical structures, and Table 1-2 shows the classification by killing targets. There are many definitions about the pesticide residue, but generally speaking, a word of "residue" means the substances remaining in or on the food, agricultural and other types of commodities or animal feed including the environmental media such as soil, air, and water resulting from the use of a pesticide[7]. In addition, all the derivatives from the pesticide that was applied to the crops, including the conversion products, metabolites, degradation products, reaction by-products, and even impurities, are considered to be "pesticide residues", which would have strong impact for humans as well as for environments.

Table.1-1. Types of pesticide categorized by the chemical structure

Type of pesticides	Representative compounds	Characteristic
Organochlorines	DDT hexachlorocyclohexane (HCH) aldrin	Organochlorine (OC) pesticides are one group of chlorinated compounds. Due to strong stability and high toxicity, some of them belong to persistent organic pollutants (POPs), which are prohibited to use in many established and even developing countries[8].
Organophosphates	parathion malathion methyl-parathion chlorpyrifos	Organophosphate (OP) pesticides are esters of phosphoric acid. They inhibit the function of neuromuscular enzyme, which is broadly required for normal functions in many insects, animals, and humans. Hydrolysis rapidly appears when this type of compounds is exposed to light, air, and soil[9].
Carbamates	sevin aldicarb carbaryl	Carbamate pesticides are one kind of chemical compounds derived from carbamic acid (NH_2COOH). Carbamate esters have a functional group which can cause the reversible inactivation for an enzyme of acteylcholinesterase[10].
Pyrethroides & pyrethrins	bifenthrin deltamethrin fenvalerate imiprothrin	Pyrethroides & pyrethrins are similar organic compounds that can be separated from the flowers of pyrethrums. The biological activity of pyrethrins arises from ketoalcoholic esters of chrysanthemic and pyrethroic acids. Pyrethroides alter nerve function, which causes paralysis in target insect pests, which makes the pests dead[11].
Phenylamide fungicides	metalaxyl mefenoxam (metalaxyl-M) furalaxyl	Phenylamide fungicides are a group of compounds that show potent eradicative anti-fungal activity, which affect nucleic acids by inhibiting the activity of rRNA synthesis and controlling pathogens[12].
Triazines	chlorazine atriazine propazine	Triazines are one category of herbicidal pesticides, which mainly inhibit plant catabolism pathway and famous for the broad spectrum and small dosage in use[13].
Dipyridyl herbicides	paraquat diquat	The dipyridyl compounds are nonselective contact herbicide, which work as redox cycling agents to kill the weeds[14].

Table.1-2. Types of pesticide by killing target

Type of pesticide	Target
Acaricide	Kill ticks and mites
Algicide	Control algae in ponds, canals, swimming pools, water tanks, and other aquatic environments
Antifouling agent	Avoid the accumulation of organisms on wetted surfaces, such as marine vessel underwater section
Antimicrobial	Kill microorganisms (such as bacteria and viruses) or stop their growth
Attractant/Repellent	Attract/Repel pests or birds to the desired/undesired location
Defoliant	Cause leaves or other foliage to drop from a plant
Disinfectant	Kill or inactivate disease-producing microorganisms on inanimate objects
Fungicide	Kill fungi or fungal spores
Fumigant	Kill or drive away the pests by producing gas or vapor
Herbicide	Kill weeds and other plants in the unnecessary place
Insect growth regulator	Disrupt the molting, maturity from pupal stage to adult, or other life processes of insects
Insecticide	Kill insects and other arthropods
Microbial pesticide	Microorganisms that kill, inhibit insects or other microorganisms
Molluscicide	Kill snails and slugs
Nematicide	Kill plant-parasitic nematodes
Plant growth regulator	Change the expected growth, flowering, or reproduction rate of plants (excluding fertilizers or other plant nutrients)
Rodenticide	Kill mice and other rodents
Wood preservative	Make wood resistant to insects or fungus

1.3. Analytical techniques

1.3.1. Current Technology of Mass Spectrometry

A variety of techniques have been developed to measure the pesticide residues in the environment. By extraction and clean-up procedures, the analytes in the sample can be measured at low concentrations. Among them, chromatography combined with mass spectrometer is known as a very important technique for the measurement of pesticides. In fact, gas chromatography-mass spectrometry (GC-MS)[15-19] and liquid chromatography-mass spectrometry (LC-MS)[20-27] are the two most common methods reported to date. With different types of ionization techniques and ion detectors, thousands of pesticides are to be analyzed and determined at ultratrace levels. For better performance in analyte separation, two-dimensional methods, *i.e.*, GC & GC and MS & MS, have been developed and used successfully in practical trace analysis. Several ionization methods such as electron ionization (EI) and chemical ionization (CI) are used as two major and popular methods in MS combined with GC[28-31], while other ionization methods such as electrospray ionization (ESI), atmospheric pressure chemical ionization (APCI), and atmospheric pressure photo-ionization (APPI) are the common techniques in MS combined with LC[32-36]. On the other hand, several mass analyzers have been developed for use in MS, *e.g.* time-of-flight, ion trapped, and quadrupole mass analyzer. All these instruments are widely used in the pesticide residue analysis and have shown excellent performance in practical applications.

1.3.2. Laser ionization Mass Spectrometry

Recently, a new type of GC-MS, which consists of a time-of-flight (TOF) mass spectrometer and a femtosecond laser as the ionization source for multiphoton ionization, has been utilized for multi-residue analysis of the pesticides in the environment[-37]. This technique has excellent sensitivity and provides subfemtogram detection limits for organic compounds. Compared with other ionization techniques such as electron ionization (EI), multiphoton ionization has an distinct advantage of providing a molecular ion referred to as "soft ionization": the energy remaining in the ionized state is minimal and usually insufficient for fragmentation of a molecular ion. Note that use of an optimal wavelength for ionization of specified pesticides will reduce the background signal significantly, which increases the signal to noise ratio and then allows the trace analysis of the constituents in the actual sample.

A femtosecond laser emitting in the far-ultraviolet region (e.g., 200 nm) would be successfully used for efficient resonance-enhanced two-photon ionization for many pesticides because of the larger molar absorptivity in this spectral region. However, the structure of the pesticide used nowadays has become more and more complicated, then majority of the pesticides may or may not have the absorption band in the far-ultraviolet region. Accordingly, it would be necessary to investigate the optimal laser wavelength of efficient ionization and background suppression. In fact, several laser wavelengths can be available by means of a technique of harmonic generation: 400 nm (second harmonic emission), 267 nm (third harmonic emission), 200 nm (fourth harmonic emission) in addition to the fundamental beam (800 nm) of the Ti:sapphire laser currently used for ionization in MS. Therefore, it is desirable to study the ionization mechanism using a laser emitting at

various wavelength for best use of laser ionization MS especially for trace analysis of pesticides in the environment.

1.4. Research subjects

In this dissertation, I employed a femtosecond laser emitting at several wavelengths as the ionization source in MS for trace analysis of pesticides at low concentrations. This dissertation is divided into four chapters as summarized below.

In Chapter 1, the aim of this research is explained in detail. The basic knowledge concerning pesticides is provided for better understandings of the motivation of this work and the contribution to agricultural and environmental sciences. Current technology regarding laser ionization MS is summarized in the following section, which is useful as a background knowledge to consider the successful approach for the pesticide analysis.

In Chapter 2, hexachlorocyclohexane, HCH, is measured by gas chromatography combined with femtosecond laser ionization MS. Many pesticides contain one or more asymmetric carbon atoms, indicating that several enantiomers are present for an isomer. Although these enantiomers are very similar to each other in the chemical structure and the spectral properties, the chemical properties such as boiling points (polarities) are not identical one another. This suggests that one of the enantiomers is biologically more effective (more toxic) and degrades more rapidly than the others in the environment. Then, it is desirable to determine the enantiomers selectively in pesticide analysis. In this chapter, hexachlorocyclohexane, HCH, was separated by GC using a column with a chiral stationary phase and measured by MS using a deep-ultraviolet (267 nm) and far-ultraviolet (200 nm)

femtosecond lasers as the ionization source. Several structural isomers, α-, β-, γ-, δ-HCH and (+/-)-α-HCH enantiomers were assigned from the data of elution order, which was theoretically predicted by calculating the stabilization energy based on molecular dynamics using a semi-empirical method.

In Chapter 3, many pesticides were determined by GC combined with MS using ultraviolet (267 nm), visible (400 nm), and near-infrared (800 nm) femtosecond lasers as the ionization source. The ionization mechanism is examined from the data of absorption spectra calculated for the neutral and ionic species. This systematic study provides us several valuable guidelines for finding an optimal wavelength for ionization. Several molecules of pesticides remain unexplained by the above guidelines, suggesting that further investigation would be needed for complete understanding of the ionization mechanism.

In Chapter 4, all the subjects obtained in this research are summarized as conclusions.

References

1. Richardson, R. *Water Sci. Technol.* **1998**, *37*, 19−25.
2. Huggett, D. B.; Khan, I. A.; Allgood, J. C.; Blosck, D. S.; Schlenk, D. *Bull. Environ. Contam. Toxicol.* **2001**, 66, 150– 155.
3. www.fao.org/agriculture/crops/thematic-sitemap/theme/pests/en/
4. Fernández-Alba, A. R., Ed. *Chromatographic-Mass Spectrometric Food Analysis for Trace Determination of Pesticide Residues*; Elsevier: Amsterdam, The Netherlands, **2005**.
5. Tomlin, C., Ed. The Pesticide Manual, 10th ed; The Royal Society of Chemistry: Cambridge. U.K., **1994**.
6. Schechter, M. *Anal. Chem.* **1951**, *23*, 538–538.
7. WHO Fact sheet, Pesticide residues in food, January **2018**
8. Ostrander, G. K. *Chem. Eng. News Archieve* **2000**, *78*, 57–58.
9. Munnecke, D. M. *J. Agric. Food Chem.* **1980**, *28*, 105–111.
10. Crosby, D. G.; Leitis, E.; Winterlin, W. L. *J. Agric. Food Chem.* **1965**, *13*, 204–207.
11. Elliott, M.; Janes, N. F.; Kimmel, E. C.; Casida, J.E. *J. Agric. Food Chem.* **1972**, *20*, 300–313.
12. http://www.frac.info/expert-fora/phenylamides/introduction
13. Hu, S.; Chen, S. *J. Agric. Food Chem.* **2013**, *61*, 8524–8532.
14. https://www.scribd.com/document/313684791/Bipyridyl-Herbicides
15. Berger, M.; Loffler, D.; Ternes, T.; Heiniger, P.; Ricking, M. *Chemosphere*, **2016**, *150*, 219–226.
16. Barrek, S.; Cren-Olivé, C.; Wiest, L.; Baudot, R.; Arnaudguilhem, C.; Grenier-Loustalot, M. *Talanta*, **2009**, *79*, 712–722.
17. Hart, E.; Coscollà, C.; Pastor, A.; Yusà, V. *Atmos. Environ.* **2012**, *62*, 118–129.

18. Huo, F.; Tang, H.; Wu, X.; Chen, D.; Zhao, T.; Liu, P.; Li, L. *J. Chromatogr. B* **2016**, *1023–1024*, 44–54.

19. Hajšlová, J.; Zrostlíková, J. *J. Chromatogr., A* **2003**, *1000*, 181.

20. Lenz, E. M.; Wilson, I. D. *J. Protein Res.* **2007**, *6*, 443– 458.

21. Moco, S.; Bino, R. J.; De Vos, C. H.; Vervoort, J. *Trends Anal. Chem*. **2007**, *26*, 855–866.

22. Xu, W.; Wang, X.; Cai, Z. *Anal. Chim. Acta*. **2013**, *790*, 1–13.

23. Trtić-Petrović, T.; Đorđević, J.; Dujaković, N.; Kumrić, K.; Vasiljević, T.; Laušević, M. *Anal. Bioanal. Chem.* **2010**, *397,* 2233–2243.

24. Bossi, R.; Vejrup, K.V.; Mogensen, B.B.; Asman, W.A.H. *J. Chromatogr. A* **2002**, *957,* 27–36.

25. Rickes, S.; Cesar, P.; José, L.; Carla, G.; Clasen, F. *Food Chem.* **2017**, *220*, 510–516.

26. Region, V.; Coscollà, C.; Hart, E.; Pastor, A.; Yusà, V. *Atmos. Environ.* **2013**, *77*, 394–403.

27. Machado, I.; Gérez, N.; Pistón, M.; Heinzen, H.; Verónica, M. *Food Chem.* **2017**, *227*, 227–236.

28. Mills, P. A.; Onley, J. H.; Gaither, R. A. *Anal. Chem.* **1963**, *46*, 186– 191.

29. Lee, S. M.; Papathakis, M. L.; Feng, M. H. C.; Hunter, G. C.; Carr, J. E. *Anal. Chem.* **1991**, 339, 376–383.

30. Nakamura, Y.; Tonogai, Y.; Sekiguchi, Y.; Tsumura, Y.; Nishida, N.; Takakura, K.; Isechi, M.; Yuasa, K.; Nakamura, M.; Kifune, N.; Yamamoto, K.; Terasawa, S.; Oshima, T.; Miyata, M.; Kamakura, K.; Ito, Y. *J. Agric. Food Chem.* **1994**, *42*, 2508–2518.

31. Fillion, J.; Hindle, R.; Lacroix, M.; Selwyn, J. *J. AOAC Int.* **1995**, *78*, 1252– 1266.

32. Cook, J.; Beckett, M. P.; Reliford, B.; Hammock, W.; Engel, M. *J. AOAC Int.* **1999**, *82*, 1419– 1435.

33. Fillion, J.; Sauvé, F.; Selwyn, J. *J. AOAC Int.* **2000**, *83*, 698–713.

34. Chun, O. K.; Kang, H. G.; Kim, M. H. *J. AOAC Int.* **2003**, *86*, 823–831.

35. Kondo, H.; Amakawa, E.; Sato, H.; Aoyagi, Y.; Yasuda, K. *J. Food Hyg. Soc. Jpn* **2003**, *44*, 161– 167.

36. Ueno, E.; Oshima, H.; Saito, I.; Matsumoto, H.; Yoshimura, Y.; Nakazawa, H. *J. AOAC Int*. **2004**, *87*, 1003–1015.

37. Li, A.; Thang, D. P.; Imasaka, T.; Imasaka, T. Analyst **2017**, *142*, 3942–3947.

Chapter 2 Determination of hexachlorocyclohexane isomers

2.1. Introduction

During the past decades, a variety of pesticides have been developed and widely used for pest control to increase the yield of crops in the agriculture. Most of them are considerably toxic and are harmful not only for insects but also for humans.[1-3] Then, the pesticides should be carefully used under controls for protection of the environment. Although some of the pesticides was prohibited for a long time ago, they remain in the environment due to extremely high stability of these compounds. It should be noted that some of the toxic pesticides are used even now in several countries when their use is more beneficial for the production of crops rather than the contamination of the soils.

Hexachlorocyclohexane, HCH, is the most abundant organochlorine compound of the pesticide in the atmosphere and also in the water.[4-8] This compound is a generic term for the isomers of 1,2,3,4,5,6,-hexachlorocyclohexane, and the isomers are denoted by Greek letters (α, β, γ, δ, ε, η, and θ-HCH).[9] A technical mixture of HCH isomers is used as a commercial product, which typically contains 60-70% α–, 5-12% β–, 10-12% γ–HCH.[10] The order of toxicity for insects is reported to be γ > α > δ >>β.[11] HCHs primarily affect the central nervous system (CNS). Although the toxicological mechanism in human body remains mostly unknown, the α-, β-, and δ-HCH isomers are considered to be CNS depressants.[12] Only α-HCH consists of chiral HCH isomers.[13] The enantiomeric ratio of (+)-α-HCH and (-)-α-HCH was measured in the North Sea water.[14] The ratio of the technical α-HCH is

reported to be 1.00 ± 0.02, the value being changed from 1.2 from 1.9 for those in the blubber, liver, and lung of neonatal northern fur seals.[15] Although α–, β–, and γ–HCHs were recently issued as new persistent organic pollutants (POPs) in the Stockholm Convention, toxic, persistent, and bio-accumulative HCH wastes remaining in the environment, mainly consisting of α-HCH (80%) and β-HCH (20%), are estimated to be 4-7 million tonne.[16]

The distribution of structural and enantiometric isomers provides us important information for assessment of the environment and is also useful for control and protection of the environmental issue. However, the concentration levels of the toxic pesticides are very low, and numerous interference species are present at high concentrations for environmental samples.[17] Therefore, it is desirable to develop a sensitive as well as selective analytical method for trace analysis of these compounds. To date, several types of analytical instruments have been utilized to date, e.g., gas chromatography/mass spectrometry (GC/MS)[18,19], liquid chromatography/mass spectrometry (LC/MS)[20-22], and liquid chromatography/tandem mass spectrometry (LC/MS-MS)[21]. In standard GC/MS, a technique of electron ionization (EI) has been successfully used, since the standard data are available for many compounds in the database and the analyte can be readily assigned. However, other ionization techniques such as photoionization provides us useful means for trace analysis. For example, femtogram detection limits are reported for dioxins and subfemtogram for polycyclic aromatic hydrocarbons based on multiphoton ionization (MPI) using an ultraviolet femtosecond laser.[23] Several pesticides have absorption bands in the far-ultraviolet region at around 200 nm, a far-ultraviolet femtosecond laser emitting at 200 nm was used for more efficient ionization in MS.[24]

In this study, I report on the separation of four structural isomers of α-, β-, γ-, δ-HCHs and two enantiomers of α-HCH, i.e., (+)-α-HCH and (-)-α-HCH, using a capillary column with a stationary phase consisting of permethylated γ-cyclodextrin (PM-γ-CD) and their determination by MS using a femtosecond laser emitting in the deep-ultraviolet (267 nm) and far-ultraviolet (200 nm) regions. The order of elution of the (+/-)-α-HCH enantiomers were compared with the data from stabilization energy by a technique based on molecular dynamics using a semi-empirical method. The mechanism of fragmentation is discussed using data obtained by quantum chemical calculations.

2.2. Experimental

2.2.1. Apparatus

The analytical instrument used in this study is reported in detail elsewhere.[25,26] Briefly, a 1-μL of sample solution was injected into a GC (6890N, Agilent Technologies, Santa Clara, CA, USA) equipped with an auto sampler (7683B, Agilent Technologies), which was combined with a time-of-flight (TOF) mass spectrometer developed in our laboratory and now commercially available (HGK-1, Hikari-GK, Fukuoka, Japan). The third and fourth harmonic emissions (267 and 200 nm) of a Ti:sapphire laser (800 nm, 35 fs, 1 kHz, 4 mJ, Elite, Coherent Inc., CA, USA) were used as ionization sources. The laser beam was focused into a molecular beam for multiphoton ionization. The analytes in the standard sample mixture containing four structural isomers of HCHs were separated using a capillary column with a chiral stationary phase (γ-DEX 120, 30 m long, 0.25 inner diameter, 0.25 film

thickness, Supelco, Bellefonte, PA, USA). The temperature of a GC oven was programed to increase from 100 °C (1 min hold) to 150 °C at a rate of 20 °C/min and then to 190 °C at a rate of 2 °C, where it was held for 15 min. The temperature was further increased to 210 °C at a rate of 30 °C and was held for 5 min. The flow rate of helium used as a carrier gas was 1 mL/min. The ions induced were accelerated toward a TOF tube and were detected by microchannel plates (F4655-11, Hamamatsu Photonics, Shizuoka, Japan). The signals were recorded by a digitizer (AP240, Acqiris, Agilent Technologies), and the data were analyzed using a home-made software programed by LabVIEW.

2.2.2. Reagents

Enantiometric isomers of (+/-)-α-HCH and δ-HCH were purchased from Wako Pure Chemical Industries, Tokyo, Japan. β-HCH was supplied from Sigma Aldrich, while γ-HCH was a product of Tokyo Chemical Industry, Tokyo, Japan. Their steric structures are shown in Fig. 2-1. Acetone (analytical grade) used as a solvent was supplied from Wako Pure Chemical Industries.

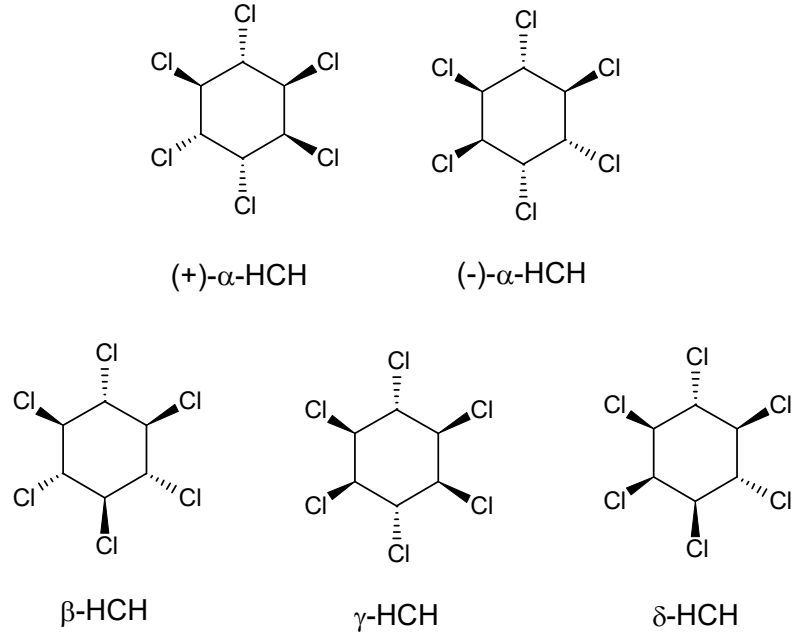

Fig. 2-1. Chemical structures of α-, β-, γ-, and δ-HCH. Two enantiomers of (+) and (-) are shown for α-HCH.

2.2.2. Quantum Chemical Calculation

To investigate the mechanism for the ionization, the spectral properties such as the ionization energies and the absorption spectra of α-, β-, γ-, and δ-HCH in the gaseous phase are necessary. For this purpose, sophisticated analytical instruments such as photoelectron spectroscopy and also for absorption spectrometry in the vacuum-ultraviolet region are required. These parameters were evaluated by Tomoko Imasaka of the Graduate School of Design, Kyushu University. The optimized geometry of the ground state and the harmonic frequencies were calculated using the B3LYP method based on density functional theory (DFT) with a cc-pVDZ basis set. The lowest 40 singlet transition energies and the oscillator strengths were calculated using time-dependent DFT (TD-DFT), and the absorption spectra

were predicted by assuming a peak with a Gaussian profile having a half width at half maximum of 0.333 eV. These calculations were performed using the Gaussian 09 and Gauss View 5 programs.[27,28] For the discussion of fragmentation, the enthalpy change by the dissociation of a molecular ion was calculated using DFT.

In order to examine the energy of interaction between (+/-)-α-HCH and PM-γ-CD, their structures were generated using Gauss View 5.0.9 and were optimized at the level of PM3 (Parameterized Model number 3) using Gaussian 09 by Tomoko Imaska. As an initial configuration of PM-γ-CD, the glycosidic oxygen atoms, i.e., Oa, Ob, Oc, and Od, were placed on the XY plane and their center of gravity was positioned at the origin of the space-fixed Cartesian coordinate of XYZ (see Fig. 2-2. for details). The methylated secondary hydroxyl groups of the PM-γ-CD, i.e., -OCH_3, were set to point toward the positive direction of the Z-axis. The (+/-)-α-HCH molecule was assumed to approach toward the wide rim of the PM-γ-CD.

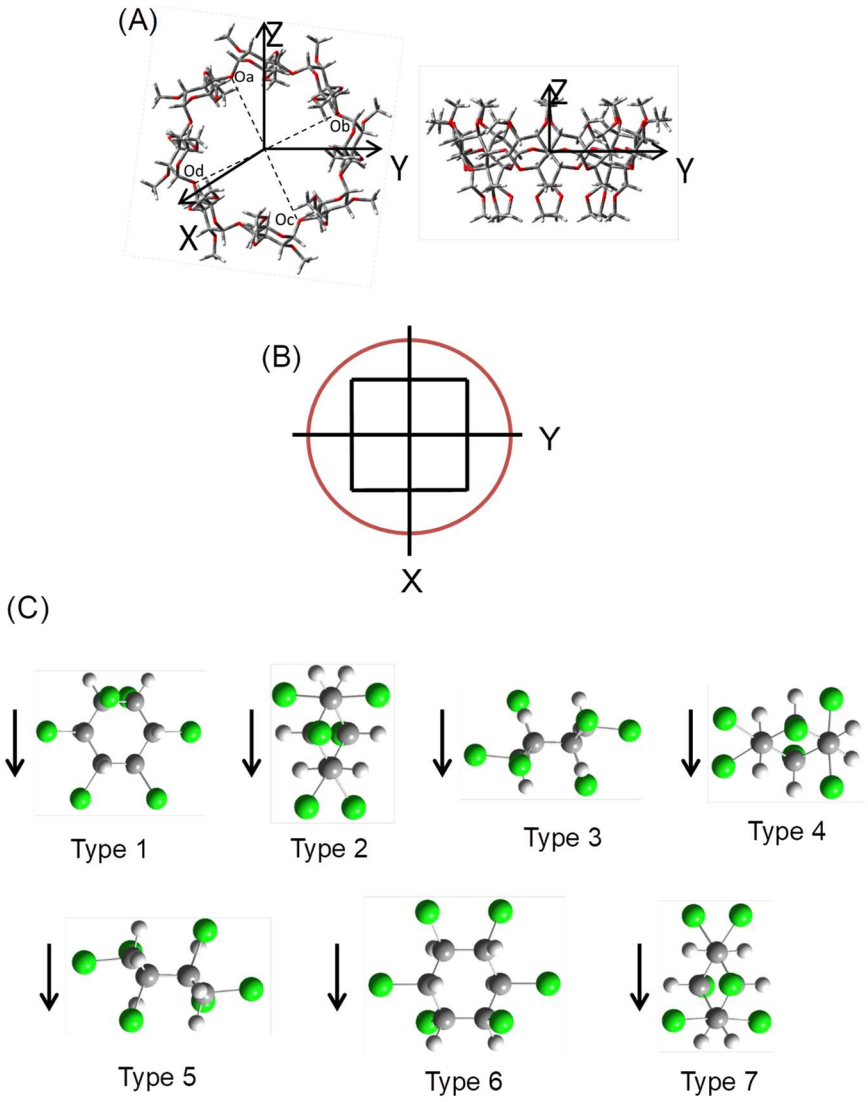

Fig. 2-2. (A) structure of permethylated γ-cyclodextrin calculated at PM3 levels. Red, oxygen; gay, carbon; white, hydrogen. (B) picture of Cartesian coordinate viewed from a ring with a larger size at a height of Z = 5 Å. The locations initially used for computer simulation are indicated as black filled circles in the picture. The spacing between the locations is 2 Å. (C) initial configuration of (+)-α-HCH isomers used in the computer simulation. Type 1, original position (not rotated); Type 2, rotated 90° along z-axis; Type 3-5, rotated 90° along y-axis and rotated 0, 90, 180° along z-axis, respectively; Type 6-7, rotated 180° along y-axis and rotated 0, 90° along z-axis, respectively. The arrow shows the direction that (+)-α-HCH approach permethylated γ-cyclodextrin.

2.3. Results and discussion

2.3.1. Spectral Properties of HCHs

The absorption spectra of HCH isomers calculated by DFT are shown in Fig. 2-3. The energy of excitation to the first singlet electronic excited state (*EE*) is located at around 200 nm while no absorption band is found at around 267 nm. The half of the energy for ionization (*IE*/2) is located at around 250 nm, suggesting two-photon ionization at 200 nm and three-photon ionization at 267 nm. Thus, all of the isomers would be ionized through a resonant two-photon ionization at 200 nm and non-resonant three-photon ionization at 267 nm. Therefore, a far-ultraviolet laser (200 nm) would be preferential for efficient ionization and also for reducing the excess energy to suppress fragmentation. The molar absorptivity at 200 nm was ca. 500, 700, 400, and 400 for α-, β-, γ-, and δ-HCHs, respectively, which was nearly identical to each other. This suggests that the ionization efficiency would not change significantly among these isomers.

2.3.2. Predicted Elution Order of (+/-)-α-HCHs

The optimized structure of the PM-γ-CD used as the stationary phase of the capillary column in GC is shown in Fig. 1 (A), and suggests that the molecule has a symmetry of C_8. The average distance from the center of gravity to a glycosidic oxygen atom, Oa, Ob, Oc, Od, of PM-γ-CD was 5.94 Å, which was similar to the value of 5.88 Å reported based on X-ray crystallography data for γ-CD.[29] The average angle of C-O-C calculated for a glycosidic oxygen was 115°, which was close to the observed value of 117°. The average distance between the oxygen atoms was 4.54 Å, which is nearly identical to the observed value (4.50

Å). Thus, the calculated structural data are in reasonably good agreement with the observed data for γ-CD, although no data were available for PM-γ-CD as a reference. It should also be noted that the calculated structure of PM-γ-CD was very similar to that obtained by increasing the number of the glycosidic units from seven to eight in the reported structure of PM-β-CD.[30]

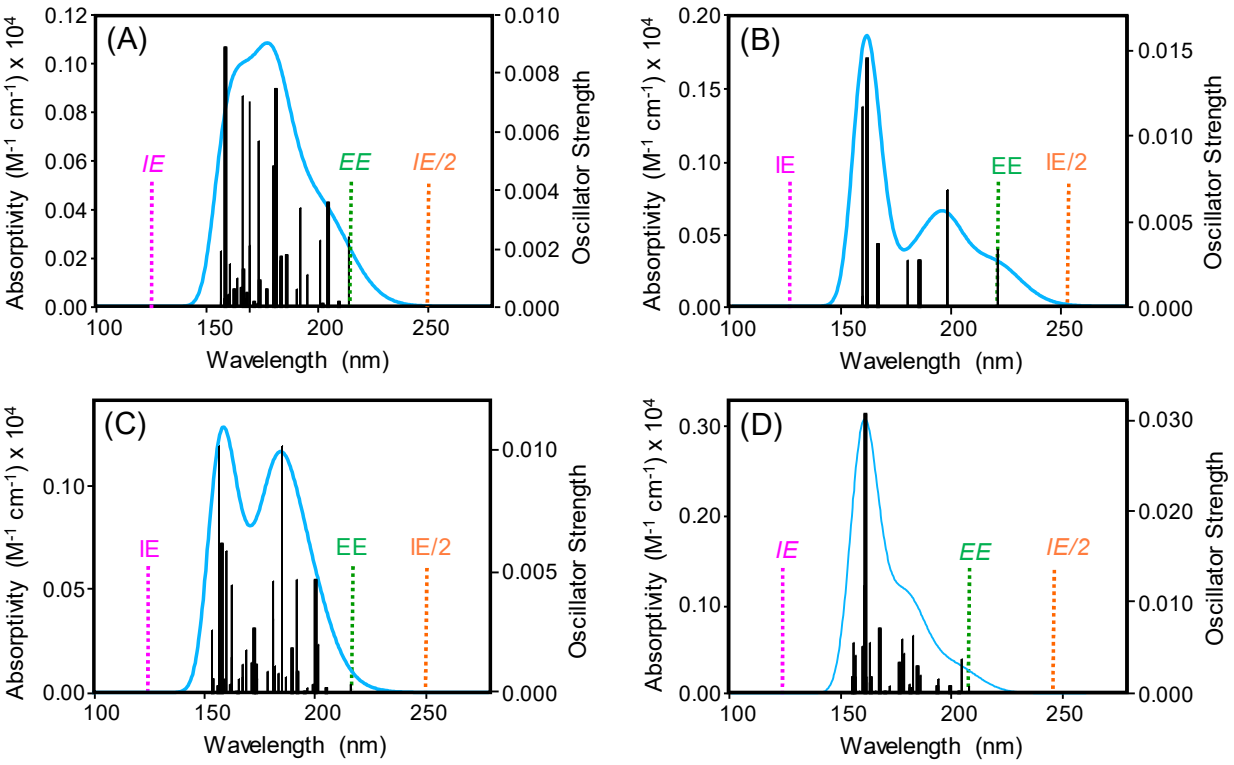

Fig. 2-3. Absorption spectra calculated for (A) α-HCH (B) β-HCH (C) γ-HCH (D) δ-HCH by DFT. *IE*, ionization energy; *IE*/2, half of ionization energy; *EE*, excitation energy to the first electronic excited state. The vertical ionization energy for these compounds are 9.91 eV (125.1 nm), 9.91 eV (125.1 nm), 9.87 eV (125.6 nm), and 10.08 eV (123.0 nm), respectively.

Since the (+/-)-α-HCH/PM-γ-CD complex consists of 258 atoms, finding an optimized structure required a long time or it was difficult to converge the data in the DFT computation: it was difficult to apply, even the Hartree-Fock method. Therefore, a semi-empirical method, i.e., PM3, was utilized in this study. A preliminary examination suggests that the calculated value for the stabilization energy by complexing was affected by the initial position and configuration of (+/-)-α-HCH. In fact, (+/-)-α-HCH with different configurations placed at various locations approaches the PM-γ-CD cage in the experiment, and enantiomeric separation was achieved by virtue of the small difference in the stabilization energy of the complex of (+/-)-α-HCH and PM-γ-CD. The (+/-)-α-HCHs with different configurations were then positioned at 3 × 3 grids above the PM-γ-CD before the calculation (see Fig. 2-2. (B)). A molecule was assumed to approach along the Z-axis toward the inner surface of the PM-γ-CD cage. To investigate the stabilization energy along the Z-axis, the structure of the (+/-)-α-HCH/PM-γ-CD complex was first optimized with no restrictions by placing the center of gravity of (+/-)-α-HCH at (0, 0, Z) where Z = 3, 4, 5, 6, 7 Å. The energy was minimal at (0, 0, 5 Å) in the cases of both (+)-α-HCH and (-)-α-HCH. Second, the initial center of gravity was set at (X, Y, Z=5 Å) where X = -1.5, 0, 1.5 and Y = -1.5, 0, 1.5, since (+/-)-α-HCH is assumed to approach from various positions toward the wider rim of the PM-γ-CD. The (+/-)-α-HCH molecule was then rotated by 0°, 90°, 180° around the z-axis of the molecule-fixed Cartesian coordinate of xyz and was also rotated by 0°, 90°, 180° around the y-axis, as shown Fig. 2-2. (C); the arrow in the figure shows the direction of approach to the PM-γ-CD. The optimization was then initiated from 126 positions/configurations/species, i.e.,

9 translational × 7 rotational × 2 (+/-)-α-HCH species. After rejecting data leading to unstable and deformed structures (12/126), the difference in the stabilization energies for the (+/-)-α-HCHs was calculated to be -0.34 ± 1.42 kcal/mol, suggesting that the (+)-α-HCH/PM-γ-CD complex is slightly more stable than the (-)-α-HCH/PM-γ-CD complex: the conclusion remained unchanged even when the conditions for the calculation and the rule for rejecting the data were modified. A small difference in the stabilization energy could be due to the very flexible structure of PM-γ-CD. Thus, (+)-α-HCH would be predicted to elute later than (-)-α-HCH in GC, as reported in the literature.[31]

2.3.3. Determination of HCHs

A sample containing a mixture of α-, β-, γ-, and δ-HCH was analyzed by GC/MPI-TOFMS using a femtosecond laser emitting at 200 nm and the result is shown in Fig. 2-4. The isomers of HCH were clearly separated by GC and a series of fragment peaks were produced in MS. The expanded view shown in the insert indicates the complete separation/resolution of (+)-α-HCH and (-)-α-HCH by GC and MS; the (-)-enantiomer elutes earlier than the (+)-enantiomer in GC.[31] The signal intensity of the peak arising from β-HCH is relatively weak, although the molar absorptivity is slightly higher than that for the other compounds at 200 nm, suggesting that a β-HCH undergoes a more inefficient ionization from the excited state. A two-dimensional display measured at 267 nm is shown in Fig.2-5. for comparison. A molecular ion is more clearly observed for α- and γ-HCHs at 200 nm than at 267 nm, which would be attributed to efficient resonant two-photon ionization at 200 nm and inefficient non-resonant three-photon ionization at 267 nm. However, no drastic changes

were observed for data measured at the different wavelengths, suggesting that the effect of resonance is minimal in femtosecond ionization.[32]

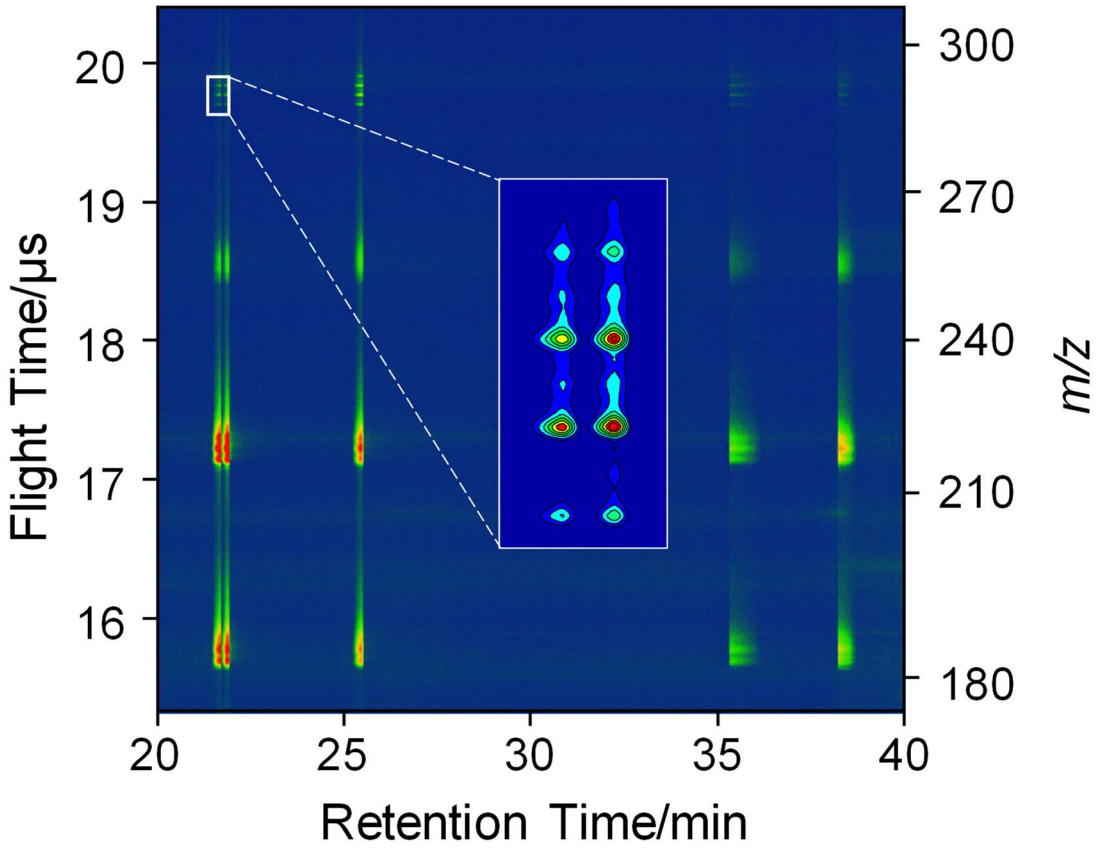

Fig. 2-4. Two-dimensional display for a sample mixture containing four isomers of α-, β-, γ, and δ-HCHs measured at 200 nm (20 μJ). The insert shows the expanded part that the molecular ions of (-) and (+) enantiomers of α-HCH appear. The concentration of the analyte was 25 ng/μL for each isomer of HCH.

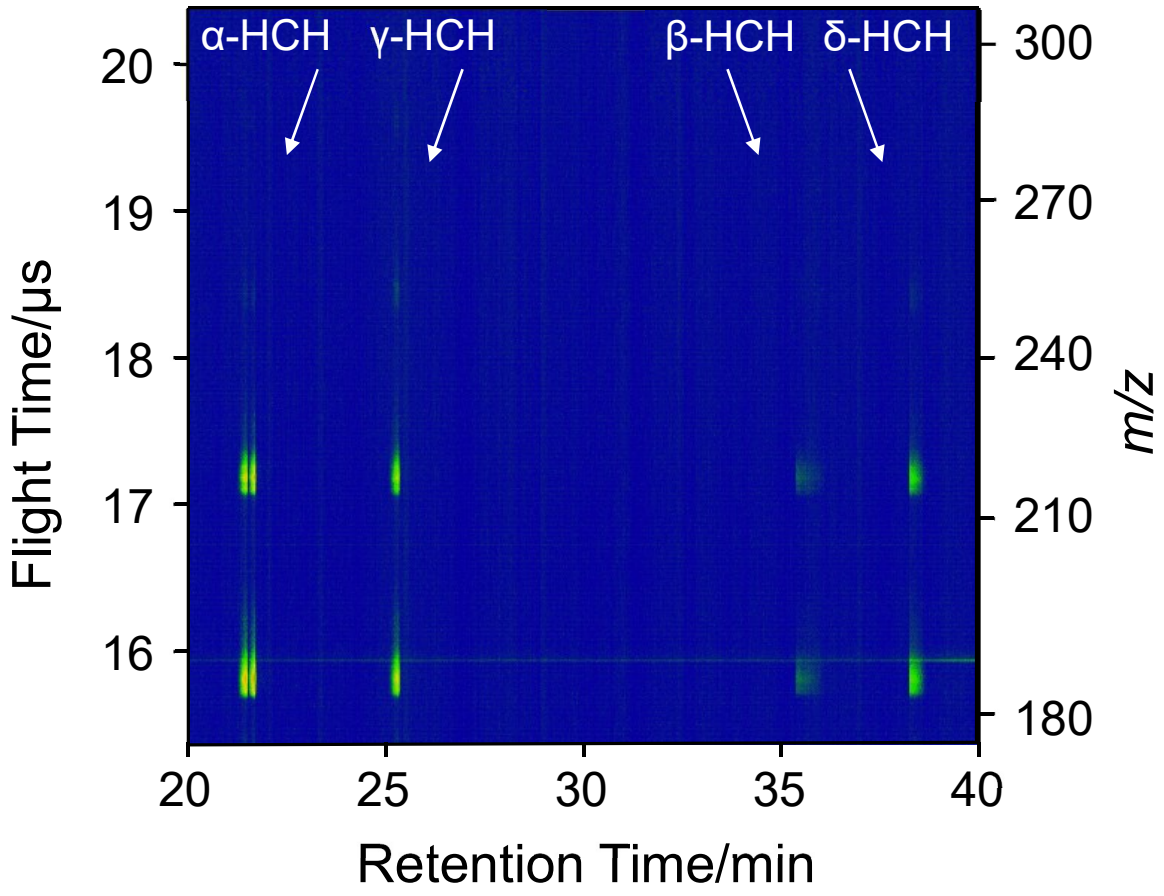

Fig. 2-5. Two-dimensional display for a sample mixture containing four isomers of α-, β-, γ, and δ-HCHs measured at 267 nm (20 μJ). The concentration of the analyte was 25 ng/mL for each isomer of HCH.

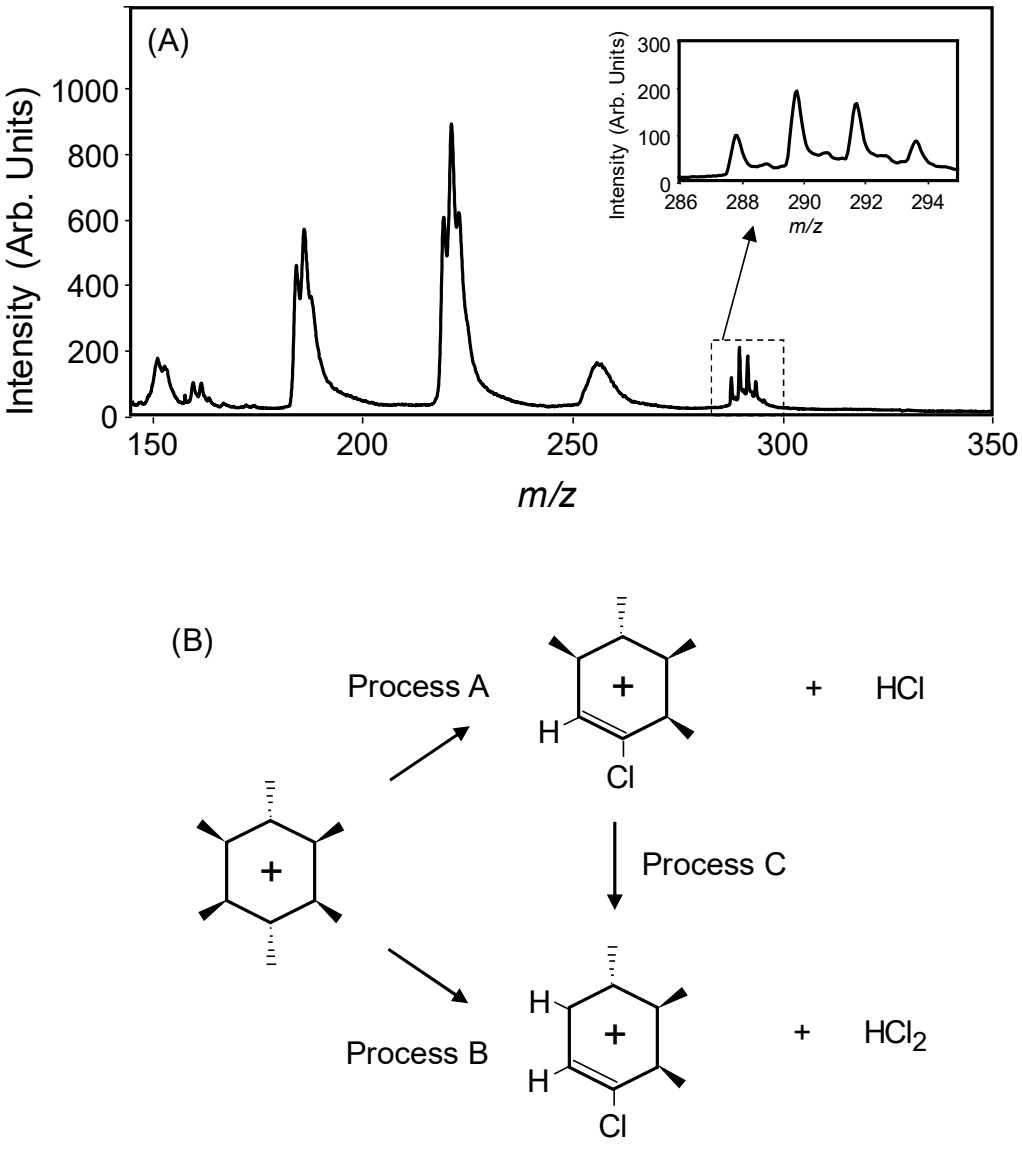

Fig. 2-6. (A) mass spectrum of γ-HCH measured at 200 nm (20 μJ) (B) scheme of the fragmentation from the molecular ion.

2.3.4. Fragmentation of HCHs

As shown in Figs. 2-4. and 2-5., the fragment patterns are similar among these isomers, although α- and γ-HCHs give rise to a more pronounced molecular ion and the signal intensity is larger when measured at 200 nm. Figure 2-6. shows the mass spectra of HCHs extracted from the data shown in Fig. 2-4.. A molecular ion corresponding to $C_6H_6{}^{35}Cl_6$ is clearly observed at *m/z* = 288, in addition to other several isotopomers of $C_6H_6{}^{35}Cl_{6-x}{}^{37}Cl_x$ where x = 1 - 3. The EI mass spectra are available for HCHs in the NIST database: the spectral region of a molecule ion is missing for α-HCH probably due to a small signal intensity.[33] The relative signal intensities of the molecular ions were apparently more enhanced in the MPI mass spectra measured at 200 nm. This result suggests that UV femtosecond ionization is more favorable for observing a molecular ion. It should be noted that the signal of the fragment, $[M\text{-}HCl]^+$ observed at around *m/z* = 253 in Fig. 2-6., is very broad, which is in contrast to the result for $[M\text{-}HCl_2]^+$ providing a slightly split structure. In this study, a linear-type TOFMS was used and the initial velocity distribution of the ion can be evaluated; the mass resolution calculated using the signal of a molecular ion was $m/\Delta m$ = 520 and this peak broadening cannot be attributed to the limited resolution of the mass spectrometer. These results suggest that a molecule easily dissociates to form fragment ions and neutral species such as HCl (process A) or HCl_2 (Process B): these processes would occur in parallel (not sequentially) in femtosecond ionization mass spectrometry. The dissociation releases the excess energy as translational energies of the ions and also of the neutral species. Concerning the fragmentation, an enthalpy change in processes A and B was calculated by DFT. In process A, the enthalpy change was -8.2, -12.0, -3.3 and -5.8 kcal/mol for α-, β-, γ-, and δ-

HCH, respectively, suggesting that the molecular ion can be stabilized by producing a fragment ion and a neutral species of HCl and that the fragmentation is less efficient for γ-HCH. Accordingly, a very broad peak was observed for the fragment of $[M\text{-}HCl]^+$ and a molecular ion remained more efficiently for γ-HCH due to a smaller change in enthalpy (-3.3 kcal/mol or -0.14 eV). In process B, the enthalpy change was 7.8, 0.0, 8.4, 6.2 kcal/mol for α-, β-, γ-, and δ-HCH, respectively. Then, a small energy is required for the dissociation of HCl_2 (e.g., 8.4 kcal/mol or 0.37 eV for γ-HCH), which is, however, much smaller than the excess energy in two-photon ionization ($6.20 \times 2 - 9.87 = 2.53$ eV): a molecular ion remained more efficiently for γ-HCH due to a larger change in enthalpy. Thus, a slightly split structure was observed for the fragment of $[M\text{-}HCl_2]^+$ and a molecular ion remained more efficiently for γ-HCH. When the third harmonic emission (267 nm) was used, the excess energy obtained through the process of three-photon ionization increases significantly ($4.64 \times 3 - 9.87 = 4.05$ eV), suggesting that a molecular ion can more easily dissociate to form fragment ions. It is interesting to note that a molecular ion was observed more efficiently at 800 nm rather than at 400 nm for benzene and halogenated ethylenes (both through non-resonant MPI processes).[34,35] Then, a fundamental beam of the Ti:sapphire laser was utilized in this study to examine the advantage of this technique for observing a molecular ion. However, it was difficult to observe a molecular ion at 800 nm under the optimized conditions used in this study. In fact, the fundamental beam (800 nm) was employed for dissociation of the protonated peptides formed by electrospray ionization (ESI).[36] Thus, moderate resonant two-photon ionization in the ultraviolet region would be more preferential, although further

studies would be necessary to conclude this discussion. It has been reported that the efficiency of non-resonant two-photon ionization can be improved significantly by optimizing the wavelength and decreasing the pulse width of the femtosecond laser (<100 fs).[32] Therefore, a tunable ultraviolet femtosecond laser, the wavelength of which can be optimized to reduce excess energy at around 250 nm, would be useful to understand the mechanism for non-resonant or nearly-resonant two-photon ionization in terms of observing a molecular ion.[37]

2.3.5. Limit of detection

Figure 2-7. shows a two-dimensional display obtained using the third harmonic emission (267 nm) at a larger pulse energy available (75 μJ). Because the signal intensity was increased and a molecular ion was observed for γ-HCH, an analytical curve was constructed and confirmed to be linear in a range of 0-12 ng/μL under present conditions. The limit of detection (LOD) was 68 pg/μL when the signal intensity was measured for a molecular ion (*m/z* = 290). The value was improved to 5.0 pg/μL when a fragment ion (*m/z* = 219) was measured. The rather poor detection limits compared with those reported for other organic compounds such as polycyclic aromatic hydrocarbons[23] can be attributed to inefficient non-resonant three-photon ionization and the efficient dissociation of a molecular ion to fragments.

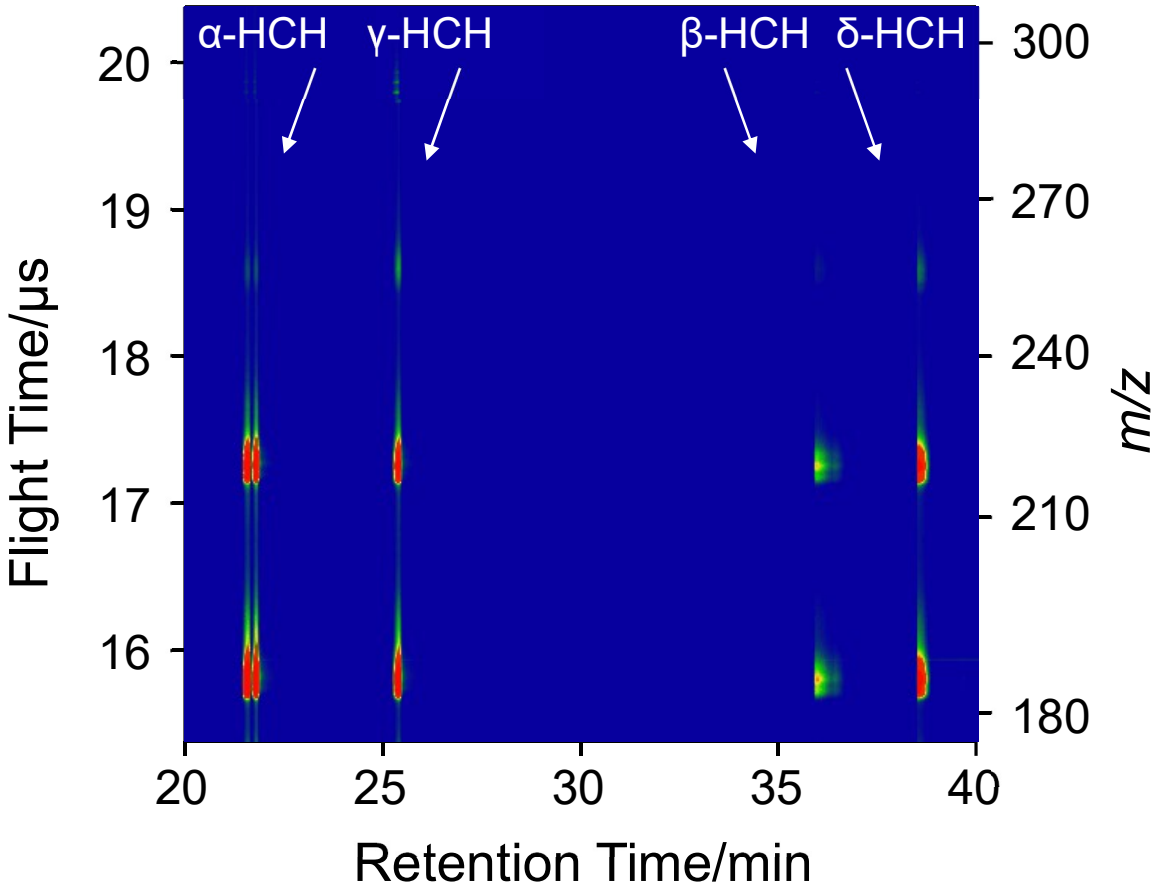

Fig. 2-7. Two-dimensional display for a sample mixture containing four isomers of α-, β-, γ, and δ-HCHs measured at 267 nm (75 μJ). The concentration of the analyte was 10 ng/mL for each isomer of HCH.

2.4. Conclusions

In this study, I report on the separation of some isomers and enantiomers of HCHs using a capillary column with a chiral stationary phase (PM-γ-CD) by GC. A molecular ion was

more clearly observed for the isomers of α- and γ-HCHs but was weak, even when a far-ultraviolet femtosecond laser (200 nm) was used for resonant two-photon ionization. This result can be explained by the efficient dissociation of neutral species such as HCl and HCl_2 from the molecular ion using data obtained by quantum chemical calculations. The isomers and enantiomers of the HCHs were separated by GC and their isotopomers were identified by MS on the two-dimensional display data, suggesting the potential advantage of this method for the comprehensive analysis of pesticides in the environment.

References

1. Bucheli, T.D.; Grüebler, F.C.; Müller, S.R.; Schwarzenbach, R.P. *Anal. Chem.* **1997**, *69*, 1569−1576.
2. Tsai, W.C.; Huang, S.D. *J. Chromatogr. A* **2009**, *1261*, 5171–5175.
3. Li, J.; Zhang, G.; Qi, S.; Li, X.; Peng, X. *Sci. Total Environ.* **2006**, *372*, 215–224.
4. Iwata, H.; Tanabe, S.; Ueda, K.; Tatsukawa, R. *Environ. Sci. Technol.* **1995**, *29*, 792–801.
5. Walker, K. *Environ. Sci. Technol.* **1999**, *33*, 4373–4378.
6. Simonich, S.L.; Hites, R.A. *Science* **1995**, *269*, 1851–1854.
7. Montgomery, J.H. Agrochemical Desk Reference, Environmental Data, Chelsea, MI, **1993**, 248–251.
8. Li, Y.; Bidleman, T.; Barrie, L.; McConnell, L. *Geophys. Res. Lett.* **1998**, *25*, 39–41.
9. Wilett, K.; Ulrich, E.; Hites, R. *Environ. Sci. Technol*. **1998**, *32*, 2197–2207.
10. Kutz, F. W.; Wood, P. H.; Bottimore, D. P. *Rev. Environ. Contam*. *Toxicol*. **1991**, *120*, 1–82.
11. Marrs, T.T.; Ballantyne, B. Pesticide Toxicology and International Regulation, John Wiley & Sons, Ltd, **2004**, 34
12. Pomes, A.; Rodriguez-Farre, E.; Sunol, C. *Dev. Brain Res.* **1993**, *73*, 85–90.
13. Cristol, S. *J. Am. Chem. Soc*. **1949**, *71*, 1894.
14. Faller, J.; Huhnerfuss, H.; Konig, W.; Krebber, R.; Ludwig, P. *Environ. Sci. Technol.* **1991**, *25*, 676–678.
15. Mössner, S.; Spraker, T.; Becker, P.; Ballschmiter, K. *Chemosphere*, **1992**, *24*, 1171–1180.
16. Vijgen, J.; Abhilash, P.; Li, Y.; Lal, F.; Forter, M.; Torres, J.; Singh, N.; Yunus, M.; Tian, C.; Schäffer, A. *Environ. Sci. Pollut. Res*. **2011**, *18*, 152–162.
17. Pinto, M.; Sontag, G.; Bernardino, R.; Noronha, J. *Microchem. J*. **2010**, *96*, 225–237.

18. Berger, M.; Loffler, D.; Ternes, T.; Heiniger, P.; Ricking, M. *Chemosphere*, **2016**, *150*, 219–226.

19. Barrek, S.; Cren-Olivé, C.; Wiest, L.; Baudot, R.; Arnaudguilhem, C.; Grenier-Loustalot, M. *Talanta*, **2009**, *79*, 712–722.

20. Xu, W.; Wang, X.; Cai, Z.: Analytical chemistry of the persistent organic pollutants identified in the Stockholm Convention: A review. *Anal. Chim. Acta*. **2013**, *790*, 1–13.

21. Trtić-Petrović, T.; Đorđević, J.; Dujaković, N.; Kumrić, K.; Vasiljević, T.; Laušević, M. *Anal. Bioanal. Chem.* **2010**, *397,* 2233–2243.

22. Bossi, R.; Vejrup, K.V.; Mogensen, B.B.; Asman, W.A.H. *J. Chromatogr. A* **2002**, *957,* 27–36.

23. Matsui, T.; Fukazawa, K.; Fujimoto, M.; Imasaka, T. *Anal. Sci.* **2012**, *28,* 445–450.

24. Hashiguchi, Y.; Zaitsu, S.; Imasaka, T. *Anal. Bioanal. Chem.***2013**, *405,* 7053–7059.

25. Matsumoto, J.; Saito, G.; Imasaka, T. *Anal. Sci*. **2002**, *18*, 567–570.

26. Matsumoto, J.; Nakano, B.; Imasaka, T. *Anal. Sci*. **2003**, *19,* 379–382.

27. Frisch, M.J., Trucks, G.W., Schlegel, H.B., Scuseria, G.E., Robb, M.A., Cheeseman, J.R., Scalmani, G., Barone, V., Mennucci, B., Petersson, G.A., Nakatsuji, H., Caricato, M., Li, X., Hratchian, H.P., Izmaylov, A.F., Bloino, J., Zheng, G., Sonnenberg, J.L., Hada, M., Ehara, M., Toyota, K., Fukuda, R., Hasegawa, J., Ishida, M., Nakajima, T., Honda, Y., Kitao, O., Nakai, H., Vreven, T., Montgomery, J.A., Jr., Peralta, J.E., Ogliaro, F., Bearpark, M., Heyd, J.J., Brothers, E., Kudin, K.N., Staroverov, V.N., Kobayashi, R., Normand, J., Raghavachari, K., Rendell, A., Burant, J.C., Iyengar, S.S., Tomasi, J., Cossi, M., Rega, N., Millam, J.M., Klene, M., Knox, J.E., Cross, J.B., Bakken, V., Adamo, C., Jaramillo, J., Gomperts, R., Stratmann, R.E., Yazyev, O., Austin, A.J., Cammi, R., Pomelli, C., Ochterski, J.W., Martin, R.L., Morokuma, K., Zakrzewski, V.G., Voth, G.A., Salvador, P., Dannenberg, J.J., Dapprich, S., Daniels, A.D., Farkas, Ö., Foresman, J.B., Ortiz, J.V., Cioslowski, J., Fox, D.J.: Gaussian 09, Revision D.01: Gaussian, Inc., Wallingford CT, **2009**

28. Dennington, R.; Keith, T.; Millam, J. Gauss View, Version 5, Semichem Inc., Shawnee Mission KS, **2009**

29. Harata, K. *Bull. Chem. Soc. Jpn.* **1987**, *60,* 2763–2767.

30. Lipkowitz, K.B.; Pearl, G.; Coner, B.; Peterson, M.A. *J. Am. Chem. Soc*. **1997**, *119,* 600-610.

31. Badea, S. L.; Vogt, C.; Gehre, M.; Fischer, A.; Danet, A. F.; Richnow, H. H. *Mass Spectrom.* **2011**, *25*, 1363-1372.

32. Kouno. H.; Imasaka, T. *Analyst* **2016**, *18*, 5274-5280.

33. http://webbook.nist.gov/cgi/cbook.cgi?ID=C319846&Units=SI&Mask=200#Mass-Spec

    http://webbook.nist.gov/cgi/cbook.cgi?ID=C319857&Units=SI&Mask=200#Mass-Spec

    http://webbook.nist.gov/cgi/cbook.cgi?ID=C58899&Units=SI&Mask=200#Mass-Spec

    http://webbook.nist.gov/cgi/cbook.cgi?ID=C319868&Units=SI&Mask=200#Mass-Spec

34. Castillejo, M.; Couris, S.; Koudoumas, E.; Martín, M. *Chem. Phys. Lett.* **1998**, *289,* 303–310.

35. Castillejo, M., Martín, M., Nalda, R. D., Couris, S., Koudoumas, E. *Chem. Phys. Lett.* **2002**, *353*, 295-303.

36. Kalcic, C. L., Gunaratne, T. C., Jones, A. D., Dantus, M., Reid, G. E. *J. Am. Chem. Soc.* **2009**, *131*, 940-942.

37. Hamachi, A., Okuno, T., Imasaka, T., Kida, Y., Imasaka, T. *Anal. Chem.* **2015**, *87*, 3027-3031.

Chapter 3 Determination of pesticides

3.1. Introduction

The use of pesticides, which have been in widespread use for a long time to increase the production of various crops, has increased rapidly during the 20th century. Most pesticides are toxic, not only to pests but also for humans. Numerous pesticides persist for a long time in the environment because they are highly stable, although some are no longer in use.[1-3] Many kinds of pesticides are widely spread in water, soil, and air. Due to their high toxicity and stability, several pesticides have been categorized as persistent organic pollutants (POPs) by the Stockholm Convention.[4,5] The concentration of pesticides in the environment is extremely low, while numerous other organic compounds are present at high concentrations.[6] In addition, many types of pesticides are present in agricultural products. Therefore, a sensitive as well as selective analytical method for the determination of pesticides, in conjunction with a simple pretreatment procedure prior to the measurement would be highly desirable.[7-11]

Several analytical methods are currently available for the determination of the pesticides. Liquid chromatography/mass spectrometry (LC/MS),[12,13] liquid chromatography/tandem mass spectrometry (LC/MS-MS),[14-17] and gas chromatography/mass spectrometry (GC/MS)[18,19] are the most popular analytical methods that have been reported. Recently, gas chromatography combined with multiphoton ionization time-of-flight mass spectrometry (GC/MPI/TOF-MS) using a femtosecond laser as the ionization source has been applied to the trace analysis of pesticides in an actual sample,[20,21] since this technique provides subfemtogram detection limits for organic compounds. In contrast to other ionization methods such as electron

ionization (EI), this technique can be used for the soft ionization of an organic molecule, which permits a molecular ion to be observed. In addition, the background signal arising from interfering substances can be significantly decreased by using a laser with an optimal wavelength for ionization.

Since the efficiency of ionization depends on the spectral properties of the analyte molecule, it is necessary to optimize the ionization conditions, such as the laser wavelength used for the pesticides to be examined. A variety of pesticides with complex chemical structures have been developed for use against highly resistant pests, which makes it more difficult to determine the optimal conditions. In most recent studies, the laser wavelength has been determined experimentally based on a trial-and-error approach. Enantiomers, in addition to several structural isomers of hexachlorocyclohexane (HCH), have recently been separated using a GC column with an optically-active stationary phase and then measured by MPI/TOF-MS.[22] In this study, a femtosecond laser emitting at 200 nm was used, and the molecular ion was more clearly observed than the case of the laser emitting at 267 nm through resonance-enhanced two-photon ionization (RE2PI), since they have strong absorption bands at 200 nm. Similar data have been reported for allergens in fragrances.[23] This approach using the laser emitting at 200 nm is useful for a more reliable identification of analytes. However, the optimal laser wavelength depends on the spectral property and then the chemical structure of the molecule. In practical trace analysis, the limit of detection (LOD) is determined by the background signal arising from interfering substances in the real sample. Therefore, it would be necessary to optimize the laser wavelength for all of the pesticides to be examined.

There are two major approaches for determining the optimal wavelength for ionization. One would involve the use of an ultraviolet (UV) laser for RE2PI (especially

for aromatic molecules), which increases the efficiency of ionization via the singlet excited state. When a laser with a pulse width of ca. 50 fs was used in a recent study, the efficiency of non-resonant two-photon ionization (NR2PI) reached a level that was nearly identical to that of RE2PI.[24] This approach can reduce the excess energy in the ionization, since the photon energy, i.e., the laser wavelength, can be adjusted to a half of the ionization energy, thus suppressing fragmentation and enhancing the signal of the molecular ion. For example, this technique has been utilized for observing a molecular ion derived from triacetone triperoxide, an explosive that is frequently used in terrorist attacks.[25] Another would be the use of a near-infrared (NIR) laser for non-resonant MPI. Although more than several photons are required for ionization, the efficiency can be improved by using a laser with a high peak power. When the molecular ion has no absorption band in the NIR region, fragmentation can be reduced and a molecular ion can be efficiently observed.[26-28] It is reported that a laser with a lower pulse energy and a shorter pulse width is preferential for observing a molecular ion and that a ring-shaped molecule is more stable against a linear molecule and is resistive against the fragmentation.[23,24,29-31] In addition, a linearly-polarized beam has been reported to be more useful to reduce the fragmentation against the circularly-polarized beam.[32] However, many types of pesticides have complicated chemical structures, and their ionization mechanisms have not yet been studied in detail. Thus, a guideline for observing a molecular ion should be examined at different wavelengths in order to achieve optimal ionization, which would also provide useful information regarding the mechanism for the ionization of a pesticide.

In this study, I measured two-dimensional displays against the retention time in GC and the mass/charge ratio (*m/z*) in MS for a sample mixture containing 51 pesticides and

calculated the LODs using femtosecond lasers emitting at 267, 400, and 800 nm as the ionization source in MS. The optimal wavelength for suppressing fragmentation was examined, and the results are compared and discussed based on spectral properties obtained by quantum chemical calculations to clarify the ionization mechanism. I also studied some exceptional cases for which additional rules were required to explain unexpected data. The present analytical technique was applied to the determination of pesticides in homogenized matrices derived from actual samples, and the results suggest that this technique has potential advantages for use in the trace analysis of the pesticides in agriculture products.

3.2. Experimental

3.2.1. Apparatus

The experimental apparatus used in the study was a combination of a commercially available GC instrument and a TOF-MS developed in this laboratory. Briefly, a GC (6890N, Agilent Technologies, Santa Clara, CA, USA) equipped with an auto injector (7683B, Agilent Technologies) was combined with a TOF-MS (HGK-1) that is commercially available from Hikari-GK, Fukuoka, Japan. The fundamental beam of a Ti:sapphire laser (800 nm, 1 kHz, 4 mJ, Elite, Coherent Co., Santa Clara, CA, USA) was converted into the second and third harmonic emissions and was used as the ionization source. The pulse energy available in this study was 220, 100, and 75 μJ at 800, 400, and 267 nm, the pulse width being 35, 37, and 62 fs at these wavelengths, respectively. The analytes were separated using an HP-5 column (a length of 30 m, a 0.25-mm inner diameter, a 0.25-μm film thickness). The temperature program of the GC oven was as

follows: initial temperature 70 °C held for 2 min, a rate of 20 °C/min to 150 °C, then 3 °C/min to 200 °C, followed by 8 °C/min to 280 °C and a hold of 10 min. The temperatures of the GC inlet port and of the transfer line between GC and MS were adjusted to 250 and 280 °C, respectively. The flow rate of helium, used as the carrier gas, was 1 mL/min. A 1-μL aliquot of sample solution was injected into the GC system. The pesticides in the molecular beam were ionized by focusing the femtosecond laser beam. The ions induced by 2PI/MPI were accelerated toward a flight tube and were detected by microchannel plates (F4655-11, Hamamatsu Photonics, Shizuoka, Japan). The signal was recorded using a digitizer (Acqiris AP240, Agilent Technologies), and the data were analyzed using a home-made software programed by Visual Basic. The two-dimensional GC/MS display was constructed using the ORIGIN software. The color scale in the picture was slightly modified to compensate for changes in the background and sensitivity using the LabVIEW software.

3.2.2. Reagents

A standard sample mixture containing 51 pesticides was purchased from Hayashi Pure Chemical Ind., Ltd, Osaka, Japan, the concentration of which was 20 μg/mL for each component. The chemical structures of those compounds are shown in Fig.3-1. The standard solution was diluted 10 fold (2 ng/μL) with acetone (analytical grade) supplied from Wako Pure Chemical Industries, Osaka, Japan.

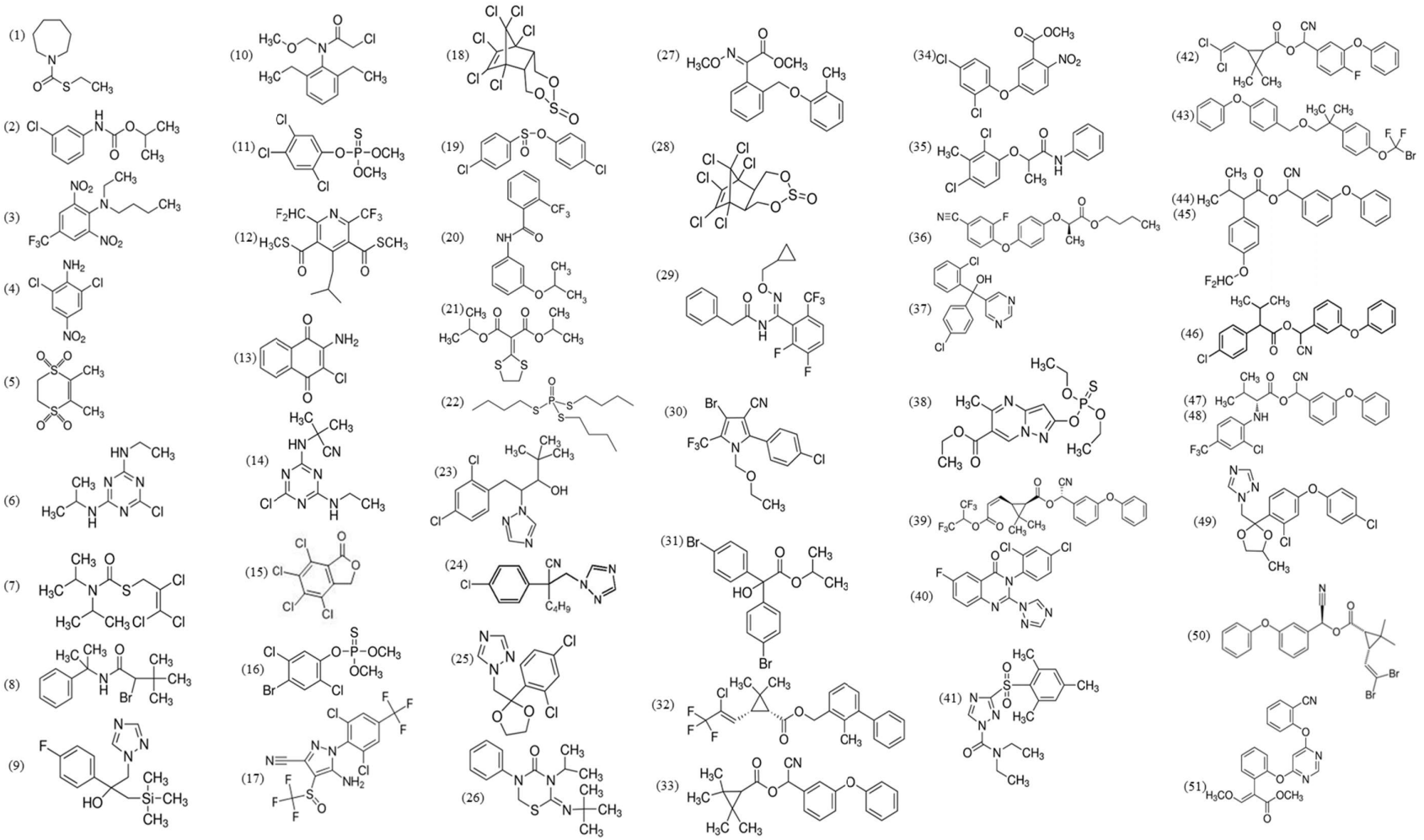

Fig. 3-1. The chemical structures of 51 pesticides.

3.2.3. Pretreatment procedure

A fruit (kabosu) and two vegetables (cucumber and pumpkin) that were examined in this study were purchased from a local supermarket in Fukuoka. The pretreatment procedure was performed by Koji Takahashi, Fukuoka Institute of Health and Environmental Sciences, as follows. The sample (20 g) in a tall 300-mL beaker was mixed with 100-mL of a 4:1 mixture of acetonitrile and water and was homogenized for 2 min. The solution was then passed through a glass-fiber filter (Advantec Toyo Kaisha, Ltd., Tokyo, Japan) to remove the fiber-like substances and was transferred to a separatory funnel (200 mL). After adding NaCl (10 g) and phosphate buffer (1 M, pH 7, 2 mL), the solution was horizontally shaken for 5 min. After phase separation, the acetonitrile layer was removed by a pipette and was then passed through a column containing anhydrous Na_2SO_4 (10 g). The solvent was removed by evaporation under reduced pressure at 40 °C using a rotary evaporator. A 2-mL solution comprised of a 3:1 mixture of acetonitrile and toluene was added to the residue and the resulting solution was loaded onto a mini-column (ENVI-Carb/NH_2, 400 mg/500 mg, 6 mL, Supelco, Bellefonte, PA, USA) conditioned using a 10-mL portion of the solvent mixture. The glassware was rinsed with a 2-mL portion of the same mixture of acetonitrile and toluene and was loaded onto the mini-column. This procedure was repeated three times. The analyte was eluted using the same solvent mixture (12 mL). The eluent was concentrated under reduced pressure in the rotary evaporator, and the residue was dissolved with acetone, transferred to a centrifuge tube, and was gently dried under a nitrogen gas flow. The residue was dissolved with acetone (1 mL) again and was used as a sample for GC analysis. Occasionally, the standard sample mixture of pesticides (2 ng/μL for each) was added to the above solution,

the final concentration being 20 pg/μL for each. The solution was stored in a refrigerator prior to the GC measurements.

3.2.4. Computational Methods

In order to find the optimum wavelength of the laser for each pesticide, quantum chemical calculations were carried out by Tomoko Imasaka, Department of Environmental Design, Kyushu University. Gaussian 09 program series package was used,[33] in an attempt to develop a further understanding of the ionization mechanism for the agricultural chemical compounds. Minimum geometries were obtained using the B3LYP method, based on density functional theory (DFT) with a cc-pVDZ basis set.[34,35] The harmonic frequencies were calculated in order to ensure an optimum geometry providing a global energy minimum. A vertical ionization energy was evaluated from the energy difference between the ground and ionic states. The lowest eighty singlet transition energies and the oscillator strengths were calculated using time-dependent DFT (TD-DFT),[36] and the predicted absorption spectra for a neutral species and a molecular ion were obtained by assuming a Gaussian profile with a half width at half maximum of 0.333 eV for each transition.

3.3. Results and discussion

3.3.1. Two-dimensional display and limits of detection

A two-dimensional display measured at 267 nm for a standard sample mixture containing 51 pesticides is shown in Fig. 3-2. Numerous signals were observed in the display. The total ion chromatogram shown at the top of the figure suggests complete separation of the components by GC. The mass spectrum can be extracted from the data measured at the retention time, at which a specific pesticide listed in Table 3-1 appears.

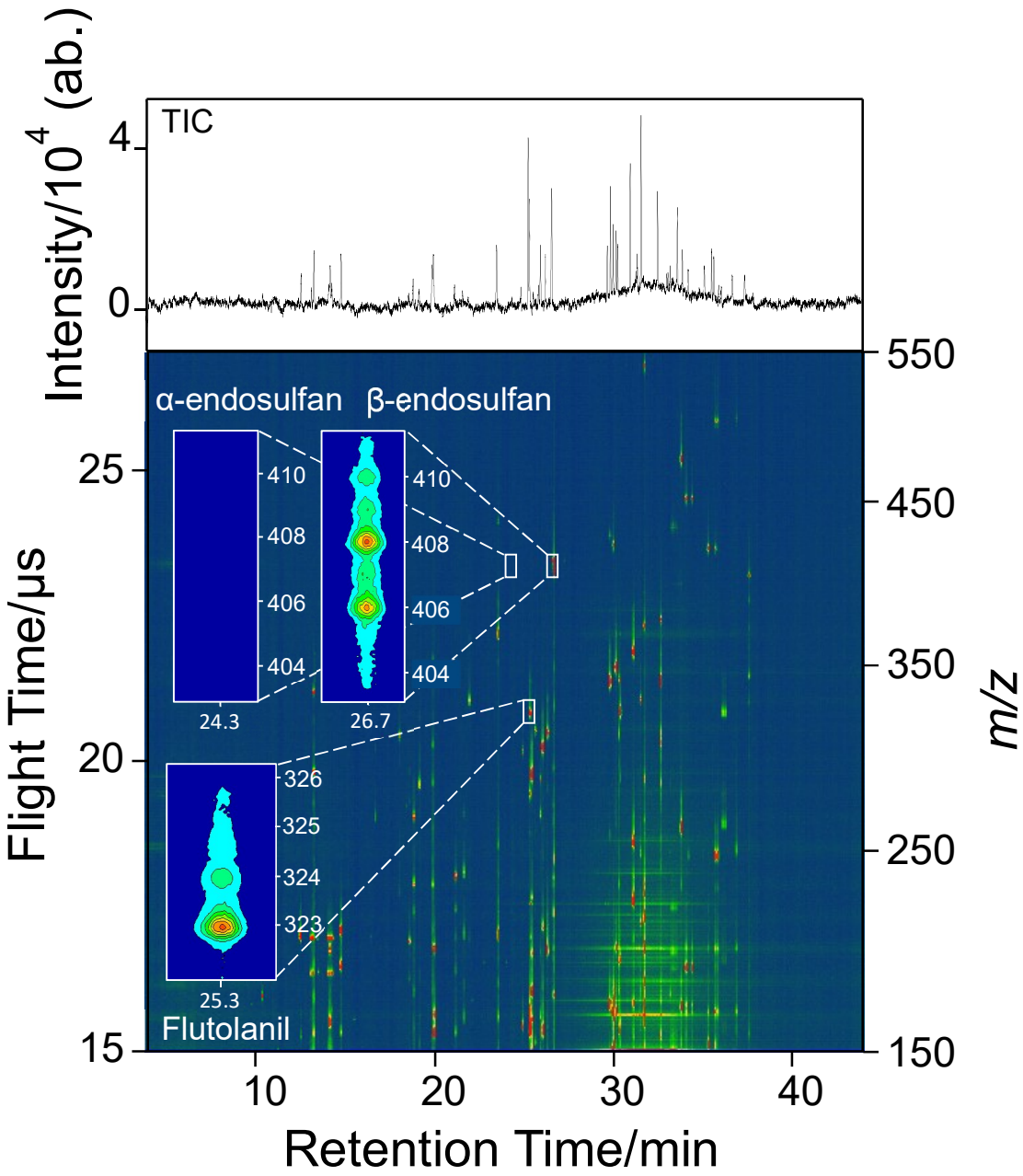

Fig. 3-2. Two-dimensional display of a standard sample mixture containing 51 pesticides measured at 267 nm. Inserts show expanded views of the regions where flutolanil, α-endosulfan, and β-endosulfan appear.

Table 3-1. Limit of detections (LODs) obtained using GC/MPI/TOFMS at 267, 400, and 800 nm for a standard sample mixture of pesticides.

Name of pesticide (Elution Order)	LOD at 267 nm (pg/μL)		LOD at 400 nm (pg/μL)		LOD at 800 nm (pg/μL)		Group
	M^+	F^+	M^+	F^+	M^+	F^+	
Molinate (1)	36	N.D.	5.4	6.8	1.41	2.8	C-1
Chlorpropham (2)	9.9	240	8.7	36	4.4	5.4	A-1
Benfluralin (3)	40	50	9.4	7.4	6.5	14	A-2
Dichloran (4)	N.D.	N.D.	N.D.	156	N.D.	82	E-1
Dimethipin (5)	40	40	18	34	4.4	2.2	E-2
Atrazine (6)	10	34	22	35	3.4	21	C-2
Triallate (7)	N.D.	230	380	43	78	11	E-3
Bromobutide (8)	189	510	67	195	31	37	C-3
Simeconazole (9)	N.D.	93	240	58	34	33	E-4
Alachlor (10)	75	88	28	35	32	27	D-1
Fenchlorphos (11)	N.D.	35	280	25	178	8.6	D-2
Dithiopyr (12)	N.D.	172	N.D.	62	N.D.	29	D-3
Quinoclamine (13)	29	17	6.1	3.4	3.2	15	A-3
Cyanazine (14)	47	280	29	56	11.2	54	C-4
Fthalide (15)	840	150	60	22	17	87	E-5
Bromophos Methyl (16)	N.D.	120	270	14	240	11.4	D-4
Fipronil (17)	340	54	N.D.	20	N.D.	430	E-6
α-Endosulfan (18)	N.D.	N.D.	N.D.	N.D.	N.D.	121	E-7
Chlorefenson (19)	146	96	80	36	40	26	A-4
Flutolanil (20)	11	5.8	5.8	5.9	6.4	11.7	A-5
Isoprothiolane (21)	7.2	31	4.5	38	9.8	54	A-6
DEF (Tribufos) (22)	78	260	58	49	48	25	D-5
Dicrobutrazole (23)	N.D.	N.D.	N.D.	N.D.	N.D.	N.D.	E-8
Myclobutanil (24)	200	220	149	30	44	18	E-9
Azaconazole (25)	N.D.	N.D.	N.D.	N.D.	N.D.	N.D.	E-10
Buprofezin (26)	22	65	15	25	22	7.1	A-7

Kresoxim methyl (27)	38	57	37	25	20	15	B-1
β-Endosulfan (28)	11.8	160	60	174	70	58	E-11
Cyflufenamid (29)	N.D.	N.D.	N.D.	N.D.	N.D.	N.D.	B-2
Chlorfenapyr (30)	N.D.	N.D.	N.D.	N.D.	N.D.	N.D.	B-3
Bromopropylate (31)	290	24	N.D.	16	N.D.	21	B-4
Bifenthrin (32)	106	15	N.D.	9.0	N.D.	3.6	A-8
Fenpropathrin (33)	12.7	63	51	84	72	37	B-5
Bifenox (34)	67	96	30	91	18	380	A-9
Clomeprop (35)	16	88	15	42	12	14	A-10
Cyhalofop-butyl (36)	6.1	24	39	41	26	16	A-11
Fenarimol (37)	75	96	52	63	39	23	C-5
Pyrazophos (38)	N.D.	N.D.	46	62	16	18	D-6
Acrinathrin (39)	8.6	6.1	N.D.	N.D.	N.D.	N.D.	A-12
Fluquinconazole (40)	8.2	6.8	24	12.5	470	15	B-6
Cafenstrole (41)	350	220	N.D.	95	N.D.	30	E-12
Cyfluthrin 1-4 (42)	310	220	N.D.	32	N.D.	42	A-13
Halfenprox (43)	38	23	N.D.	23	N.D.	13	A-14
Flucythrinate 1 (44)	56	45	N.D.	59	N.D.	60	A-15
Flucythrinate 2 (45)	55	67	N.D.	59	N.D.	60	A-16
Fenvalerate 1-2 (46)	44	61	N.D.	90	N.D.	44	A-17
Fluvalinate 1 (47)	78	40	N.D.	39	N.D.	44	A-18
Fluvalinate 2 (48)	9.2	6.6	N.D.	39	N.D.	44	A-19
Difenoconazole 1-2 (49)	N.D.	5.3	N.D.	34	N.D.	71	E-13
Deltamethrin (50)	380	120	N.D.	51	N.D.	70	B-7
Azoxystrobin (51)	52	148	100	37	62	32	B-8

A molecular ion was clearly observed as a major peak for many pesticides. As shown in the expanded view, a series of isotopomers, i.e., $[M]^+$, $[M+1]^+$, and $[M+2]^+$, which contains zero, one, or two ^{13}C atoms in a molecule, was observed for flutolanil (20), an

agricultural fungicide. The fragment ions can also be assigned from the *m/z* values. These results suggest that the separation and resolution of the GC and MS are sufficient for these samples and that the method is applicable to these types of analyses. It should be noted that, in most cases, the pesticides in the sample contain aromatic rings as shown in Figure 3-1 and, therefore, can be efficiently ionized through RE2PI. A two-dimensional display measured at 400 nm is shown in Figure 3-3. As shown in the expanded view, molecular ions for alachlor (10) and isoprothioane (21) can be clearly observed. The data collected at 800 nm are shown in Figure 3-4. As shown in the insert, an $[M+2]^+$ signal is more clearly observed for dimethipin (5) than molinate (1), due to the larger number of sulfur atoms in the molecule; there are two major isotopes for sulfur, i.e., ^{32}S and ^{34}S. Although many signal peaks were observed, due to the larger pulse energy of the laser at longer wavelengths, the intensities of the signals, especially for high *m/z* values, would be relatively low. These results suggest that fragmentation is more efficient in the visible (VIS) and near-infrared (NIR) regions.

Table 3-1 shows the LODs for the pesticides measured at 267, 400, and 800 nm using the signals arising from molecular and fragment ions. Molecular ions were observed for 38 pesticides at 267 nm, which is in contrast to 30 pesticides at 400 and 800 nm. On the other hand, the fragment ions were observed as major signals for 45 and 46 compounds at 400 and 800 nm, respectively, which is slightly larger than the value of 43 at 267 nm. As a rule of thumb, a laser emitting at 267 nm appears to be slightly better for observing a molecular ion than the laser emitting at 400 and 800 nm. The lowest LODs among the three data sets measured at the different wavelengths are marked in Table 3-1. Compounds that elute earlier (smaller and nonpolar compounds) appear to be preferentially ionized at 800 nm. Only a limited number of compounds appear to be ionized at 400 nm. On the

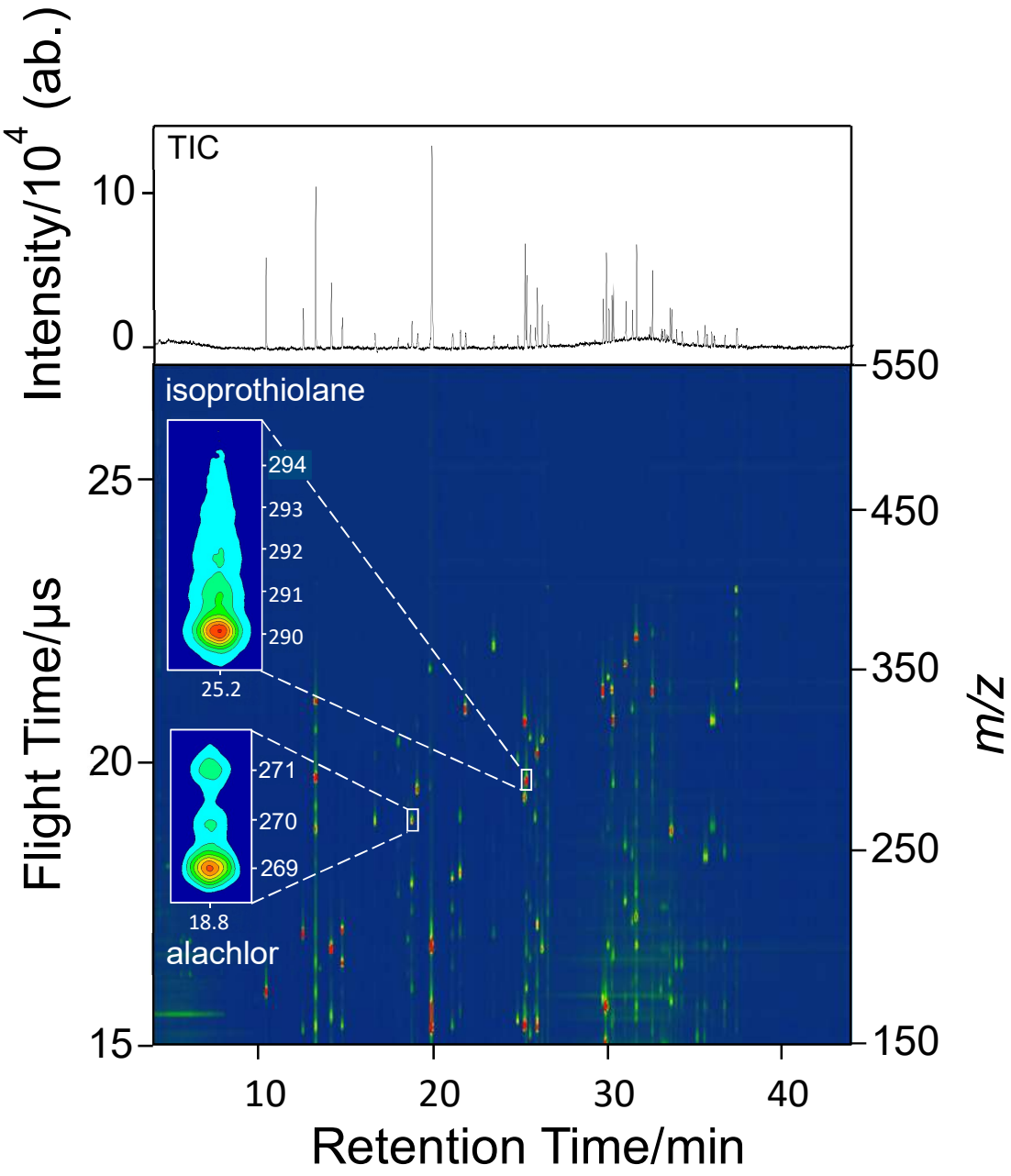

Fig. 3-3. Two-dimensional display of a standard sample mixture containing 51 pesticides measured at 400 nm. Inserts show expanded views of the regions where alachlor and isoprothiolane appear.

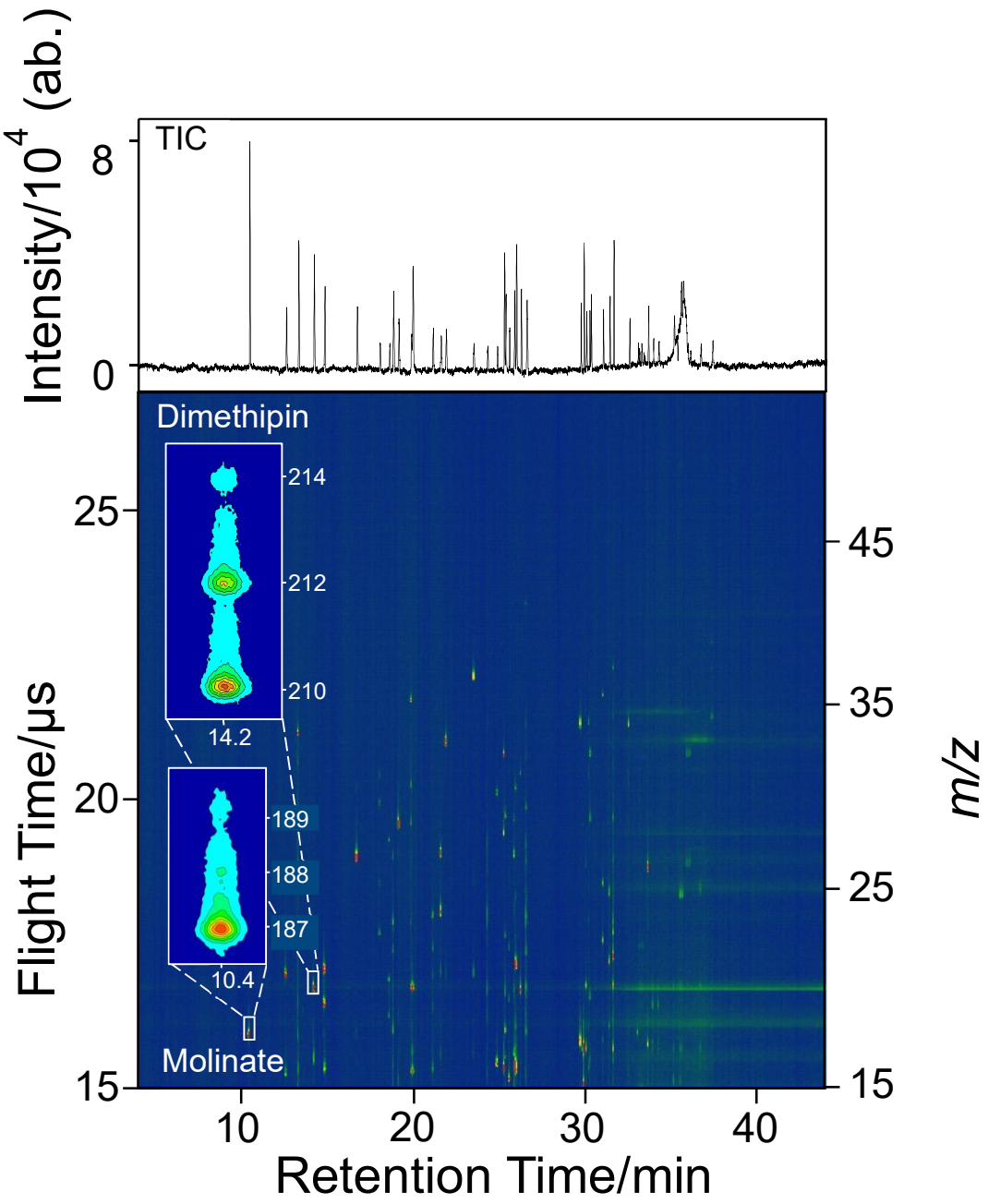

Fig. 3-4. Two-dimensional display of a standard sample mixture containing 51 pesticides measured at 800 nm. Inserts show expanded views of the regions where molinate and dimethipin appear.

other hand, compounds that elute later (larger and polar compounds) are more extensively ionized at 267 nm.

3.3.2. Optimum wavelength for ionization

Absorption spectra were calculated for all the pesticides in both neutral and ionic forms, in addition to other spectral parameters, including excitation and ionization energies based on quantum chemical calculation. The results are shown in Fig. S-1, which were used for studies related to the ionization mechanism in the following subsections, where the pesticides were tentatively grouped into five categories (Groups A- E).

3.3.2.1 Optimum both at 267 and 800 nm (Group A)

When the neutral form of the pesticide has an absorption band at 267 nm, the molecule can be ionized through efficient RE2PI. In addition, when the molecular ion has no absorption band at 800 nm, the molecule can be ionized through MPI with a minimum excess energy and remains as a molecular ion, since it does not absorb additional photons for dissociation. In this case, the pesticide molecule would be predicted to be efficiently ionized and provide a molecular ion, the value for the LOD being low both at 267 and 800 nm. Flutolanil (20) represents a typical compound of this group. This molecule can be efficiently ionized, and the LODs shown in Table 3-1 were found to be 11 and 6.4 pg/μL at 267 and 800 nm, respectively. Clomeprop (35) represents a similar example. These aromatic molecules have low LODs at 267 nm (16 pg/μL), due to small excess energies in 2PI. It has been reported that fragmentation is minimal at ≤ 1 eV and was more significant at >3 eV.[24] The situation is nearly identical for aromatic molecules such as quinoclamine (13) and non-aromatic molecules such as isoprothiolane (21) as well. Other

molecules such as cyhalofop-buthyl (36), chlorpropham (2), buprofezin (26), benfluralin (3), bifenox (34), and chlorefenson (19) can also be classified in this category. Although other molecules such as acrinathrin (39), halfenprox (43), flucythrinate (44/45), fenvalerate (46), fluvalinate (47/48), bifenthrin (32), and cyfluthrin (42) have reasonable LODs in the ionization at 267 nm, it was more difficult to detect them by ionization at 800 nm in MS, even though the molecular ions had either no or a small absorption band at 800 nm in the calculated absorption spectrum. It is, at present, difficult to explain the above findings with confidence. However, these molecules have strong absorption bands in the region above 1000 nm, suggesting a considerable degree of molar absorptivity in the actual absorption spectrum, due to high vibrational levels on the excited electronic state of the molecular ion, since these molecules have a long/large side chain and then numerous low-frequency vibrational modes (see the chemical structures shown in Figure 3-1). Note that the calculated spectrum was made by assuming a spectral bandwidth of 0.333 eV for all the electronic transitions (see the section of Computational Method) and by neglecting the Franck Condon factors for individual vibrational modes. Accordingly, the molecular ion would actually absorb the photons at 800 nm, which then undergoes dissociation to form fragments.

3.3.2.2 Optimum at 267 nm but not at 800 nm (Group B)

Fluquinconazole (40), a fungicide that functions as a sterol demethylation inhibitor, has an absorption band at 267 nm (3.92×10^4 $M^{-1}cm^{-1}$), and the molecular ion has an absorption band at 800 nm (0.25×10^4 $M^{-1}cm^{-1}$). The LOD was determined to be 8.2 pg/μL at 267 nm, which is a lower value (470 pg/μL) than that obtained at 800 nm. The LODs observed using the fragment ions were 6.8 pg/μL at 267 nm and 15 pg/μL at 800 nm.

Then, the poor LOD observed at 800 nm using the molecular ion can be attributed to the absorption of an additional NIR photon from the ionized state. It should also be noted that only fragment ions were observed in EI-MS, as shown in the figures cited in Table 3-2. To be easier to understand, the mass spectra of EI-MS are also cited in Fig.S-2. On the other hand, a molecular ion can be observed by optimizing the laser wavelength in photoionization, suggesting that the present technique has a distinct advantage over EI-MS and would be useful for more reliable analyses and for reducing background arising from interfering substances in the sample. Other molecules such as fenpropathrin (33), azozystrobin (51), kresoxim methyl (27) can be classified in this category. As expected, it was difficult to determine chlorfenapyr (30), bromopropylate (31), deltamethrin (50), and cyflufenamid (29) using the laser emitting at 800 nm. However, it was also difficult to measure these compounds even using the laser emitting at 267 nm, although they have absorption bands in this spectral region. These exceptions are likely due to the presence of bromine atoms and a cyclopropyl group in the molecule, which are dissociative or reactive and form small fragments.

Table 3-2. Source of the mass spectrum of the pesticides measured by electron ionization (70 eV).

Name of Pesticide	Data sources
Molinate (1)	http://webbook.nist.gov/cgi/cbook.cgi?ID=C2212671&Mask=200
Chlorpropham (2)	http://webbook.nist.gov/cgi/cbook.cgi?ID=C101213&Mask=200
Benfluralin (3)	http://webbook.nist.gov/cgi/cbook.cgi?ID=C1861401&Mask=200
Dichloran (4)	http://webbook.nist.gov/cgi/inchi?ID=C99309&Mask=200
Dimethipin (5)	http://webbook.nist.gov/cgi/cbook.cgi?ID=C55290647&Mask=200
Atrazine (6)	http://webbook.nist.gov/cgi/cbook.cgi?ID=C1912249&Mask=200
Triallate (7)	http://webbook.nist.gov/cgi/cbook.cgi?ID=C2303175&Mask=200
Bromobutide (8)	http://webbook.nist.gov/cgi/cbook.cgi?ID=C74712199&Mask=200

Simeconazole (9)	https://pubchem.ncbi.nlm.nih.gov/compound/Simeconazole#section=Spectral-Properties
Alachlor (10)	http://webbook.nist.gov/cgi/cbook.cgi?ID=C15972608&Mask=200
Fenchlorphos (11)	http://webbook.nist.gov/cgi/cbook.cgi?ID=C299843&Mask=200
Dithiopyr (12)	https://pubchem.ncbi.nlm.nih.gov/compound/Dithiopyr#section=Kovats-Retention-Index
Quinoclamine (13)	http://webbook.nist.gov/cgi/cbook.cgi?ID=C2797515&Mask=200
Cyanazine (14)	http://webbook.nist.gov/cgi/cbook.cgi?ID=C21725462&Mask=200
Fthalide (15)	http://webbook.nist.gov/cgi/cbook.cgi?ID=C27355222&Mask=200
Bromophos Methyl (16)	http://webbook.nist.gov/cgi/cbook.cgi?ID=C2104963&Mask=200
Fipronil (17)	https://pubchem.ncbi.nlm.nih.gov/compound/fipronil#section=Top
α-Endosulfan (18)	http://webbook.nist.gov/cgi/cbook.cgi?ID=C959988&Mask=200
Chlorefenson (19)	http://webbook.nist.gov/cgi/inchi?ID=C80331&Mask=200
Flutolanil (20)	http://webbook.nist.gov/cgi/cbook.cgi?ID=C66332965&Mask=200
Isoprothiolane (21)	http://webbook.nist.gov/cgi/cbook.cgi?ID=C50512351&Mask=200
DEF (Tribufos) (22)	http://webbook.nist.gov/cgi/cbook.cgi?ID=C78488&Mask=200
Dicrobutrazole (23)	http://webbook.nist.gov/cgi/cbook.cgi?ID=C75736333&Mask=200
Myclobutanil (24)	https://pubchem.ncbi.nlm.nih.gov/compound/myclobutanil#section=Spectral-Properties
Azaconazole (25)	http://www.massbank.jp/jsp/Dispatcher.jsp?type=disp&id=MSJ01062&site=24
Buprofezin (26)	http://webbook.nist.gov/cgi/cbook.cgi?ID=C69327760&Mask=200
Kresoxim methyl (27)	http://webbook.nist.gov/cgi/cbook.cgi?ID=C143390890&Mask=200
β-Endosulfan (28)	http://webbook.nist.gov/cgi/cbook.cgi?ID=C33213659&Mask=200
Cyflufenamid (29)	Chinese Journal of Magnetic Resonance, 2016, 33(1): 142-152
Chlorfenapyr (30)	http://webbook.nist.gov/cgi/cbook.cgi?ID=C122453730&Mask=200
Bromopropylate (31)	https://pubchem.ncbi.nlm.nih.gov/compound/Bromopropylate#section=GC-MS
Bifenthrin (32)	https://pubchem.ncbi.nlm.nih.gov/compound/5281872#section=Spectral-Properties

Fenpropathrin (33)	http://webbook.nist.gov/cgi/cbook.cgi?ID=C39515418&Mask=200
Bifenox (34)	http://webbook.nist.gov/cgi/inchi?ID=C42576023&Mask=200
Clomeprop (35)	Korean Journal of Environmental Agriculture, 2012, 31(2): 157-163
Cyhalofop-butyl (36)	Bulletin of the Nagano Research Institute for Health and Pollution, 2000, 22(3):17-21
Fenarimol (37)	http://webbook.nist.gov/cgi/cbook.cgi?ID=C60168889&Mask=200
Pyrazophos (38)	http://webbook.nist.gov/cgi/cbook.cgi?ID=C13457186&Mask=200
Acrinathrin (39)	i. http://www.massbank.jp/jsp/Dispatcher.jsp?type=disp&id=MSJ01060&site=24 ii. Analytical Sciences, 1997, 13(5): 817-819
Fluquinconazole (40)	Biomedical Chromatography, 2014, 28(6): 774-781
Cafenstrole (41)	Not availalbe
Cyfluthrin (42)	http://webbook.nist.gov/cgi/cbook.cgi?ID=C68359375&Mask=200
Halfenprox (43)	http://webbook.nist.gov/cgi/inchi?ID=C111872583&Mask=200
Flucythrinate (44/45)	http://www.restek.fr/compound/view/70124-77-5/Flucythrinate%201
Fenvalerate (46)	http://webbook.nist.gov/cgi/cbook.cgi?ID=C51630581&Mask=200
Fluvalinate (47/48)	http://webbook.nist.gov/cgi/inchi?ID=C69409945&Mask=200
Difenoconazole (49)	http://webbook.nist.gov/cgi/cbook.cgi?ID=C119446683&Mask=200
Deltamethrin (50)	http://webbook.nist.gov/cgi/cbook.cgi?ID=C52918635&Mask=200
Azoxystrobin (51)	http://webbook.nist.gov/cgi/cbook.cgi?ID=C131860338&Mask=200

3.3.2.3 Optimum at 800 nm but not at 267 nm (Group C)

Molinate (1), a herbicide used to control water grass in rice, which has no absorption band both at 267 and 800 nm is a typical example of this category. It can, however, be ionized through NR2PI at 267 nm. As expected, it had a low LOD value (1.41 pg/μL) when the laser emitting at 800 nm was employed. This suggests that using the laser emitting at 800 nm is advisable when the molecular ion has no absorption band at the laser wavelength. On the other hand, the LOD value was moderate (36 pg/μL) at 267 nm. A similar situation was observed for atrazine (6) and cyanazine (14), both of which

provided low LODs at 800 nm and low/moderate LODs at 267 nm. These data suggest that the molecules can be efficiently ionized through NR2PI when the laser pulse width is reduced to ca. 50 fs, as reported previously.[24] Fenarimol (37) and bromobutide (8) can also be classified in this category.

3.3.2.4 Not optimum both at 267 and 800 nm (Group D)

Dithiopyr (12), a herbicide developed for selective weed control in turf and ornamental grasses, has no or a small absorption band at 267 nm but the molecular ion has an absorption band at around 800 nm. For this reason, it was difficult to detect the molecular ion at a concentration of 20 pg/μL. Other compounds such as fenchlorphos (11), bromophos methyl (16), in addition to pyrazophos (38) with a bulky side chain, DEF (tribufos) (22) with long chains, and alachlor (10) with flexible chains, have rather poor LODs, as expected. Fragmentation would be accelerated by associating with the low frequency modes of the bully/long/flexible side chain, the trend of which has been reported in the reference.[23]

3.3.2.5 Miscellaneous molecules (Group E)

There are several compounds that cannot be explained from the rules described above. For example, dichloran (4) is a simple molecule with no long/flexible side chain and has a strong absorption band at 267 nm (3.9×10^3 $M^{-1}cm^{-1}$) and a small excess energy (0.8 eV) at 267 nm. It is, however, difficult to observe any signal at this concentration. In addition, the molecular ion has no absorption band at around 800 nm and is predicted to remain in MS. However, only fragment ions can be observed when the molecules are ionized at 800 nm. In EI-MS, a molecular ion can be observed, although the fragment

ions are observed as major ions. This is the only case where a molecular ion can be observed not in 2PI/MPI-MS but in EI-MS. No reasonable explanation can be provided for this, based on the findings reported herein. However, it is well known that this molecule can form an intra-molecular charge-transfer complex due to $–NH_2$ and NO_2 functional groups combined at the para-position of the aromatic ring, which would play an important role in the photoionization process. Similar data have been observed for an intra-molecular charge-transfer molecule of *p*-nitroaniline, in which fragmentation has been reported to be more significant at higher pulse energies (0.1→0.6 mJ) and longer pulse widths (0.1→5 ps) at 790 nm.[37]

Other mysterious molecules are the α- and β-endosulfan isomers (18) (28). The retention times are very different from each other due to the different chemical structures of the isomers (*cf.* Fig. 3-2) and then their different physical properties such as polarity that determines the melting point (α isomer, 109.28 ºC; β isomer, 213.28 ºC). The spectral properties of the molecules are, however, very similar as shown in Figure S-1 and these molecules would be expected to be ionized through NR2PI at 267 nm. It should be noted that measuring α-endosulfan was difficult by ionizations at 267 and 800 nm, which is in contrast to β-endosulfan (the LODs are 11.8 and 70 pg/μL at 267 and 800 nm, respectively) (see the insert of Fig. 3-2). Note that the major ion observed at 267 nm was a molecular ion. On the other hand, no significant difference is observed between α- and β-endosulfans in the mass spectrum obtained by EI, although the intensities of the molecular ions are much smaller than those of the fragment ions.

Other interesting compounds include molecules that contain a functional group of 1,2,4-triazole, i.e., azaconazole (25), difenoconazole (49), dicrobutrazole (23), and cafenstrole (41). It is difficult even to measure these compounds, although they have a

small leading-edge absorption band at the longer wavelength side of the absorption spectrum at around 267 nm and the molecular ion does not have a strong absorption band at around 800 nm. Other molecules that can be grouped in this category would be simeconazole (9), fipronil (17), and myclobutanil (24). These molecules seldom provide a molecular ion in EI-MS. It should be noted that these molecules all contain a strained functional group or a flexible/bulky side chain. It would be predicted that this type of molecule would be more difficult to detect, due to a large distortion and the small barrier for dissociation. Note that fluquinconazole (40), with no side chain, provides a molecular ion efficiently at 267 nm (see Section 3.3.2.2).

There are a few other exceptional cases, which cannot be explained by the rules reported to date. For example, fthalide (15) and triallate (7) have a strong absorption band at around 267 nm but the LOD values were poor (830 pg/μL and ND). On the other hand, the LOD calculated from the signal of a molecule ion was very low for dimethipin (5) (4 pg/μL) at 800 nm (see Section 3.3.1 and Fig. 3-4), although it has a strong absorption band at 800 nm for the molecular ion. Further investigations will be necessary for arriving at a coherent explanation for these compounds.

3.3.3 Pesticides in an actual sample

In this study, samples extracted from a fruit (kabosu) and vegetables (cucumber and pumpkin) were measured at 267 and 800 nm. A two-dimensional display obtained for the sample extracted from kabosu and measured at 267 nm is shown in Fig. 3-5. (a). Numerous signal spots appeared in the data. However, none of the signals could be assigned to the pesticides examined in this study. The same findings were obtained for the vegetable samples. These results suggest that fruit and vegetables obtained in a

supermarket are not contaminated by the pesticides. To study validity of the method, the standard mixture of pesticides was added to the solution extracted from actual samples. Many additional signals appeared in the two-dimensional display, in addition to signals arising from contaminants, as shown in Fig. 3-5. (b). These signals can be assigned to the pesticides by comparing the data with those obtained in Fig. 3-2. The same samples were also measured using the NIR laser. A pattern similar to that shown in Fig. 3-5. was observed in the two-dimensional display, as shown in Fig. 3-6. A careful examination of the data shown in Figs. 3-5. and 3-6. indicated that the larger ions such as the molecular ions derived from larger pesticides that elute later in GC were more pronounced when the UV laser was used (see the area specified by a tilted elliptical circle with a broken line). This result suggests that 2PI in the UV is superior to MPI in the NIR for more sensitive as well as reliable determination of the pesticides.

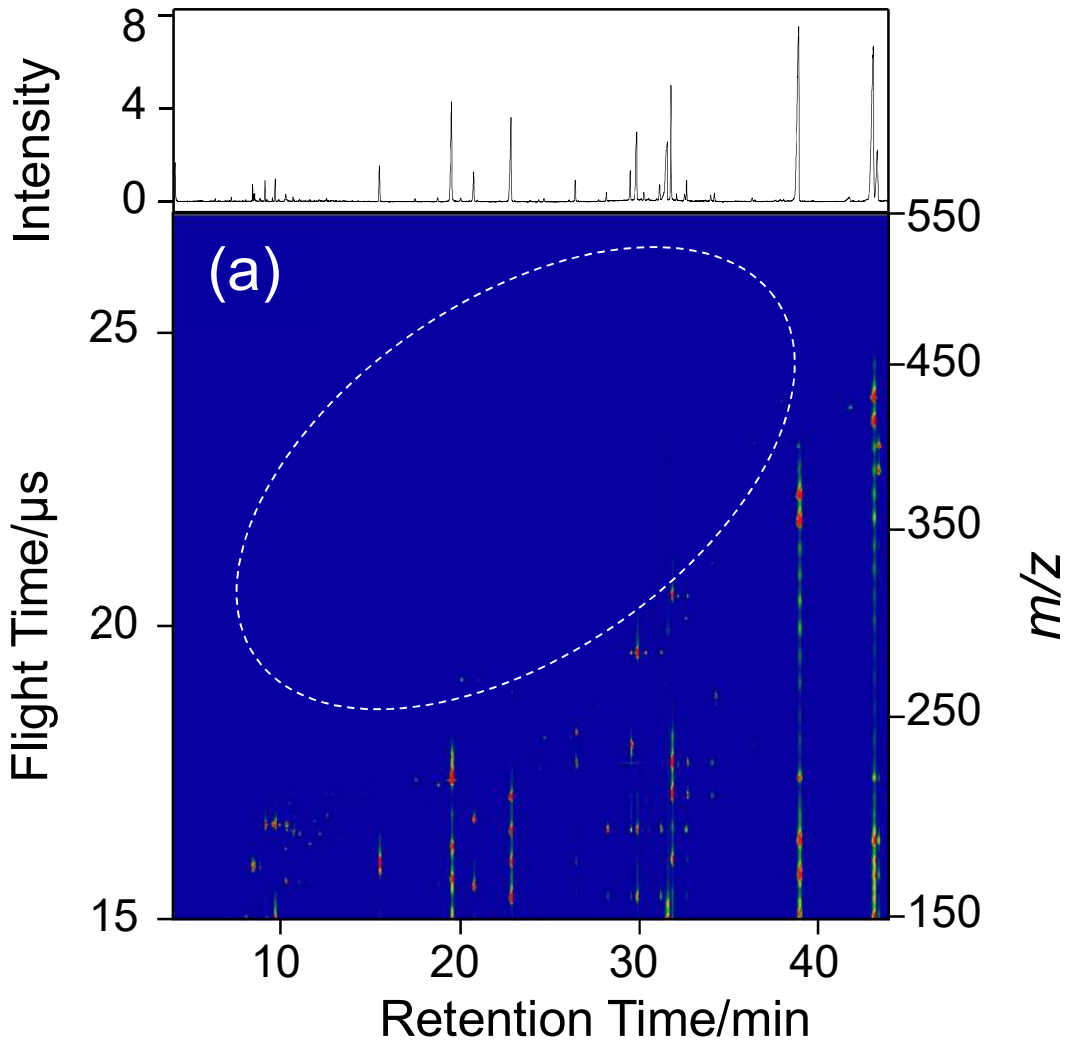
Intensity
8
4
0
(a)
Flight Time/μs
25
20
15
10
20
30
40
Retention Time/min
550
450
350
250
150
m/z

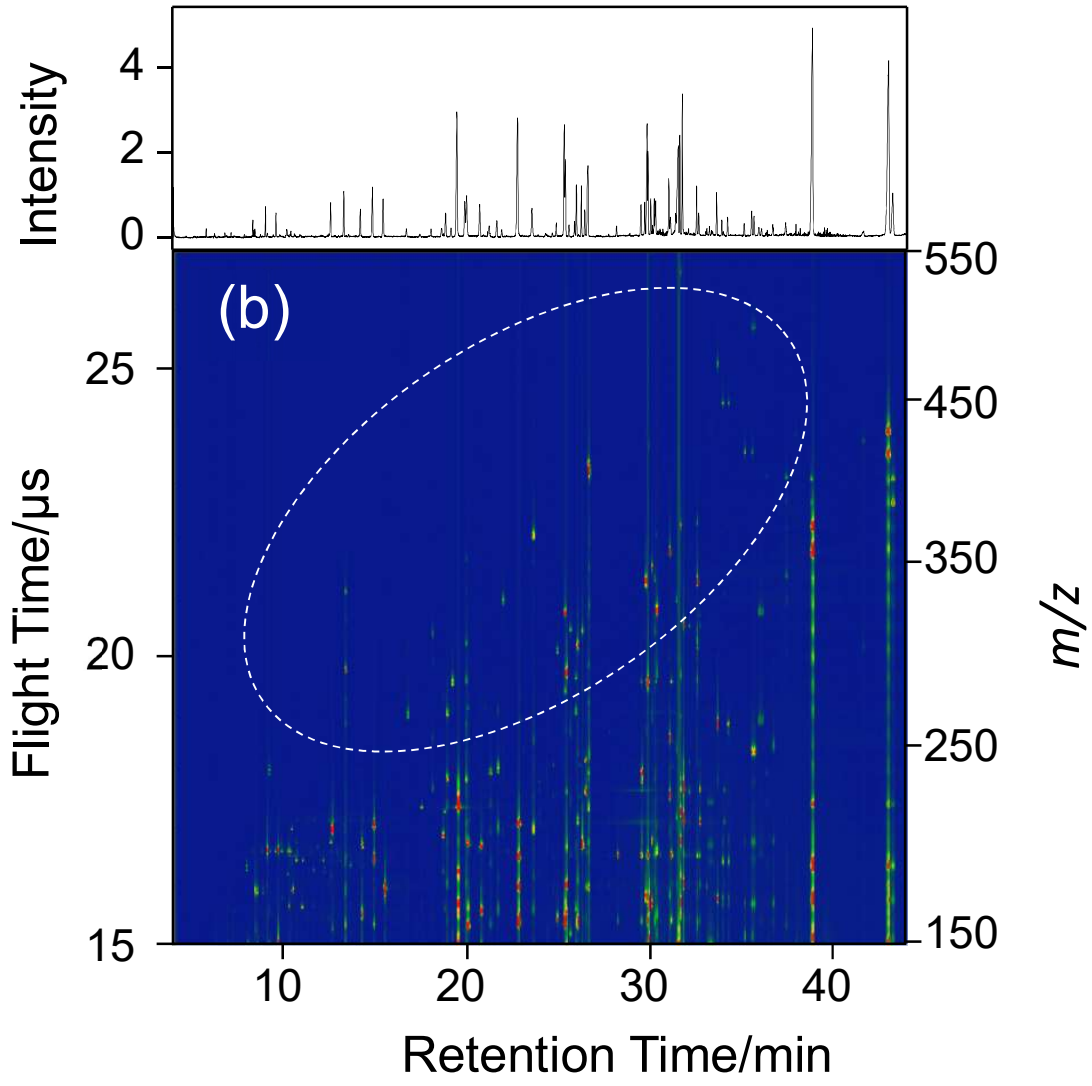

Fig. 3-5. Two-dimensional display measured at 267 nm. (a) kabosu (b) kabosu and 51 pesticides. A tilted elliptical circle (broken line) is drawn as a guide line to provide a visual check of the locations of the data spots.

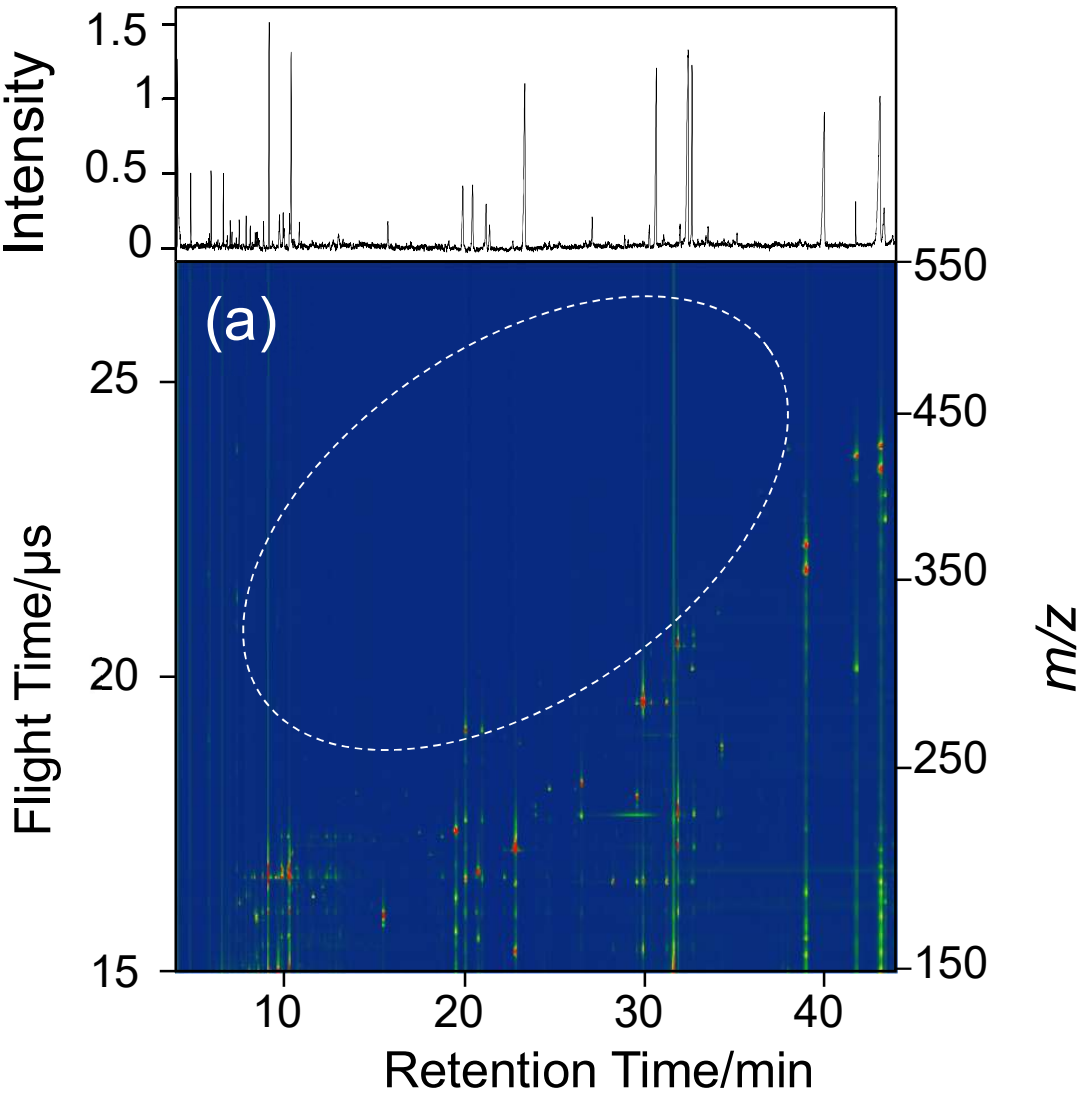
Intensity
1.5
1
0.5
0
(a)
Flight Time/μs
25
20
15
10
20
30
40
Retention Time/min
550
450
350
250
150
m/z

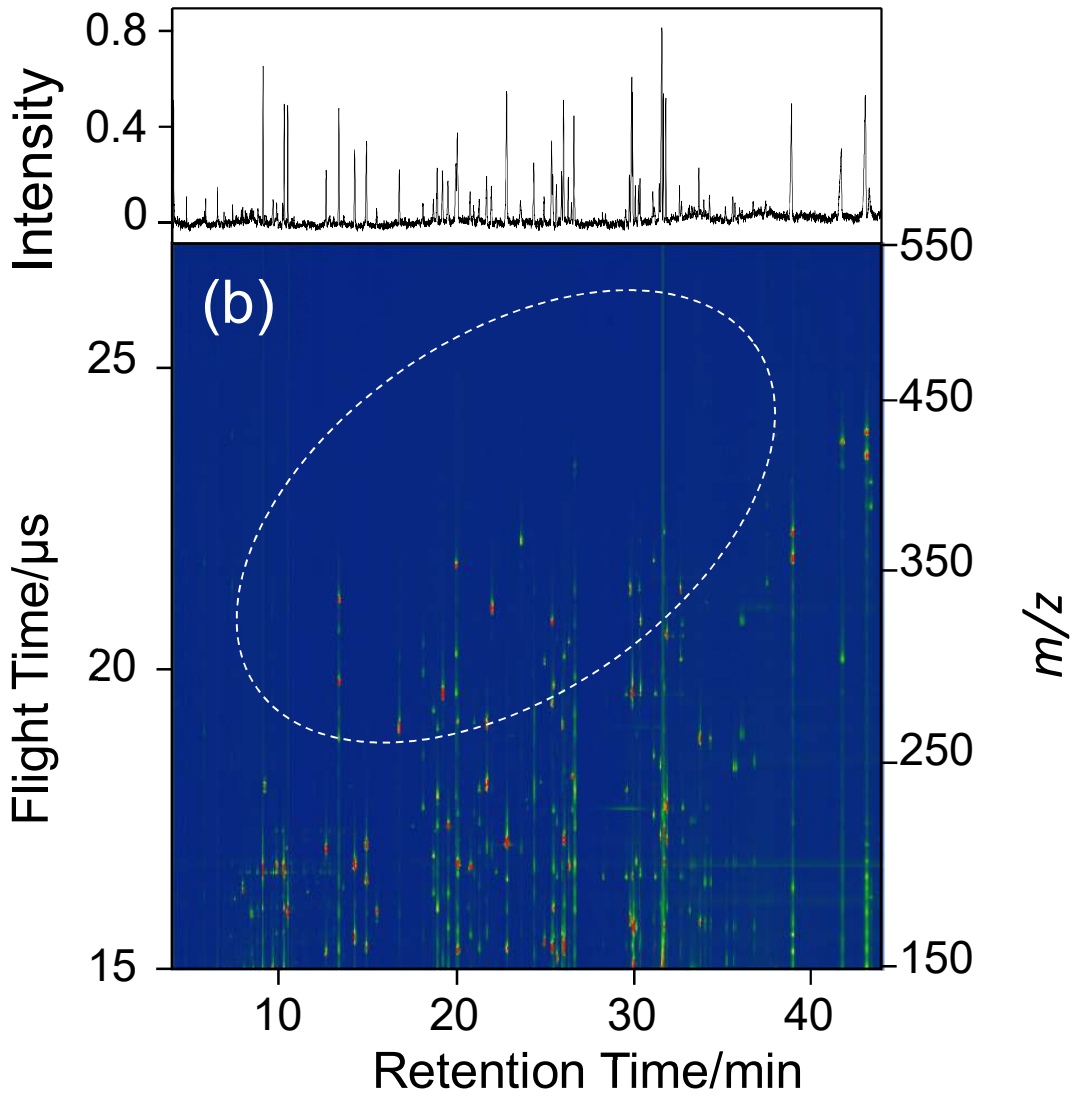

Fig. 3-6. Two-dimensional display measured at 800 nm. (a) kabosu (b) kabosu and 51 pesticides. A tilted elliptical circle (broken line) is drawn as a guide line to permit a visual check of the locations of the data spots.

3.4. Conclusion

The two-dimensional display was obtained for a sample mixture containing 51 pesticides, and the LODs obtained at 267, 400, and 800 nm were compared. The findings indicate that MS measured at 267 nm procedure was slightly more sensitive than MS measured at 400 and 800 nm, although the results depended on the pesticides examined. The data were evaluated using spectral properties obtained by quantum chemical calculations. As a rule of thumb, when a molecule has an absorption band at 267 nm, a laser emitting at 267 nm can be successfully used for efficient ionization through RE2PI and for observing a molecular ion. Note that the efficiency of NR2PI becomes nearly comparable to that of RE2PI when the laser pulse width was reduced to ca. 50 fs. When a molecular ion shows no or a small absorption band at 800 nm, a laser emitting at 800 nm can be preferentially used for observing a molecular ion and provides a low LOD. In addition, a strained functional group or a bulky/long/flexible side chain accelerates the degree of fragmentation. However, there were several exceptional cases for which it was difficult to explain using the above rules. For example, dichloran (4), which forms an intramolecular charge-transfer complex, was difficult to detect both at 267 and 800 nm, even though it has a strong absorption band at 267 nm and the molecular ion has no absorption band at 800 nm. It is interesting to note that α- and *β*-endosulfan (18, 28) have nearly the same spectral properties, *e.g.*, spectral shape, molar absorptivity, ionization energy, *etc.*, for both neutral and ionic species but the former was difficult to detect but the latter was easily detected by photoionization MS.

Selectivity in photoionization can be tuned by changing the laser wavelength, which is preferential for enhancing an analyte signal and for suppressing background arising from interfering substances. This favorable effect can reduce the time required for sample

pretreatment, thus reducing the cost of an analysis. Moreover, the data obtained at different wavelengths can be used to narrow down the candidate compounds that remain unassigned in a comprehensive analysis by GC/MS. In order to demonstrate the potential advantage of the methodology, GC/MPI/TOF-MS was used to analyze pesticides in some typical foods. In fact, the pesticides in homogenized matrix obtained from kabosu were separated and measured on a two-dimensional display, suggesting that this technique performs at a level sufficient to permit its use in practical trace analyses of pesticides in actual samples.

References

1. Barrek, S.; Cren-Olivé, C.; Wiest, L.; Baudot, R.; Arnaudguilhem, C.; Grenier-Loustalot, M. F. *Talanta* **2009**, *79*, 712–722.

2. Bernardi, G.; Kemmerich, M.; Ribeiro, L. C.; Adaime, M. B.; Zanella, R.; Prestes, O. D. *Talanta* **2016**, *161*, 40–47.

3. Domínguez, I.; Romero González, R.; Arrebola Liébanas, F. J.; Martínez Vidal, J. L.; Garrido Frenich, A. *Trends Environ. Anal. Chem.* **2016**, *12*, 1–12.

4. Xu, W.; Wang, X.; Cai, Z. *Anal. Chim. Acta* **2013**, *790*, 1–13.

5. Muir, D.; Lohmann, R. *Trends Anal. Chem.* **2013**, *46*, 162–172.

6. Kosikowska, M.; Biziuk, M. *Trends Anal. Chem.* **2010**, *29*, 1064–1072.

7. Li, N.; Chen, J.; Shi, Y. *Talanta* **2015**, *141*, 212–219.

8. Bresin, B.; Piol, M.; Fabbro, D.; Mancini, M. A.; Casetta, B.; Bianco, C. D. *J. Chromatogr. A* **2015**, *1376*, 167–171.

9. Costa, A. I. G.; Queiroz, M. E. L. R.; Neves, A. A.; De Sousa, F. A.; Zambolim, L. *Food Chem.* **2015**, *181*, 64–71.

10. Farajzadeh, M. A.; Feriduni, B.; Mogaddam, M. R. A. *Anal. Chim. Acta* **2015**, *885*, 122–131.

11. Ali, M.; Khoshmaram, L.; Nabil, A. A. A. *J. Food Compos. Anal.* **2014**, *34*, 128–135.

12. Rickes, S.; Cesar, P.; José, L.; Carla, G.; Clasen, F. *Food Chem.* **2017**, *220*, 510–516.

13. Region, V.; Coscollà, C.; Hart, E.; Pastor, A.; Yusà, V. *Atmos. Environ.* **2013**, *77*, 394–403.

14. Machado, I.; Gérez, N.; Pistón, M.; Heinzen, H.; Verónica, M. *Food Chem.* **2017**, *227*, 227–236.

15. Nortes-Méndez, R.; Robles-Molina, J.; López-Blanco, R.; Vass, A.; Molina-Díaz, A.; Garcia-Reyes, J. F. *Talanta* **2016**, *158*, 222–228.

16. Timofeeva, I.; Shishov, A.; Kanashina, D.; Dzema, D.; Bulatov, A. *Talanta* **2017**, *167*, 761–767.

17. Alves, J.; Maria, J.; Ferreira, S.; Talamini, V.; Fátima, J.D; Medianeira, T.; Damian, O.; Bohrer M.; Zanella, R.; Beatriz, C.; Bottoli, G. *Food Chem.* **2016**, *213*, 616–624.

18. Hart, E.; Coscollà, C.; Pastor, A.; Yusà, V. *Atmos. Environ.* **2012**, *62*, 118–129.

19. Huo, F.; Tang, H.; Wu, X.; Chen, D.; Zhao, T.; Liu, P.; Li, L. *J. Chromatogr. B* **2016**, *1023–1024*, 44–54.

20. Hashiguchi, Y.; Zaitsu, S.; Imasaka, T. *Anal. Bioanal. Chem.* **2013**, *405*, 7053–7059.

21. Li, A.; Imasaka, T.; Uchimura, T.; Imasaka, T. *Anal. Chim. Acta* **2011**, *701*, 52–59.

22. Yang, X.; Imasaka, T.; Li, A.; Imasaka, T. *J. Am. Soc. Mass Spectrom.* **2016**, *27*, 1999–2005.

23. Shibuta, S.; Imasaka, T.; Imasaka, T. *Anal. Chem.* **2016**, *88*, 10693–10700.

24. Kouno, H.; Imasaka, T. *Analyst* **2016**, *141*, 5274–5280.

25. Hamachi, A.; Okuno, T.; Imasaka, T.; Kida, Y.; Imasaka, T. *Anal. Chem.* **2015**, *87*, 3027–3031.

26. Yatsuhashi, T.; Nakashima, N. *J. Photochem. Photobiol. C: Photochem. Rev.* **2007**, https://doi.org/10.1016/j.jphotochemrev.2017.12.001

27. Konar, A.; Shu, Y.; Lozovoy, V.; Jackson, J.; Levine, B.; Dantus, M. *J. Phys. Chem. A* **2014**, *118*, 11433–11450.

28. Li, A.; Thang, D. P.; Imasaka, T.; Imasaka, T. Analyst **2017**, *142*, 3942–3947.

29. Markevitch, A. N.; Smith, S. M.; Romanov, D. A.; Schlegel, H. B.; Ivanov, M. Y.; Levis, R. J. *Phys. Rev. A* **2003**, *68*, 011402.

30. Tanaka, M.; Panja, S.; Murakami, M.; Yatsuhashi, T.; Nakashima, N. *Chem. Phys. Lett.* **2006**, *427*, 255–258.

31. Lezius, M.; Blanchet, V.; Ivanov, M. Y.; Stolow, A. *J. Chem. Phys.* **2002**, *117*, 1575–1588.

32. Murakami, M.; Tanaka, M.; Yatsuhashi, T.; Nakashima, N. *J. Chem. Phys*. **2007**, *126*, 104304.

33. Frisch, M. J.; Trucks, G. W.; Schlegel, H. B.; Scuseria, G. E.; Robb, M. A.; Cheeseman, J. R.;

Scalmani, G.; Barone, V.; Mennucci, B.; Petersson, G. A.; Nakatsuji, H.; Caricato, M.; Li, X.; Hratchian, H. P.; Izmaylov, A. F.; Bloino, J.; Zheng, G.; Sonnenberg, J. L.; Hada, M.; Ehara, M.; Toyota, K.; Fukuda, R.; Hasegawa, J.; Ishida, M.; Nakajima, T.; Honda, Y.; Kitao, O.; Nakai, H.; Vreven, T.; Montgomery, J. A., Jr.; Peralta, J. E.; Ogliaro, F.; Bearpark, M.; Heyd, J. J.; Brothers, E.; K. N. Kudin,; Staroverov, V. N.; Kobayashi, R.; Normand, J.; Raghavachari, K.; Rendell, A.; Burant, J. C.; Iyengar, S. S.; Tomasi, J.; Cossi, M.; Rega, N.; Millam, J. M.; Klene, M.; Knox, J. E.; Cross, J. B.; Bakken, V.; Adamo, C.; Jaramillo, J.; Gomperts, R.; Stratmann, R. E.; Yazyev, O.; Austin, A. J.; Cammi, R.; Pomelli, C.; Ochterski, J. W.; Martin, R. L.; Morokuma, K.; Zakrzewski, V. G.; Voth, G. A.; Salvador, P.; Dannenberg, J. J.; Dapprich, S.; Daniels, A. D.; Farkas, O.; Foresman, J. B.; Ortiz, J. V.; Cioslowski, J.; Fox, D. J. *Gaussian 09*, revision D.01; Gaussian Inc.: Wallingford, CT, **2009**.

34. Becke, A. D. *J. Chem. Phys.* **1993**, *98*, 5648–5652.

35. Dunning, Jr. T. H. *J. Chem. Phys. Lett.* **1989**, *90*, 1007–1023.

36. Bauernschmitt, R.; Ahlrichs, R. *Chem. Phys. Lett.* **1996**, *256*, 454–464.

37. Moore, N. P.; Menkir, G. M.; Markevitch, A. N.; Graham, P.; Levis, R. J. In *Laser Control and Manipulation of Molecules*; Bandrauk, A. D.; Fujimura, Y.; Gordon, R. J., Ed.; American Chemical Society: Washington, DC, 2002; pp 207–220.

Chapter 4 Conclusion

In Chapter 1, a history of the development of pesticides is briefly introduced in the beginning of this chapter. The positive and negative sides of the pesticides to human being has been described for better understanding of the function of the pesticides. The definition of "pesticide" by the Food and Agriculture Organization is provided for the readers involved in the other academic fields different from the agriculture. A figure indicating the world pesticide demand shows the rapid production rate in developing countries in Asia, Africa, and central & south America. "Silent Spring", a book published in 1962 reports environmental pollution by wide-spread DDT. Since then, many scientists are more concentrating their attentions for solving the environmental issues. The pesticides can be classified according to the chemical structures and also by the killing targets to realize their functions. Current technology of mass spectrometry is briefly summarized and is followed by a technique of laser ionization mass spectrometry. As described, there are several ionization methods in mass spectrometry, e.g., electron ionization. Among them, a laser ionization technique using a tunable femtosecond laser provides an excellent tool for ionization of various pesticides. The research subjects explained in the following chapters are briefly introduced at the end of this chapter.

In Chapter 2, one of the popular pesticides, i.e., HCH was measured in this chapter. Structural and enantiometric isomers were separated by a GC column with a chiral stationary phase. Then, far- and deep- ultraviolet femtosecond laser emitting at 200 and 267 nm were used as the ionization source for multiphoton ionization in mass spectrometry. The

elution order of the enantiomers, i.e., (+)-α-HCH and (-)-α-HCH, observed in the experiment was compared with the predicted data obtained from the stabilization energies of the complexes with permethylated γ-cyclodextrin used as a stationary phase of the capillary column. When a far-ultraviolet laser emitting at 200 nm was used, resonance-enhanced two-photon ionization (RE2PI) was found to be a major process for these compounds. The molecular ions of HCHs were clearly observed, although the fragment ions dominantly appeared in the mass spectrum. The experimental data, which was unpredicted from quantum chemical calculation was explained by efficient dissociation of a molecular ion. The result achieved in this study suggests that the analytical instrument has a potential advantage for the determination of the pesticide with structural and enantiometric isomers in the environment and their elution order can be predicted from the data obtained by quantum chemical calculation.

In Chapter 3, three different kinds of femtosecond laser emitting at 267 nm (ultraviolet), 400 nm (visible) and 800 nm (near-infrared) were used as the ionization source. Gas chromatography (GC) combined with the home-made mass spectrometry (MS) was employed for the measurement of a standard sample mixture containing 51 pesticides. A two-dimensional display of the GC/MS was successfully used for the determination of these compounds. Two laser wavelengths, i.e., 267 nm and 800 nm, were examined to have optimal conditions for trace analysis and to find the rule to explain the efficiency of ionization. The data were compared with those obtained using quantum chemical calculations, in which numerous spectrometric properties such as the excitation and ionization energies and the absorption spectrum and the oscillator strengths were calculated

for the neutral and ionized species. As a result of this, several additional rules were found for explanation of the observed data. The sample of pesticides in the homogenized matrix obtained from kabosu and other vegetables were measured and the constituents were clearly separated and identified in the data, providing an excellent performance in the practical trace analysis of the multi-residue of pesticides in the environment.

In Chapter 4, all the studies in this dissertation are summarized in this chapter as mentioned.

Acknowledgement

Firstly, I would like to express my deep gratitude to my Prof. Totaro Imasaka. The professional, rigorous, conscientious and hard-working spirits in every research work as well as daily life will always be my role model. I benefit a lot from every discussion with him, all of those will be my precious wealth not only in my future research, but also my whole life.

Secondly, I would like to thank Tomoko Imasaka, Graduate School of Design, Kyushu University for the quantum chemical calculations and Koji Takahashi, Fukuoka Institute of Health and Environmental Sciences for the preparation of actual samples. Also, I express my gratitude to Prof. Noritada Kaji, Prof. Toshihiko Imato, Prof. Chihaya Adachi for the work of my graduation.

Next, I would like to give my acknowledgement to all the members of the laboratory. From teachers to students, from academic staff to secretaries, although the people in the laboratory come from different countries with different background and cultures, the timely help from them never stop, which makes me firmly believe that people all over the world could live and work in harmony and make the contribution to the cause of human development together.

Last but not the least, I would like to thank my family. They inspire me to follow my dreams no matter what happens, encourage me in all my pursuits selflessly.

Fukuoka, Japan

Xixiang Yang

February 28, 2018

Appendix

Fig. S-1. Chemical structure and absorption spectrum of the pesticides calculated for neutral and ionic species.

Fig. S-2. Mass spectrum of the pesticide measured based on electron ionization (70 eV).

Fig. S-1. Chemical structure and absorption spectrum of the pesticides calculated for neutral and ionic species.

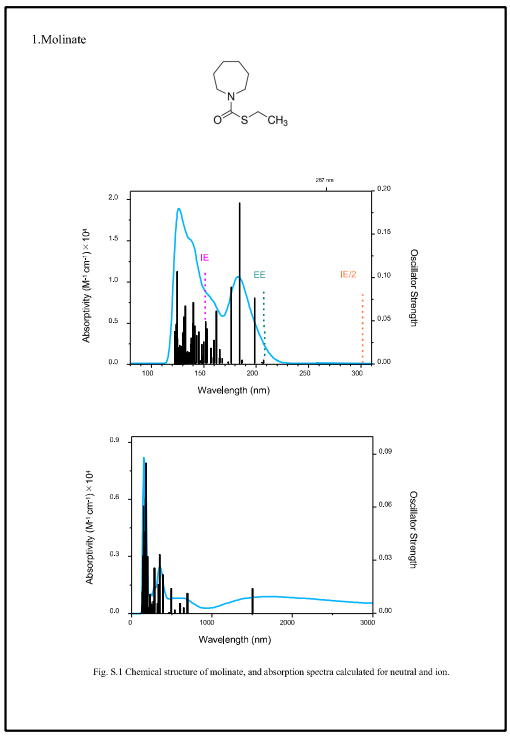

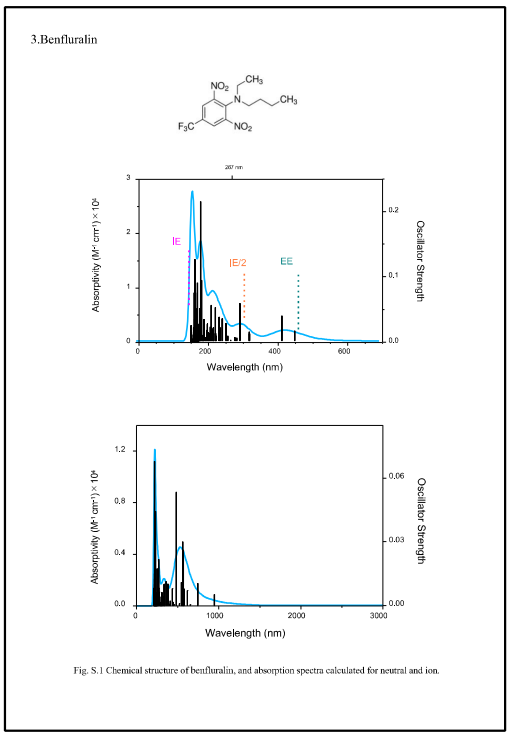

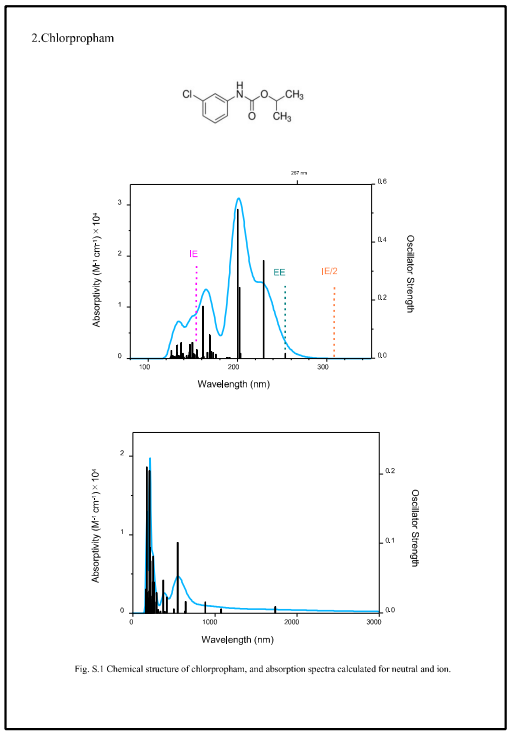

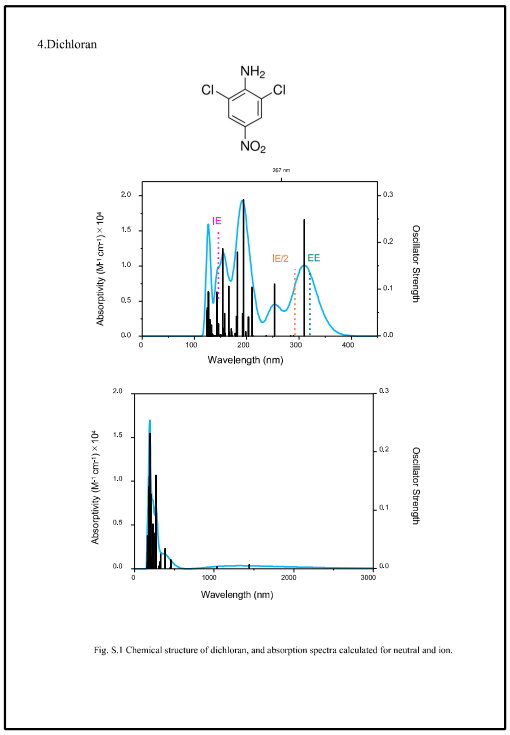

5.Dimethipin

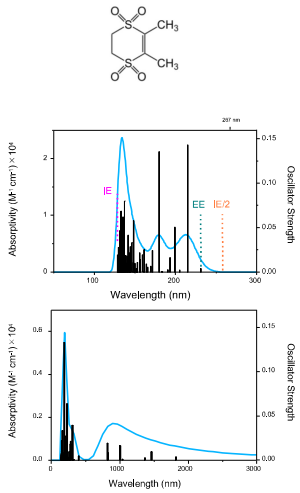

Fig. S.1 Chemical structure of dimethipin, and absorption spectra calculated for neutral and ion.

7.Triallate

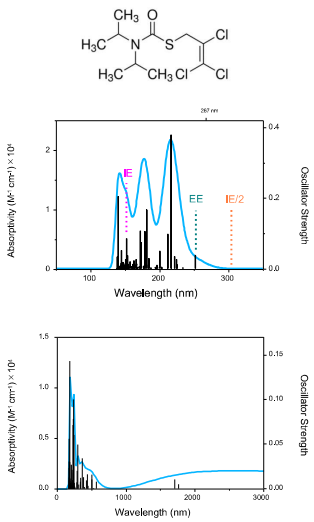

Fig. S.1 Chemical structure of triallate, and absorption spectra calculated for neutral and ion.

6.Atrazine

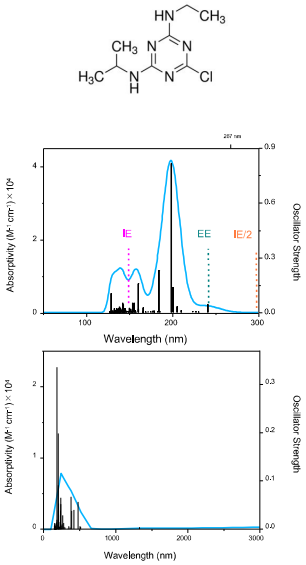

Fig. S.1 Chemical structure of atrazine, and absorption spectra calculated for neutral and ion.

8.Bromobutide

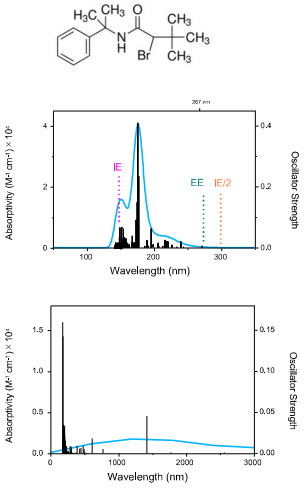

Fig. S.1 Chemical structure of bromobutide, and absorption spectra calculated for neutral and ion.

9.Simeconazole

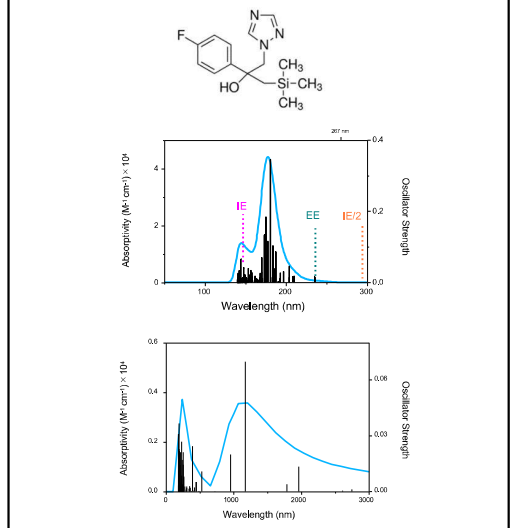

Fig. S.1 Chemical structure of simeconazole, and absorption spectra calculated for neutral and ion.

11.Fenchlorphos

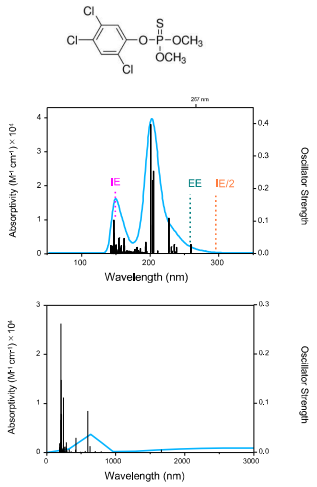

Fig. S.1 Chemical structure of fenchlorphos, and absorption spectra calculated for neutral and ion.

10.Alachlor

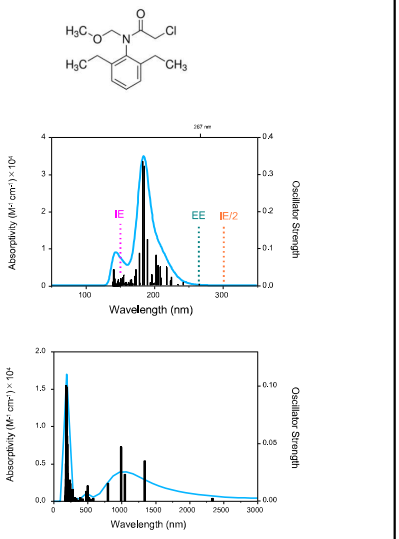

Fig. S.1 Chemical structure of alachlor, and absorption spectra calculated for neutral and ion.

12.Dithiopyr

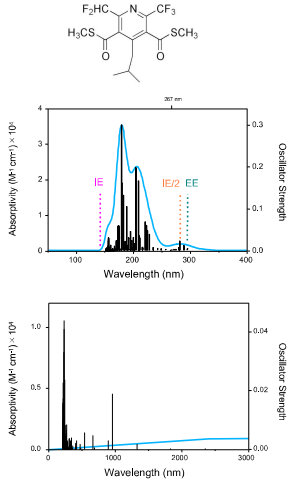

Fig. S.1 Chemical structure of dithiopyr, and absorption spectra calculated for neutral and ion.

13.Quinoclamine

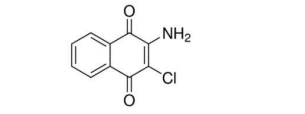

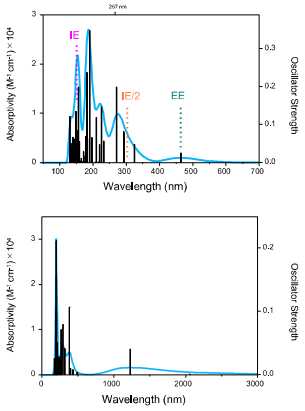

Fig. S.1 Chemical structure of quinoclamine, and absorption spectra calculated for neutral and ion.

15.Fthalide

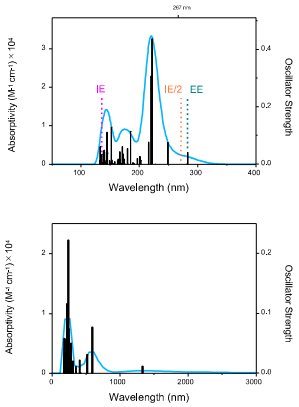

Fig. S.1 Chemical structure of fthalide, and absorption spectra calculated for neutral and ion.

14.Cyanazine

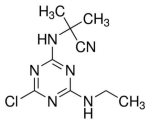

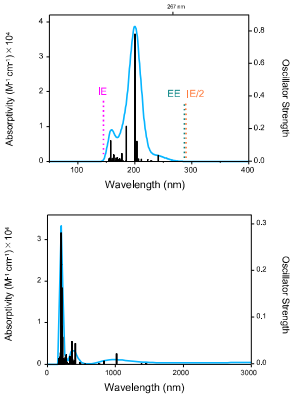

Fig. S.1 Chemical structure of cyanazine, and absorption spectra calculated for neutral and ion.

16.Bromophos methyl

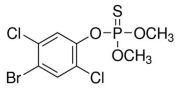

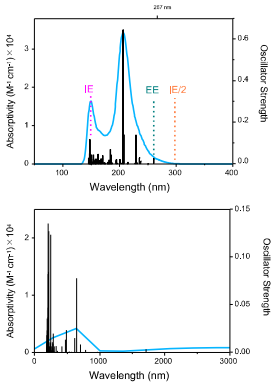

Fig. S.1 Chemical structure of bromophos methyl, and absorption spectra calculated for neutral and ion.

17.Fipronil

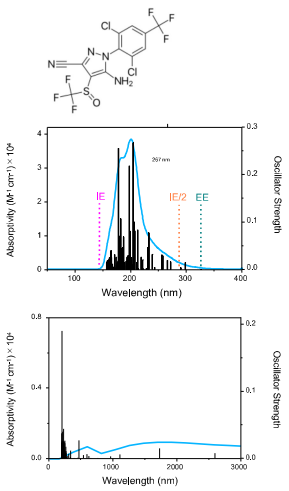

Fig. S.1 Chemical structure of fipronil, and absorption spectra calculated for neutral and ion.

19.Chlorefenson

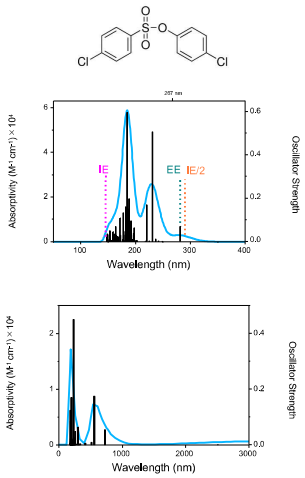

Fig. S.1 Chemical structure of chlorefenson, and absorption spectra calculated for neutral and ion.

18.α-Endosulfan

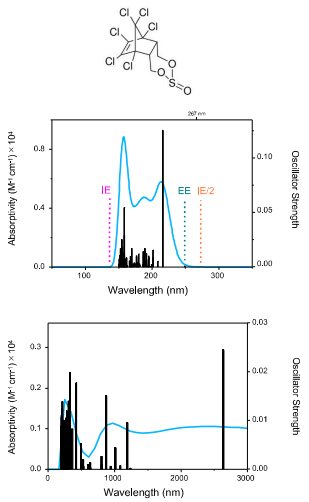

Fig. S.1 Chemical structure of α-endosulfan, and absorption spectra calculated for neutral and ion.

20.Flutolanil

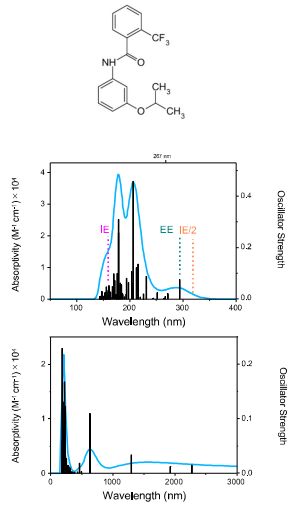

Fig. S.1 Chemical structure of flutolanil, and absorption spectra calculated for neutral and ion.

21.Isoprothiolane

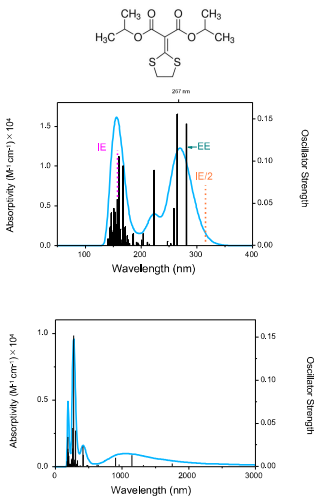

Fig. S.1 Chemical structure of isoprothiolane, and absorption spectra calculated for neutral and ion.

22.DEF (Tribufos)

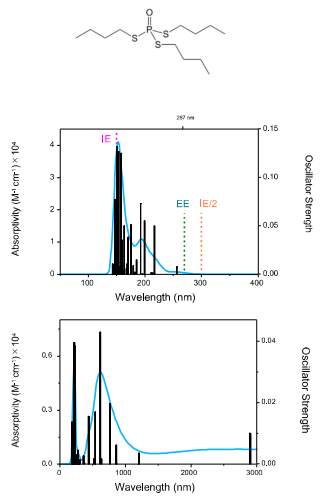

Fig. S.1 Chemical structure of DEF(tribufos), and absorption spectra calculated for neutral and ion.

23.Dicrobutrazole (R)

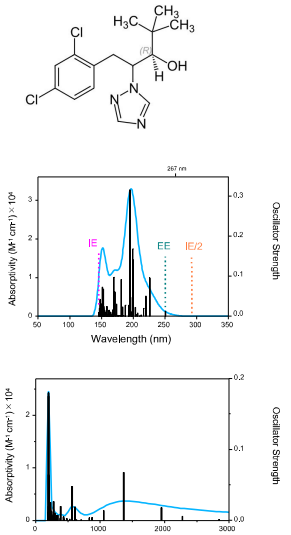

Fig. S.1 Chemical structure of dicrobutrazole (R), and absorption spectra calculated for neutral and ion.

23.Dicrobutrazole (S)

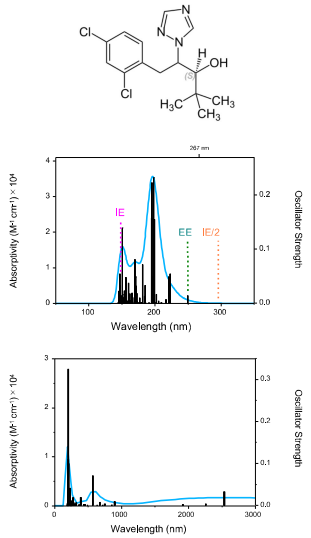

Fig. S.1 Chemical structure of dicrobutrazole (S), and absorption spectra calculated for neutral and ion.

24.Myclobutanil

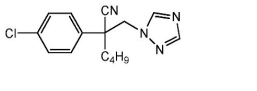

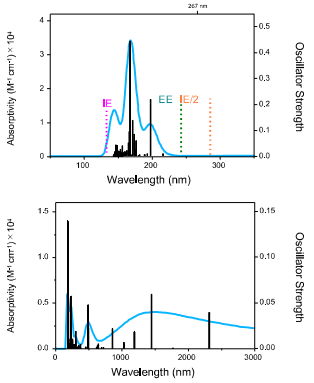

Fig. S.1 Chemical structure of myclobutanil, and absorption spectra calculated for neutral and ion.

25.Azaconazole

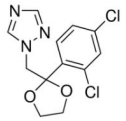

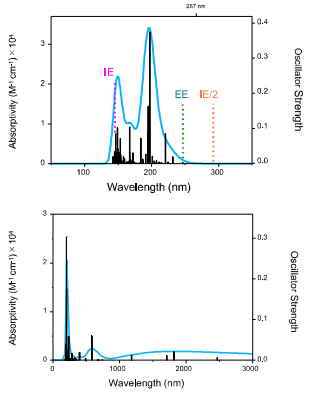

Fig. S.1 Chemical structure of azaconazole, and absorption spectra calculated for neutral and ion.

26.Buprofezin

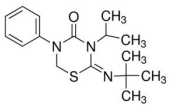

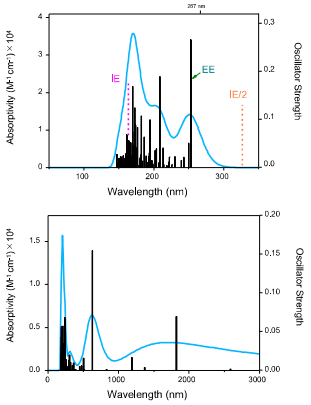

Fig. S.1 Chemical structure of buprofezin, and absorption spectra calculated for neutral and ion.

27.Kresoxim methyl

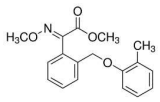

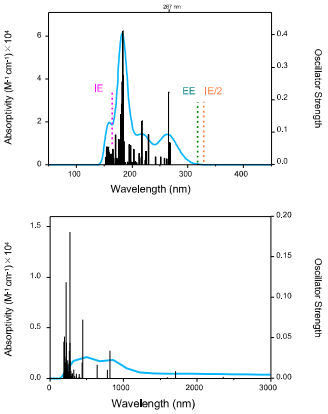

Fig. S.1 Chemical structure of kresoxim methyl, and absorption spectra calculated for neutral and ion.

28.β-Endosulfan

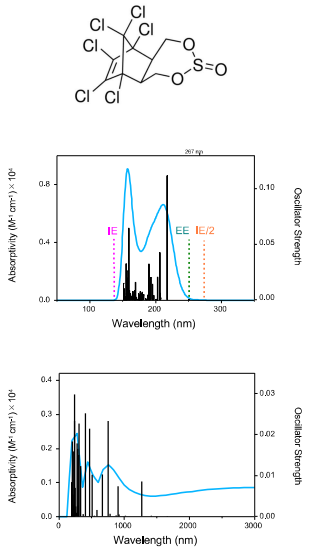

Fig. S.1 Chemical structure of β-endosulfan, and absorption spectra calculated for neutral and ion.

30.Chlorfenapyr

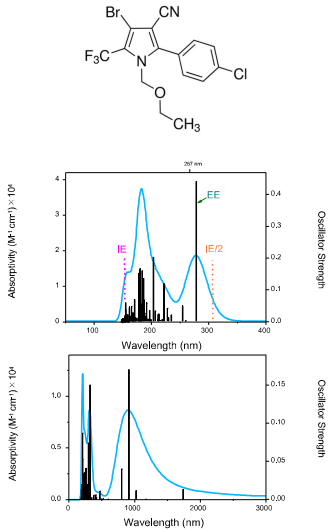

Fig. S.1 Chemical structure of chlorfenapyr, and absorption spectra calculated for neutral and ion.

29.Cyflufenamid

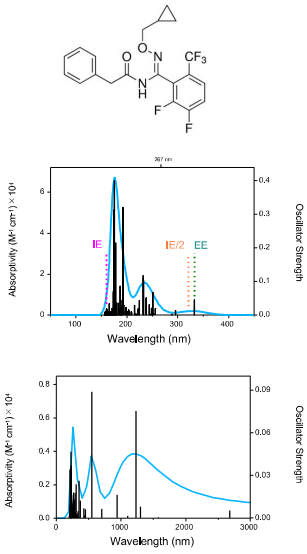

Fig. S.1 Chemical structure of cyflufenamid, and absorption spectra calculated for neutral and ion.

31.Bromopropylate

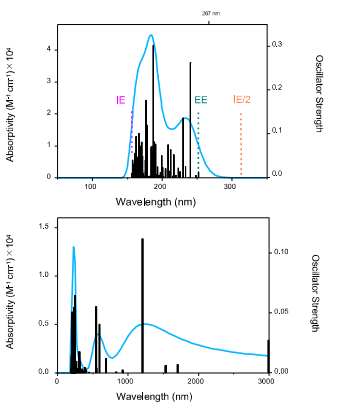

Fig. S.1 Chemical structure of bromopropylate, and absorption spectra calculated for neutral and ion.

32.Bifenthrin

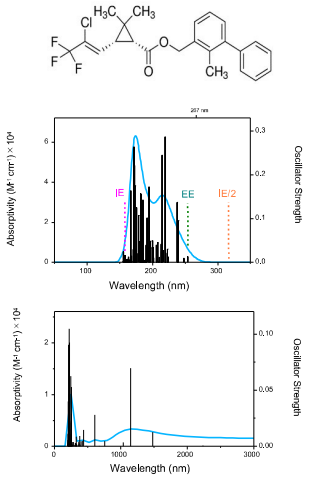

Fig. S.1 Chemical structure of bifenthrin, and absorption spectra calculated for neutral and ion.

33.Fenpropathrin

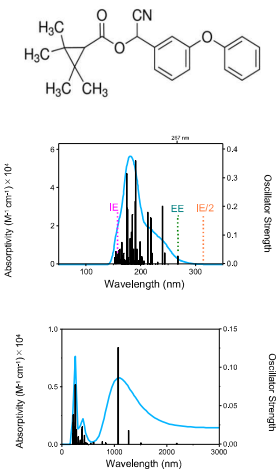

Fig. S.1 Chemical structure of fenpropathrin, and absorption spectra calculated for neutral and ion.

34.Bifenox

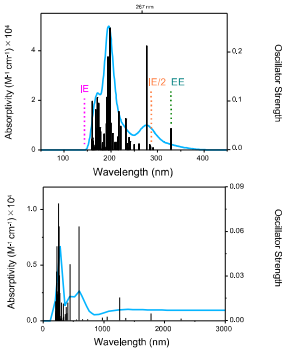

Fig. S.1 Chemical structure of bifenox, and absorption spectra calculated for neutral and ion.

35.Clomeprop

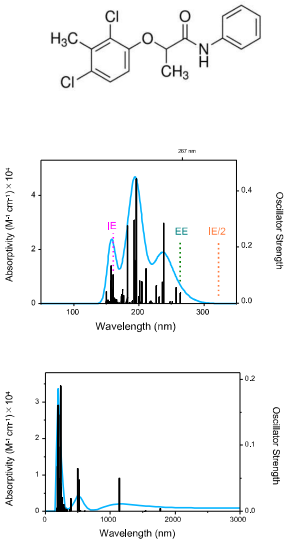

Fig. S.1 Chemical structure of clomeprop, and absorption spectra calculated for neutral and ion.

36.Cyhalofop-butyl

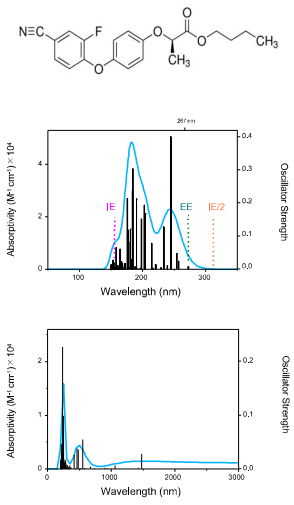

Fig. S.1 Chemical structure of cyhalofop-butyl, and absorption spectra calculated for neutral and ion.

38.Pyrazophos

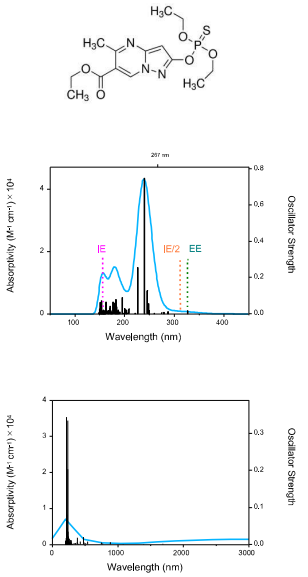

Fig. S.1 Chemical structure of pyrazophos, and absorption spectra calculated for neutral and ion.

37.Fenarimol

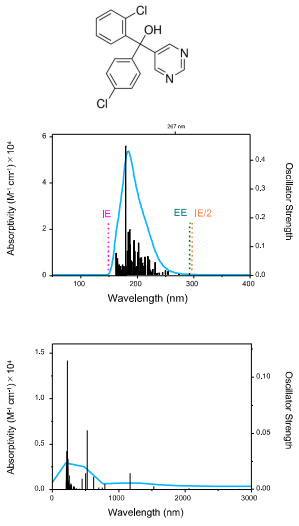

Fig. S.1 Chemical structure of fenarimol, and absorption spectra calculated for neutral and ion.

39.Acrinathrin

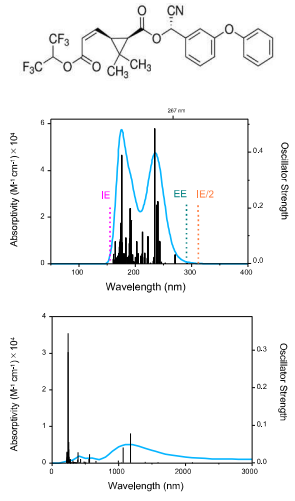

Fig. S.1 Chemical structure of acrinathrin, and absorption spectra calculated for neutral and ion.

40.Fluquinconazole

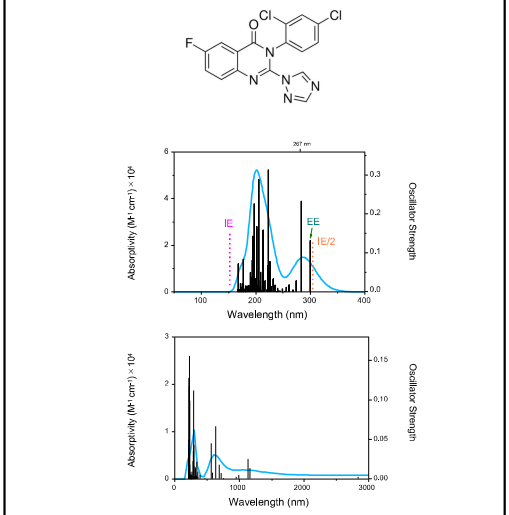

Fig. S.1 Chemical structure of fluquinconazole, and absorption spectra calculated for neutral and ion.

41.Cafenstrole

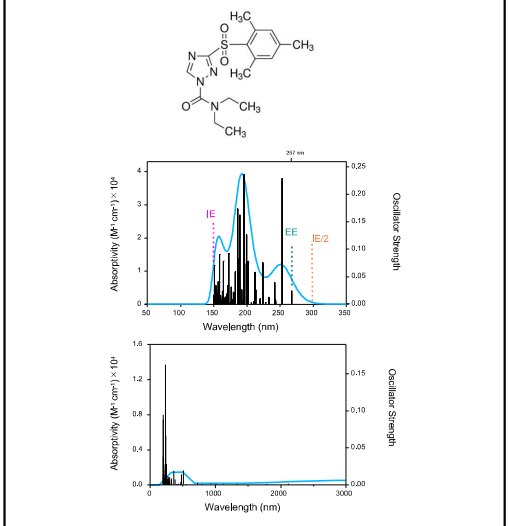

Fig. S.1 Chemical structure of cafenstrole, and absorption spectra calculated for neutral and ion.

42.Cyfluthrin

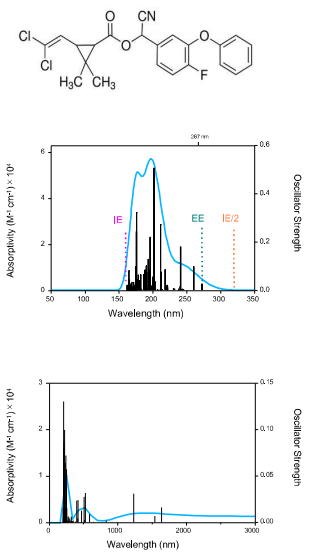

Fig. S.1 Chemical structure of cyfluthrin , and absorption spectra calculated for neutral and ion.

43.Halfenprox

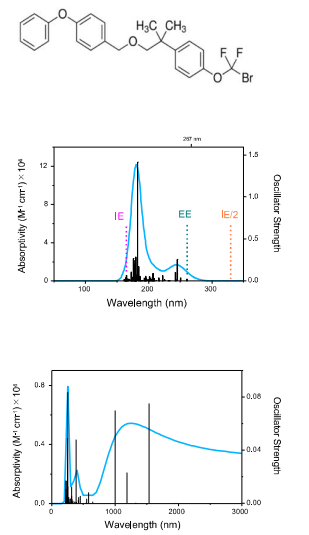

Fig. S.1 Chemical structure of halfenprox, and absorption spectra calculated for neutral and ion.

44/45.Flucythrinate

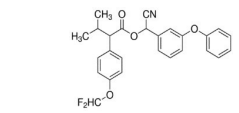

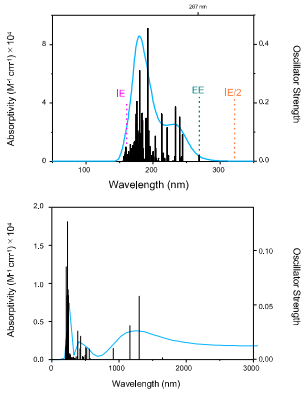

Fig. S.1 Chemical structure of flucythrinate 2, and absorption spectra calculated for neutral and ion.

46.Fenvalerate 2

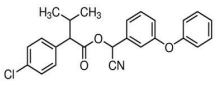

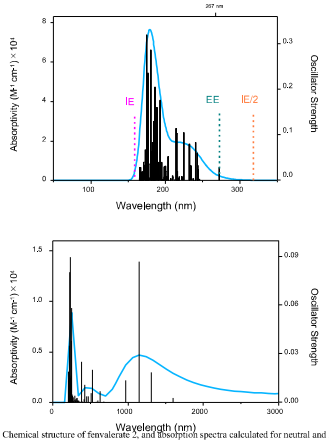

Fig. S.1 Chemical structure of fenvalerate 2, and absorption spectra calculated for neutral and ion.

46.Fenvalerate 1

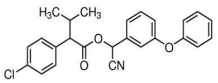

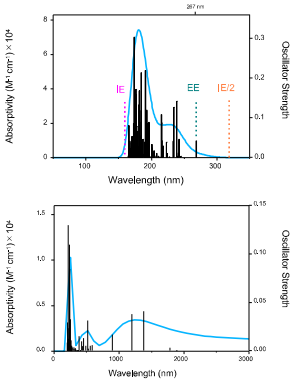

Fig. S.1 Chemical structure of fenvalerate 1, and absorption spectra calculated for neutral and ion.

46.Fenvalerate 3

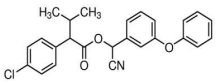

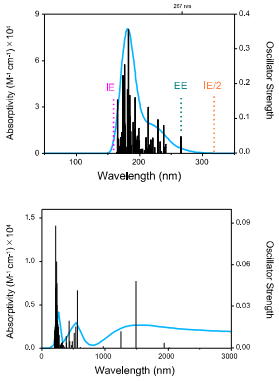

Fig. S.1 Chemical structure of fenvalerate 3, and absorption spectra calculated for neutral and ion.

46.Fenvalerate 4

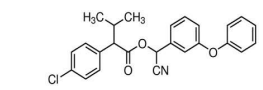

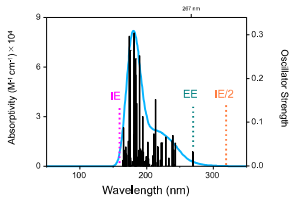

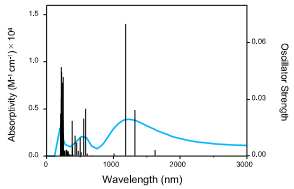

Fig. S.1 Chemical structure of fenvalerate 4, and absorption spectra calculated for neutral and ion.

48.Fluvalinate 2

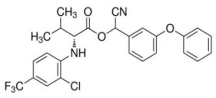

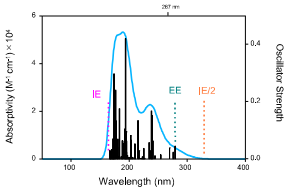

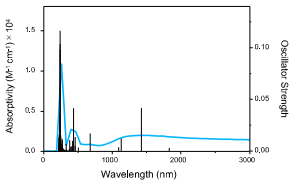

Fig. S.1 Chemical structure of fluvalinate 2, and absorption spectra calculated for neutral and ion.

47.Fluvalinate 1

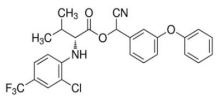

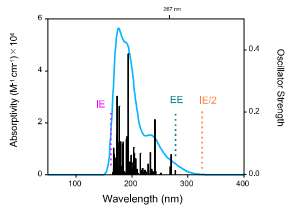

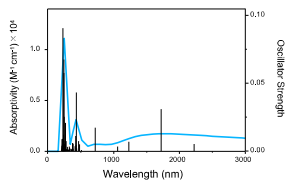

Fig. S.1 Chemical structure of fluvalinate 1, and absorption spectra calculated for neutral and ion.

Fluvalinate 3

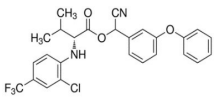

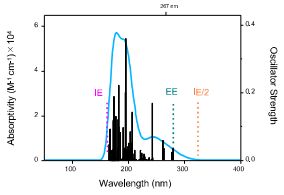

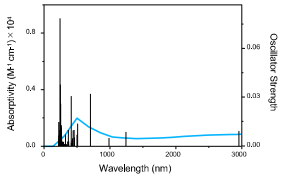

Fig. S.1 Chemical structure of fluvalinate 3, and absorption spectra calculated for neutral and ion.

Fluvalinate 4

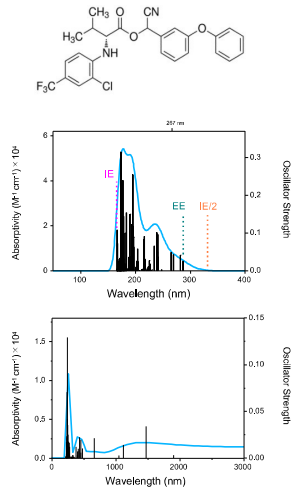

Fig. S.1 Chemical structure of fluvalinate 4, and absorption spectra calculated for neutral and ion.

49.Difenoconazole 2

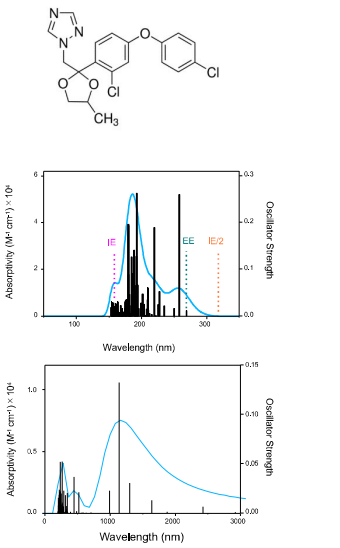

Fig. S.1 Chemical structure of difenoconazole 2, and absorption spectra calculated for neutral and ion.

49.Difenoconazole 1

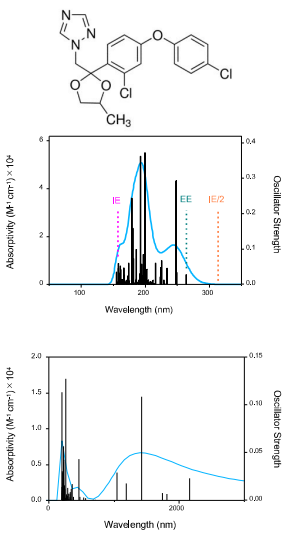

Fig. S.1 Chemical structure of difenoconazole 1, and absorption spectra calculated for neutral and ion.

49.Difenoconazole 3

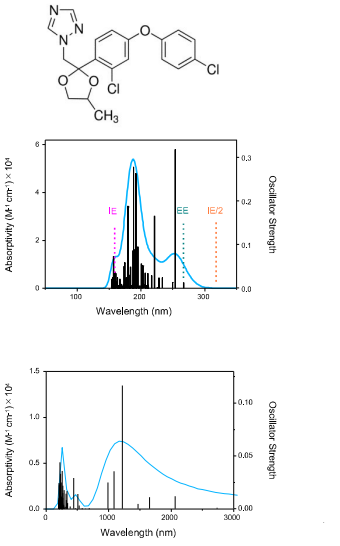

Fig. S.1 Chemical structure of difenoconazole 3, and absorption spectra calculated for neutral and ion.

49.Difenoconazole 4

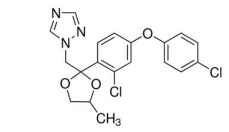

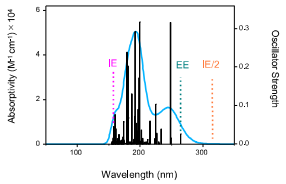

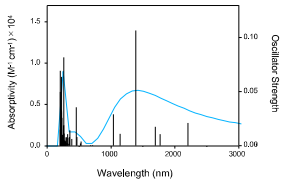

Fig. S.1 Chemical structure of difenoconazole 4, and absorption spectra calculated for neutral and ion.

51.Azoxystrobin

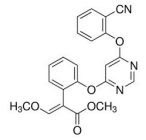

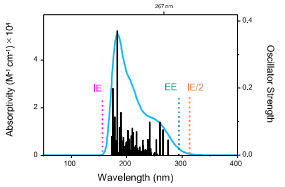

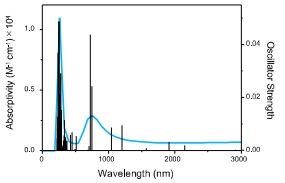

Fig. S.1 Chemical structure of azoxystrobin, and absorption spectra calculated for neutral and ion.

50.Deltamethrin

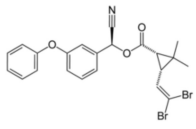

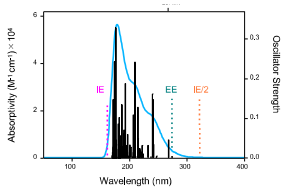

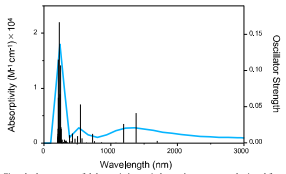

Fig. S.1 Chemical structure of deltamethrin, and absorption spectra calculated for neutral and ion.

Fig. S-2. Mass spectrum of the pesticide measured based on electron ionization (70 eV).

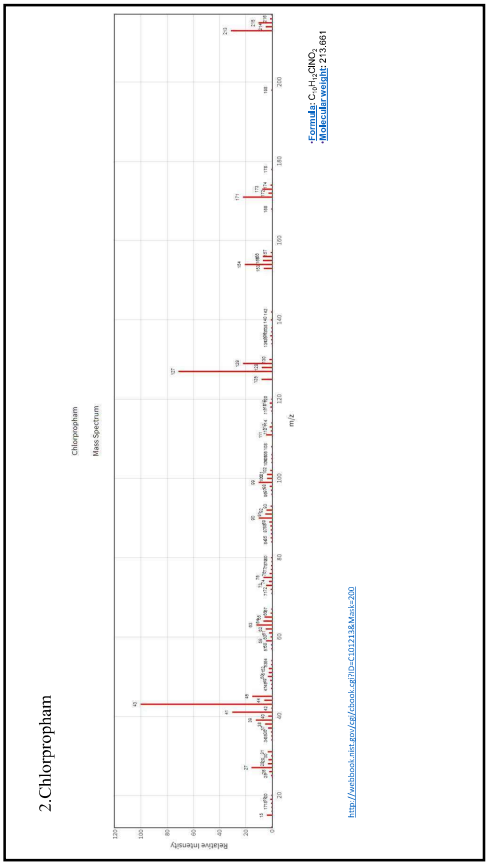

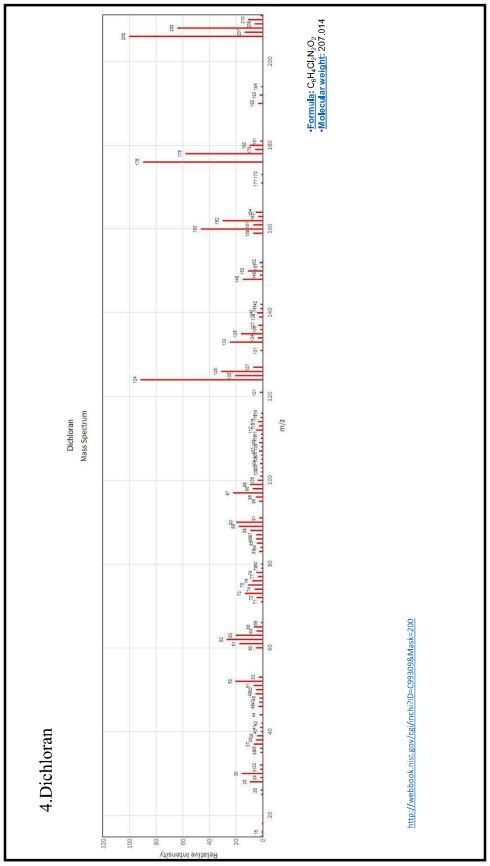

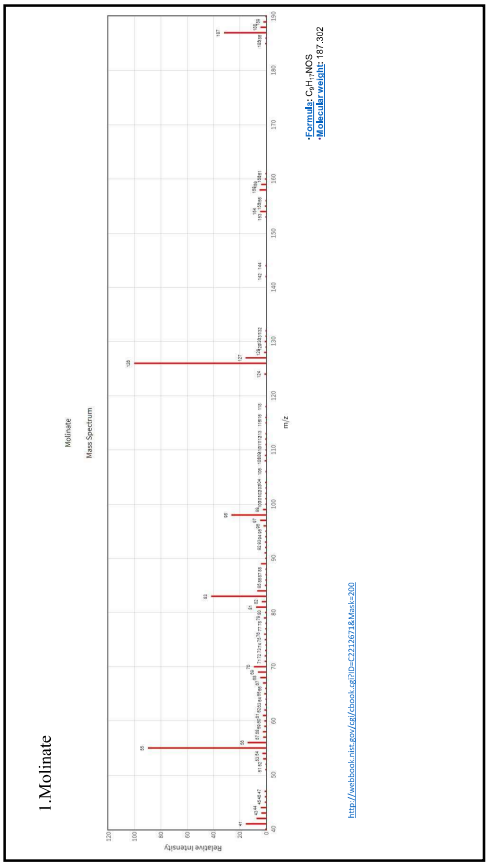

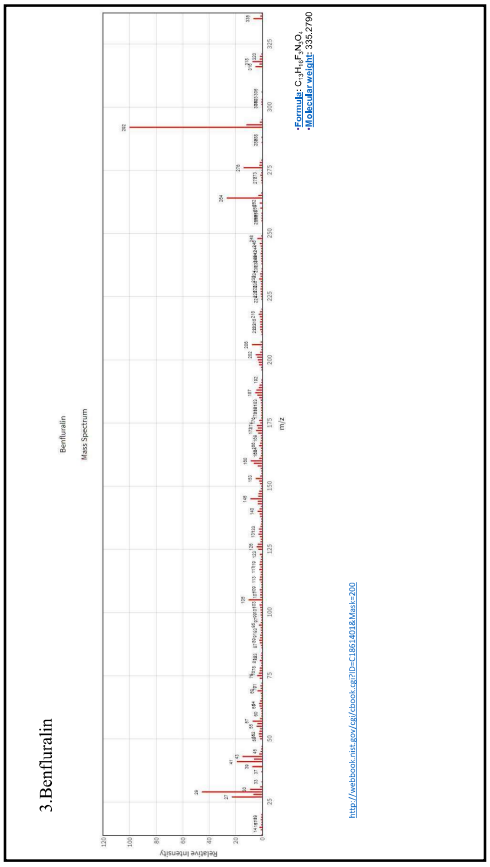

5. Dimethipin

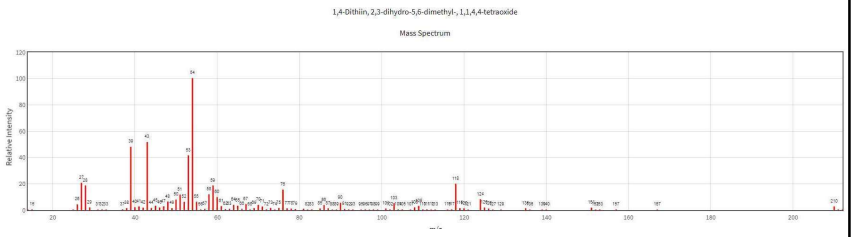

·Formula: $C_6H_{10}O_4S_2$
·Molecular weight: 210.271

http://webbook.nist.gov/cgi/cbook.cgi?ID=C52906478&Mask=200

6.Atrazine

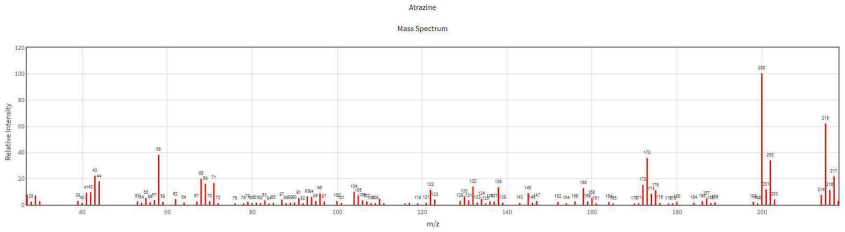

·Formula: $C_8H_{14}ClN_5$
·Molecular weight: 215.683

http://webbook.nist.gov/cgi/cbook.cgi?ID=C1912249&Mask=200

7.Triallate

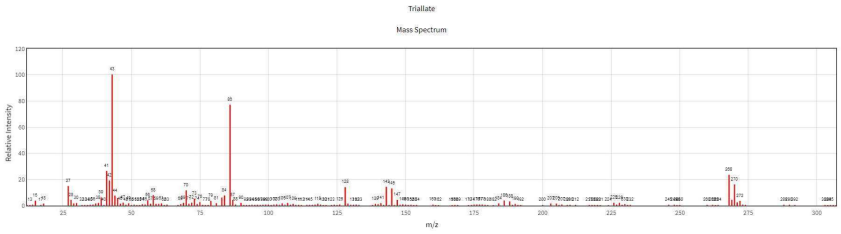

·Formula: $C_{10}H_{16}Cl_3NOS$
·Molecular weight: 304.664

http://webbook.nist.gov/cgi/cbook.cgi?ID=C2303175&Mask=200

8.Bromobutide

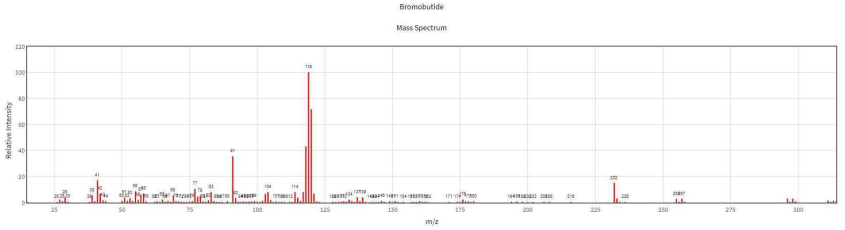

·Formula: $C_{15}H_{22}BrNO$
·Molecular weight: 312.245

http://webbook.nist.gov/cgi/cbook.cgi?ID=C74712199&Mask=200

9.Simeconazole

4.2.1 GC-MS

NIST Number	378696
Library	Main library
Total Peaks	181
m/z Top Peak	121
m/z 2nd Highest	83
m/z 3rd Highest	195
Thumbnail	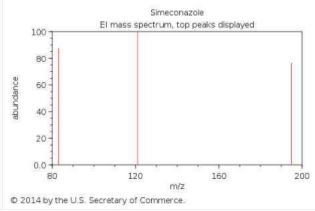

•Formula: $C_{14}H_{20}FN_2OSi$
•Molecular weight: 293.417

https://pubchem.ncbi.nlm.nih.gov/compound/Simeconazole#section=Spectral-Properties

10. Alachlor

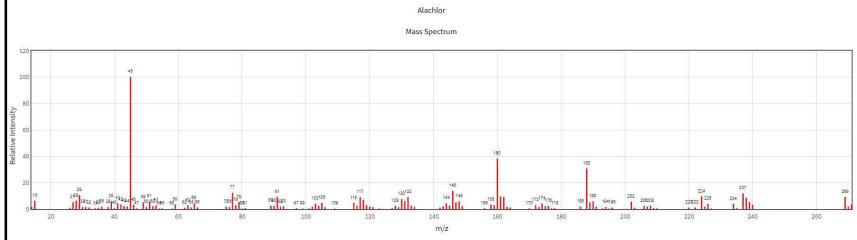

•Formula: $C_{14}H_{20}ClNO_2$
•Molecular weight: 269.767

http://webbook.nist.gov/cgi/cbook.cgi?ID=C15972608&Mask=200

11.Fenchlorphos

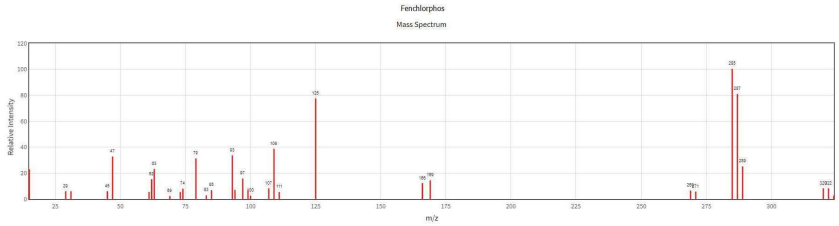

•Formula: $C_8H_8Cl_3O_3PS$
•Molecular weight: 321.545

http://webbook.nist.gov/cgi/cbook.cgi?ID=C299843&Mask=200

12.Dithiopyr

4.3.1 GC-MS

	1 of 2	2 of 2
NIST Number	372983	366511
Library	Main library	Replicate library
Total Peaks	311	280
m/z Top Peak	354	354
m/z 2nd Highest	286	286
m/z 3rd Highest	306	306
Thumbnail	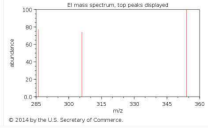	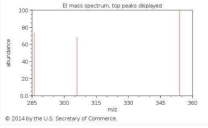

https://pubchem.ncbi.nlm.nih.gov/compound/Dithiopyr#section=Kovats-Retention-Index

•Formula: $C_{15}H_{16}F_5NO_2S_2$
•Molecular weight: 401.415

13.Quinoclamine

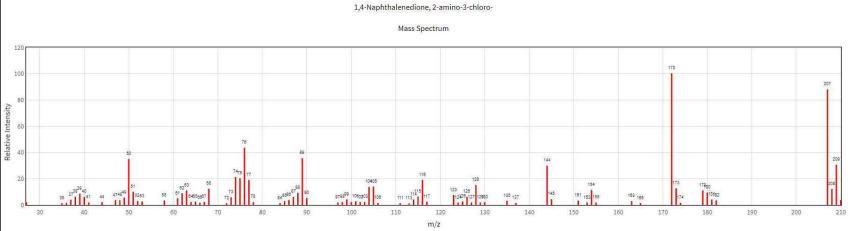

•Formula: $C_{10}H_6ClNO_2$
•Molecular weight: 207.613

http://webbook.nist.gov/cgi/cbook.cgi?ID=C797515&Mask=200

14.Cyanazine

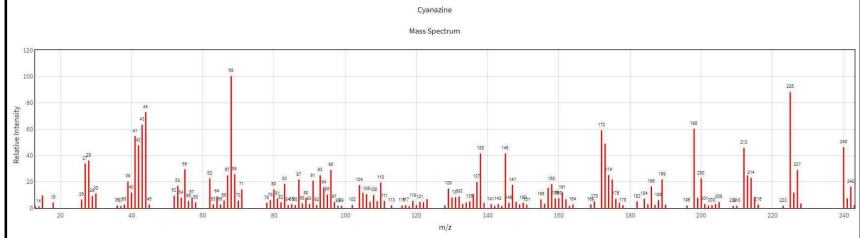

•Formula: $C_9H_{13}ClN_6$
•Molecular weight: 240.693

http://webbook.nist.gov/cgi/cbook.cgi?ID=C21725462&Mask=200

15.Fthalide

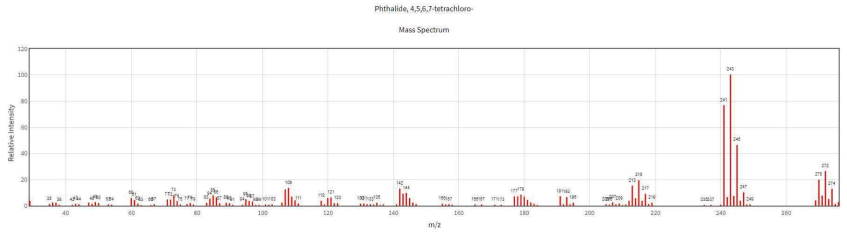

•Formula: $C_8H_2Cl_4O_2$
•Molecular weight: 271.912

http://webbook.nist.gov/cgi/cbook.cgi?ID=C27355222&Mask=200

16.Bromophos methyl

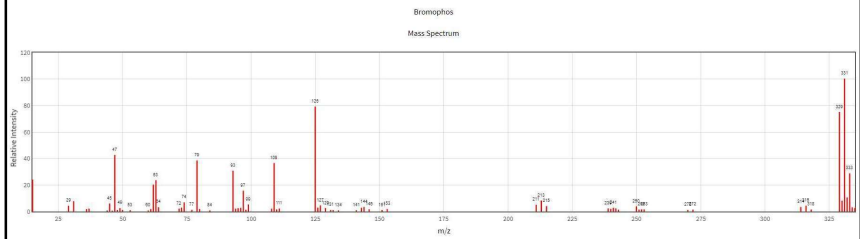

•Formula: $C_8H_8BrCl_2O_3PS$
•Molecular weight: 365.996

http://webbook.nist.gov/cgi/cbook.cgi?ID=C2104963&Mask=200

17. Fipronil

4.3.2 GC-MS

NIST Number	373137
Library	Main library
Total Peaks	320
m/z Top Peak	367
m/z 2nd Highest	369
m/z 3rd Highest	213
Thumbnail	no-1-[2,6-dichloro-4-(trifluoromethyl)phenyl]-4-(trifluoromethylsulfinyl)pyrazo EI mass spectrum, top peaks displayed

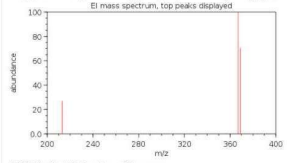

© 2014 by the U.S. Secretary of Commerce.

https://pubchem.ncbi.nlm.nih.gov/compound/fipronil#section=Top

•Formula: $C_{12}H_4Cl_2F_6N_4OS$
•Molecular weight: 437.148

18. α-Endosulfan

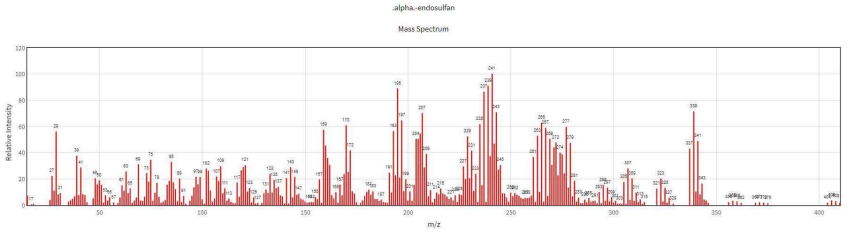

•Formula: $C_9H_6Cl_6O_3S$
•Molecular weight: 406.925

http://webbook.nist.gov/cgi/cbook.cgi?ID=C959988&Mask=200

19. Chlorefenson

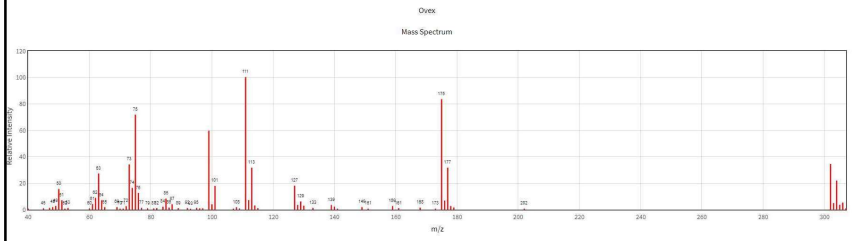

•Formula: $C_{12}H_8Cl_2O_3S$
•Molecular weight: 303.161

http://webbook.nist.gov/cgi/inchi?ID=C80331&Mask=200

Other names: Ovex、CPCBS、Ovotox、PCPCBS、Ovatran、Ovotran、Ovochlor、Estonmite、Orthotran、Genite 883、Chlorfenson、Lethalaire G-58、4-Chlorobenzenesulfonic acid 4-chlorophenyl、p-Chlorobenzenesulfonic acid p-chlorophenyl ester、4-Chlorobenzenesulfonic acid 4-chlorophenyl ester

20. Flutolanil

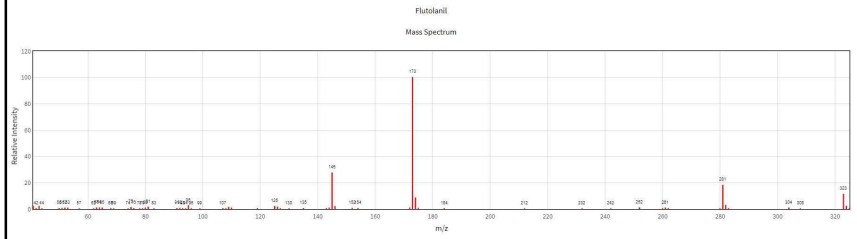

•Formula: $C_{17}H_{16}F_3NO_2$
•Molecular weight: 323.3096

http://webbook.nist.gov/cgi/cbook.cgi?ID=C66332965&Mask=200

21. Isoprothiolane

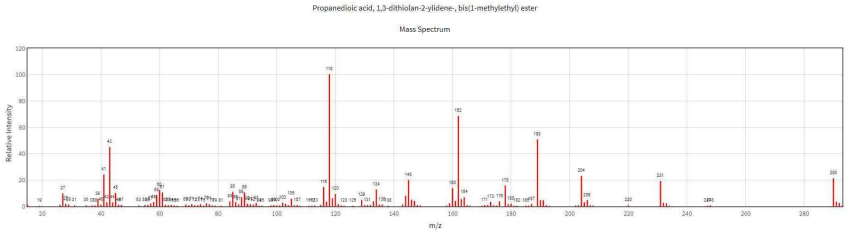

·Formula: $C_{12}H_{18}O_4S_2$
·Molecular weight: 290.399

http://webbook.nist.gov/cgi/cbook.cgi?ID=C50512351&Mask=200

22. DEF (Tribufos)

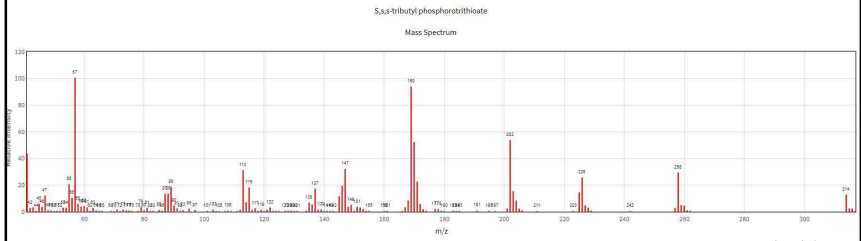

·Formula: $C_{12}H_{27}OPS_3$
·Molecular weight: 314.511

http://webbook.nist.gov/cgi/cbook.cgi?ID=C78488&Mask=200

23.Dicrobutrazole

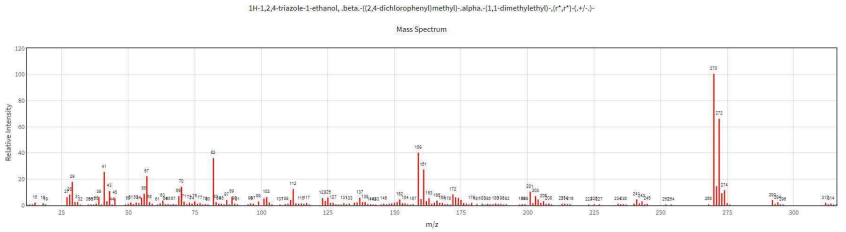

·Formula: $C_{15}H_{17}Cl_2N_3O$
·Molecular weight: 328.237

http://webbook.nist.gov/cgi/cbook.cgi?ID=C75736333&Mask=200

24.Myclobutanil

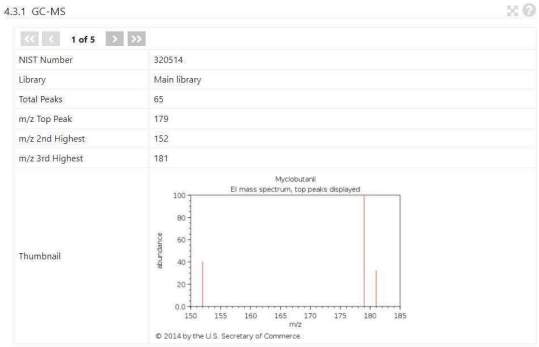

·Formula: $C_{15}H_{17}ClN_4$
·Molecular weight: 288.775

https://pubchem.ncbi.nlm.nih.gov/compound/myclobutanil#section=Spectral-Properties

25.Azaconazole

```
ACCESSION: MSJ01062
RECORD_TITLE: Azaconazole; GC-EI-Q; MS; Positive; M+*
DATE: 2016.12.28
AUTHORS: Shimadzu Corporation., Kyoto, Japan
LICENSE: CC BY
COPYRIGHT: Shimadzu Cooperation., Kyoto, Japan
PUBLICATION: Shimadzu Collection of Pesticide GCMS Data

CH$NAME: Azaconazole
CH$COMPOUND_CLASS: Non-Natural Product; Pesticides
CH$FORMULA: C12H11Cl2N3O2
CH$EXACT_MASS: 299.02283
CH$SMILES: Clc(c3)cc(Cl)c(c3)C(O2)(OCC2)Cn(c1)ncn1
CH$IUPAC: InChI=1S/C12H11Cl2N3O2/c13-9-1-2-10(11(14)5-9)12(18-3-4-19-12)6-17-8-15-7-16-17/h1-2,5,7-8H,3-4,6H2
CH$LINK: INCHIKEY AKNQMEBLVAWSNZ-UHFFFAOYSA-N
CH$LINK: PUBCHEM CID:43233

AC$INSTRUMENT: GCMS-QP2010 Plus, Shimadzu
AC$INSTRUMENT_TYPE: GC-EI-Q
AC$MASS_SPECTROMETRY: MS_TYPE MS
AC$MASS_SPECTROMETRY: ION_MODE POSITIVE
AC$MASS_SPECTROMETRY: IONIZATION EI
AC$CHROMATOGRAPHY: COLUMN_NAME Rtx-5MS(RESTEK), 0.32 mm I.D. x 30 m, df=0.25 microm
AC$CHROMATOGRAPHY: COLUMN_TEMPERATURE 80 C (1 min)-20 C/min - 180 C - 5 C/min - 330C (10 min)
AC$CHROMATOGRAPHY: INJECTION_TEMPERATURE 260 C
AC$CHROMATOGRAPHY: RETENTION_TIME 13.4 min

MS$FOCUSED_ION: ION_TYPE M*+
MS$FOCUSED_ION: PRECURSOR_M/Z 299.02
```

http://www.massbank.jp/jsp/Dispatcher.jsp?type=disp&id=MSJ01062&site=24

Other names: 1H-1,2,4-Triazole, 1-[[2-(2,4-dichlorophenyl)-1,3-dioxolan-2-yl]methyl]-; 1-[[2-(2,4-Dichlorophenyl)-1,3-dioxolan-2-yl]methyl]-1H-1,2,4-triazole; Azoconazole; R-28644

PKSNUM_PEAK: 79
PKSPEAK: m/z int. rel.int.

40 8 8	113 7 7
42 43 43	115 4 4
43 16 16	123 31 31
44 15 15	124 9 9
45 5 5	125 23 23
50 23 23	135 7 7
51 7 7	136 16 16
52 5 5	137 11 11
53 8 8	138 77 77
55 85 85	139 15 15
58 5 5	140 25 25
60 8 8	145 164 164
61 6 6	146 11 11
62 6 6	147 132 132
63 11 11	149 25 25
67 6 6	159 44 44
71 9 9	161 14 14
73 21 21	172 7 7
74 46 46	173 684 684
75 69 69	174 60 60
82 62 62	175 422 422
84 10 10	176 29 29
85 16 16	177 73 73
86 396 396	178 5 5
87 34 34	182 21 21
88 6 6	183 7 7
89 15 15	184 13 13
91 7 7	186 7 7
96 5 5	217 999 999
97 11 11	218 102 102
99 29 29	219 695 695
100 9 9	220 62 62
101 13 13	221 98 98
102 5 5	222 9 9
103 8 8	262 11 11
106 5 5	264 13 13
107 5 5	281 7 7
108 88 88	//
109 70 70	
110 48 48	
111 26 26	
112 6 6	

- **Formula**: $C_{12}H_{11}Cl_2N_3O_2$
- **Molecular weight**: 300.141

26.Buprofezin

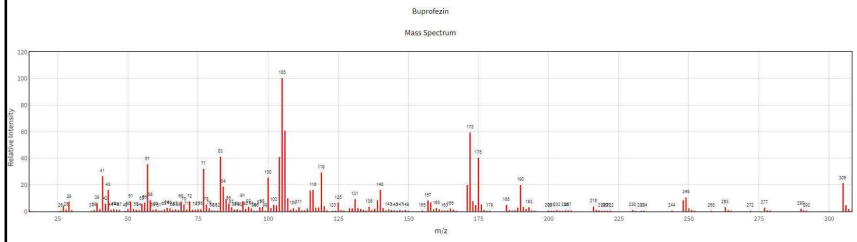

- **Formula**: $C_{16}H_{23}N_3OS$
- **Molecular weight**: 305.438

http://webbook.nist.gov/cgi/cbook.cgi?ID=C69327760&Mask=200

27.Kresoxim methyl

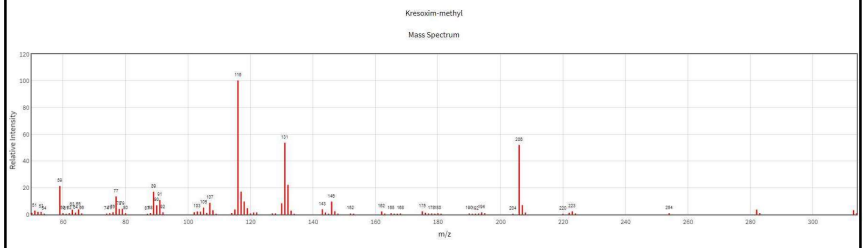

- **Formula**: $C_{18}H_{19}NO_4$
- **Molecular weight**: 313.3478

http://webbook.nist.gov/cgi/cbook.cgi?ID=C143390890&Mask=200

28. β-Endosulfan

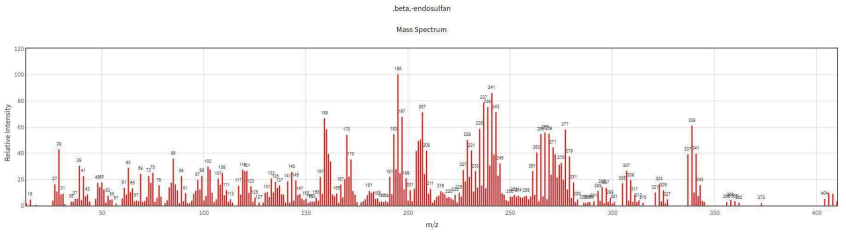

- **Formula**: $C_9H_6Cl_6O_3S$
- **Molecular weight**: 406.925

http://webbook.nist.gov/cgi/cbook.cgi?ID=C33213659&Mask=200

29.Cyflufenamid

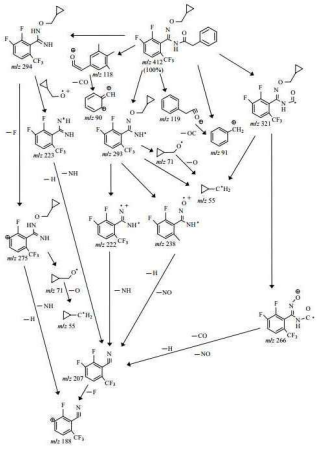

图 2 环氟菌胺的主要碎片离子和裂解途径

Fig.2 The main fragment ions and major fragmentation pathways of cyflufenamid

•Formula: $C_{20}H_{17}F_5N_2O_2$
•Molecular weight: 412.36

30.Chlorfenapyr

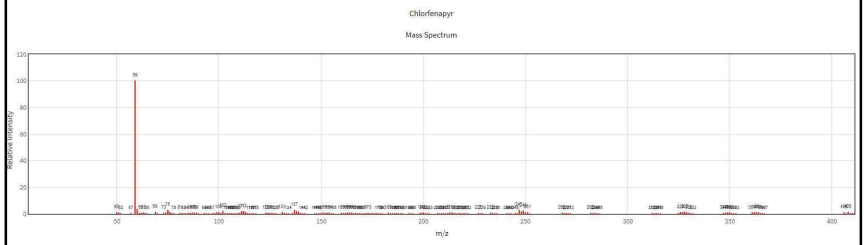

•Formula: $C_{15}H_{11}BrClF_3N_2O$
•Molecular weight: 407.613

http://webbook.nist.gov/cgi/cbook.cgi?ID=C122453730&Mask=200

31.Bromopropylate

4.4.3 GC-MS

NIST Number	55735
Library	Main library
Total Peaks	20
m/z Top Peak	341
m/z 2nd Highest	183
m/z 3rd Highest	185
Thumbnail	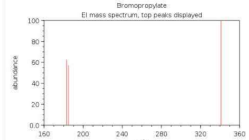

© 2014 by the U.S. Secretary of Commerce.

•Formula: $C_{17}H_{16}Br_2O_3$
•Molecular weight: 428.115

https://pubchem.ncbi.nlm.nih.gov/compound/Bromopropylate#section=GC-MS

32.Bifenthrin

4.3.1 GC-MS

NIST Number	291832
Library	Main library
Total Peaks	144
m/z Top Peak	181
m/z 2nd Highest	165
m/z 3rd Highest	166
Thumbnail	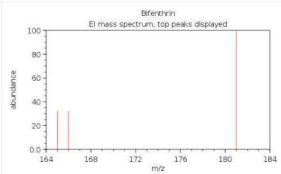

© 2014 by the U.S. Secretary of Commerce.

•Formula: $C_{23}H_{22}ClF_3O_2$
•Molecular weight: 422.868

https://pubchem.ncbi.nlm.nih.gov/compound/5281872#section=Spectral-Properties

33.Fenpropathrin

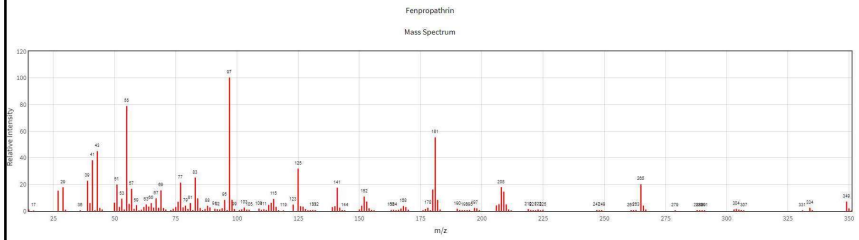

•Formula: $C_{22}H_{23}NO_3$
•Molecular weight: 349.4229

http://webbook.nist.gov/cgi/cbook.cgi?ID=C39515418&Mask=200

34.Bifenox

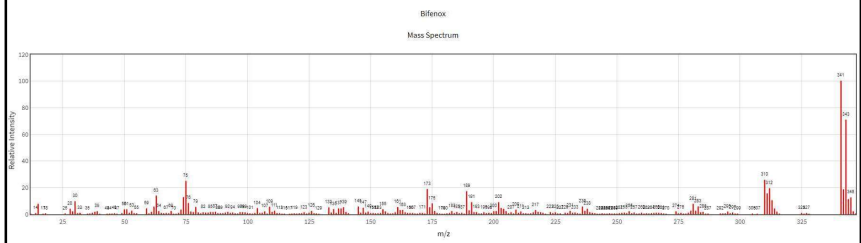

•Formula: $C_{14}H_9Cl_2NO_5$
•Molecular weight: 310.132

http://webbook.nist.gov/cgi/inchi?ID=C42576023&Mask=200

35.Clomeprop

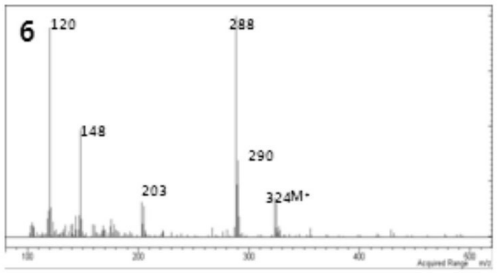

•Formula: $C_{16}H_{15}Cl_2NO2$
•Molecular weight: 324.201

Fig. 5. Mass spectra of 6 pesticides. 6. Clomeprop

Korean Journal of Environmental Agriculture Volume 31, Issue 2, 2012. pp.157-163
DOI : 10.5338/KJEA.2012.31.2.157

36.Cyhalofop-butyl

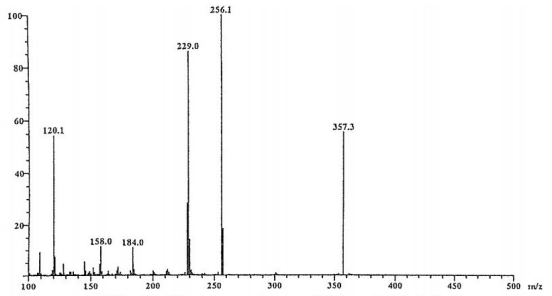

•Formula: $C_{20}H_{20}FNO_4$
•Molecular weight: 357.381

Fig. 3 EI mass spectrum of Cyharofop-butyl.

37.Fenarimol

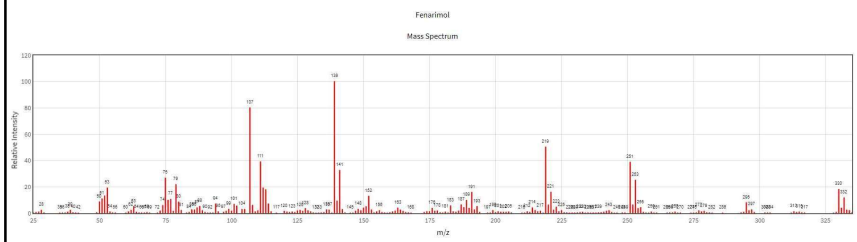

•**Formula**: $C_{17}H_{12}Cl_2N_2O$
•**Molecular weight**: 331.196

http://webbook.nist.gov/cgi/cbook.cgi?ID=C60168889&Mask=200

38.Pyrazophos

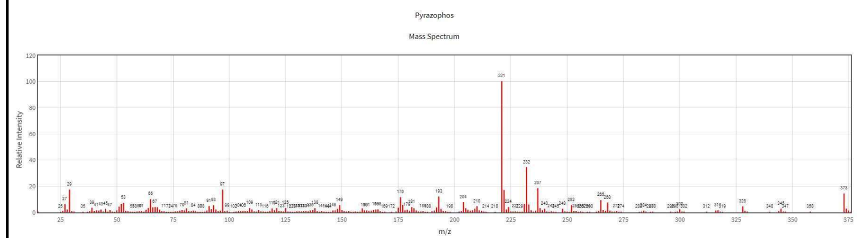

•**Formula**: $C_{14}H_{20}N_3O_5PS$
•**Molecular weight**: 373.364

http://webbook.nist.gov/cgi/cbook.cgi?ID=C13457186&Mask=200

39.Acrinathrin

ACCESSION: MSJ01060
RECORD_TITLE: Acrinathrin; GC-EI-Q; MS
DATE: 2016.12.21
AUTHORS: Shimadzu Corporation., Kyoto, Japan
LICENSE: CC BY
COPYRIGHT: Shimadzu Cooperation., Kyoto, Japan
PUBLICATION: Shimadzu Collection of Pesticide GCMS Data
COMMENT: A diostereomer of Acrinathrin

CH$NAME: Acrinathrin
CH$COMPOUND_CLASS: Non-Natural Product; Pesticides
CH$FORMULA: C26H21F6NO5
CH$EXACT_MASS: 541.13239
CH$SMILES: CC1(C)C(C1/C=C/C(=O)OC(C(F)(F)F)C(F)(F)F)C(=O)O[C@H](C#N)c3cccc(Oc2ccccc2)c3
CH$IUPAC: InChI=1S/C26H21F6NO5/c1-24(2)18(11-12-20(34)38-23(25(27,28)29)26(30,31)32)21(24)22(35)37-1
CH$LINK: INCHIKEY YLFSVIMMRPNPFK-PYWOBYHFSA-N

AC$INSTRUMENT: GCMS-QP2010 Plus, Shimadzu
AC$INSTRUMENT_TYPE: GC-EI-Q
AC$MASS_SPECTROMETRY: MS_TYPE MS
AC$MASS_SPECTROMETRY: ION_MODE POSITIVE
AC$MASS_SPECTROMETRY: IONIZATION EI
AC$CHROMATOGRAPHY: COLUMN_NAME Ptx-5MS(RESTEK), 0.32 mm I.D. x 30 m, df=0.25 microm
AC$CHROMATOGRAPHY: COLUMN_TEMPERATURE 80 C (1 min)-20 C/min - 180 C - 5 C/min - 330C (10 min)
AC$CHROMATOGRAPHY: INJECTION_TEMPERATURE 260 C
AC$CHROMATOGRAPHY: RETENTION_TIME 19.2 min

MS$FOCUSED_ION: ION_TYPE M*+
MS$FOCUSED_ION: PRECURSOR_M/Z 541.13

PK$NUM_PEAK: 176
PK$PEAK: m/z int. rel.int.
40 344 344
41 126 126
45 21 21
48 60 60
49 22 22
50 96 96
51 191 191
52 205 205
53 270 270
54 136 136
55 51 51
56 50 50
57 40 40
59 28 28
63 193 193
65 128 128
67 123 123
69 258 258
70 213 213
77 552 552
78 110 110
79 389 389
81 45 45
83 393 393
89 13 13
91 187 187
92 76 76
93 999 999
95 90 90
97 22 22
99 96 96
100 90 90
102 135 135
104 27 27
105 46 46
107 137 137
110 20 20
113 6 6
114 33 33
115 41 41
117 34 34
120 97 97
121 143 143
122 103 103
124 53 53
125 37 37
128 27 27
129 18 18
132 60 60
134 110 110
137 15 15
139 92 92
140 104 104
141 300 300
142 49 49
143 5 5
144 84 84
148 40 40
149 23 23
151 33 33
153 50 50
154 51 51
160 26 26
164 23 23
165 122 122
167 29 29
168 11 11
169 115 115
170 32 32
172 7 7
174 35 35
180 168 168
181 631 631
182 92 92
183 114 114
187 14 14
197 28 28
198 55 55
199 13 13
200 57 57
201 11 11
203 39 39
205 11 11
208 125 125
209 181 181
210 155 155
211 38 38
212 8 8
215 47 47
223 11 11
225 56 56
228 20 20
231 13 13
234 11 11
236 17 17
237 31 31
243 14 14
245 19 19
246 7 7
247 257 257
248 21 21
250 7 7
252 16 16
258 7 7
259 25 25
261 105 105
262 26 26
263 24 24
272 6 6
275 10 10
277 39 39
279 21 21

ANALYTICAL SCIENCES OCTOBER 1997, VOL. 13

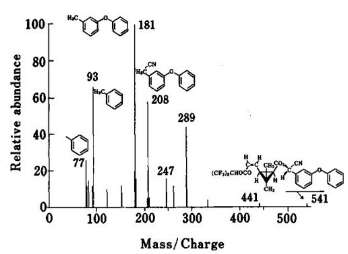

•**Formula**: $C_{26}H_{21}F_6NO_5$
•**Molecular weight**: 541.446

① http://www.massbank.jp/jsp/Dispatcher.jsp?type=disp&id=MSJ01060&site=24
② Analytical Sciences, Vol. 13 (1997) No. 5 P 817-819
http://doi.org/10.2116/analsci.13.817

40.Fluquinconazole

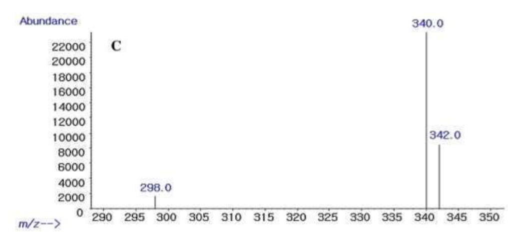

•**Formula**: $C_{16}H_8Cl_2FN_5O$
•**Molecular weight**: 376.172

Biomedical Chromatography, Volume 28, Issue 6, June 2014 ,Pages 774–781
DOI: 10.1002/bmc.3094

41.Cafenstrole

42.Cyfluthrin

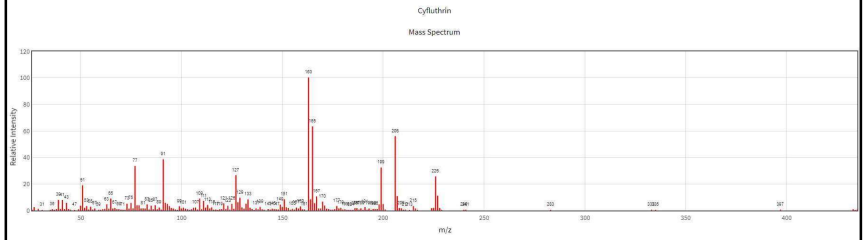

•Formula: $C_{22}H_{18}Cl_2FNO_3$
•Molecular weight: 434.288

http://webbook.nist.gov/cgi/cbook.cgi?ID=C68359375&Mask=200

43.Halfenprox

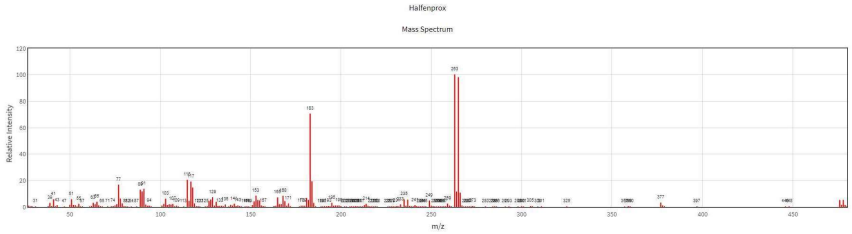

•Formula: $C_{24}H_{23}BrF_2O_3$
•Molecular weight: 477.338

http://webbook.nist.gov/cgi/inchi?ID=C111872583&Mask=200

44/45.Flucythrinate

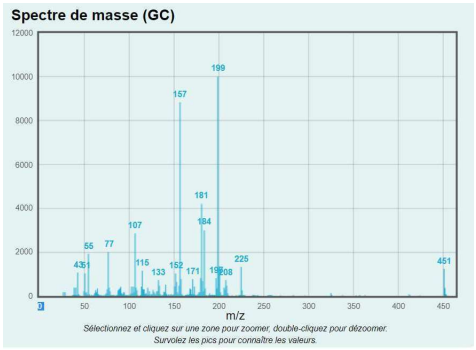

•Formula: $C_{26}H_{23}F_3NO_4$
•Molecular weight: 451.4619

http://www.restek.fr/compound/view/70124-77-5/Flucythrinate%201

46.Fenvalerate

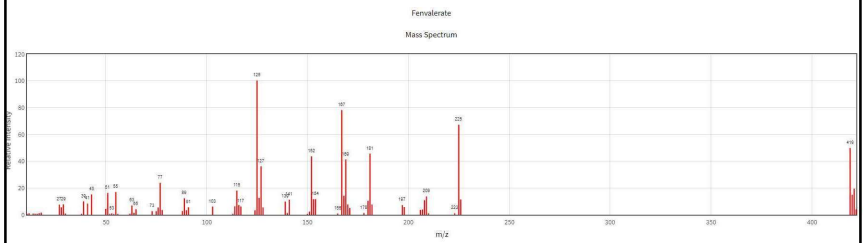

•Formula: $C_{25}H_{22}ClNO_3$
•Molecular weight: 419.900

http://webbook.nist.gov/cgi/cbook.cgi?ID=C51630581&Mask=200

47/48.Fluvalinate

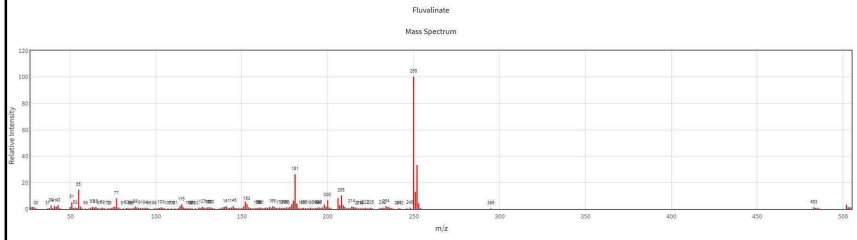

•Formula: $C_{26}H_{22}ClF_3N_2O_3$
•Molecular weight: 502.913

http://webbook.nist.gov/cgi/inchi?ID=C69409945&Mask=200

49.Difenoconazole

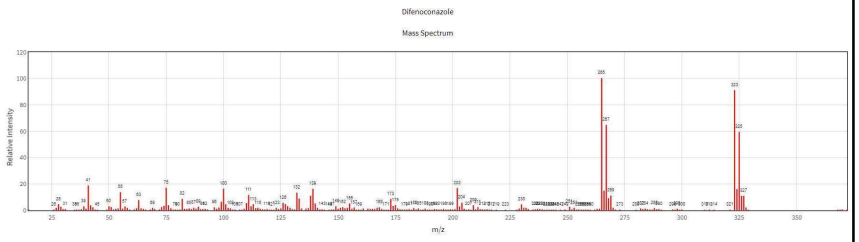

•Formula: $C_{19}H_{17}Cl_2N_3O_3$
•Molecular weight: 406.263

http://webbook.nist.gov/cgi/cbook.cgi?ID=C119446883&Mask=200

50.Deltamethrin

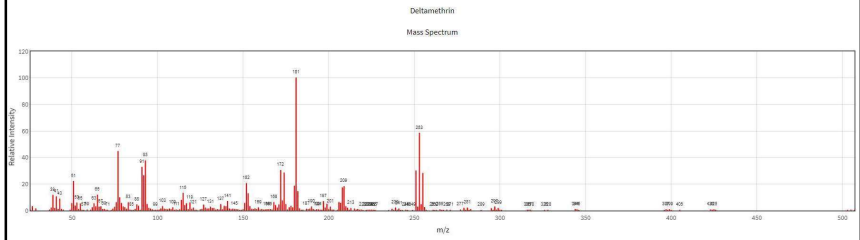

•Formula: $C_{22}H_{19}Br_2NO_3$
•Molecular weight: 505.199

http://webbook.nist.gov/cgi/cbook.cgi?ID=C52918635&Mask=200

51.Azoxystrobin

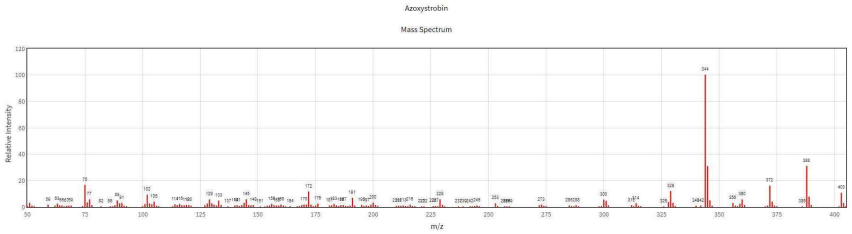

- Formula: $C_{22}H_{17}N_3O_5$
- Molecular weight: 403.3875

http://webbook.nist.gov/cgi/cbook.cgi?ID=C13180338&Mask=200